CAPILLARY INSTABILITIES IN THIN, SOLID FILMS

by

EVA JIRAN

B. A. Sc., Engineering Science
University of Toronto (1983)

Submitted to the Department of
Materials Science and Engineering
in Partial Fulfillment of
the Requirements for the Degree of

DOCTOR OF PHILOSOPHY

at the

Massachusetts Institute of Technology

February 1990

© Massachusetts Institute of Technology 1990. All rights reserved

Signature of Author _____
Department of Materials Science and Engineering
January 12, 1990

Certified by _____
Carl V. Thompson
Associate Professor, Electronic Materials
Thesis Supervisor

Accepted by _____
Linn W. Hobbs
Chairman, Departmental Committee on Graduate Students

MASSACHUSETTS INSTITUTE
OF TECHNOLOGY

MAR 08 1990

ARCHIVES

LIBRARIES

CAPILLARY INSTABILITIES IN THIN, SOLID FILMS

by

EVA JIRAN

Submitted to the Department of Materials Science and Engineering
on January 12, 1990 in partial fulfillment of the
requirements for the Degree of Doctor of Philosophy in
Materials Science and Engineering

ABSTRACT

Very thin films, less than 1000Å thick, are used in a variety of applications, including as catalysts and for thin film reactions to form patterned silicides in electronic devices. These very thin films are subject to capillary instability because of their high surface to volume ratios and will agglomerate well below their melting temperatures. We have measured and modeled the temperature and film thickness dependence of agglomeration.

In order to develop a general understanding of agglomeration in very thin films, we have studied continuous as well as patterned films of gold on fused silica substrates. Two in situ techniques were used to monitor agglomeration: 1) heating and video recording in a transmission electron microscope, and 2) measurement of the intensity of laser light transmitted through a sample heated in a furnace with a controlled atmosphere. Electron microscopy allowed investigation of the role of the microstructure of the gold film and analysis of light transmission during heating allowed determination of temperature-dependent and film thickness-dependent agglomeration rates.

We found that the material removed from the substrate as the film recedes accumulates at the film edge. The thickened edge is subject to instabilities and decomposes, exposing thinner areas of the film. The transformation rate is controlled by void growth through these thin areas and the void develops a dendritic or cellular morphology. A previously published model was modified to take this observation into account. The resulting rate equation is independent of time and has an inverse cubic dependence on film thickness.

Agglomeration in continuous films occurs by nucleation and growth of voids. In order to observe only the growth component of the process, lithographically defined lines were used to simulate a perforated film. The observed agglomeration rate from transmission experiments with gold lines in oxygen was constant as proposed in the model and the observed thickness dependence was $h^{-3.1}$, again, in very good agreement with the model. This data was also used to extract an activation energy for surface diffusion of 1.4 eV.

The agglomeration of continuous films was modeled as two dimensional void nucleation and void growth with a constant rate. The proposed transformation curve based on a constant number of nuclei and a constant growth rate fit observed transformation curves very well. Growth rates measured in 600Å thick continuous gold films annealed in oxygen were in agreement with growth rates measured in patterned films of the same thickness.

Thesis Supervisor: Carl V. Thompson

Title: Associate Professor of Electronic Materials

TABLE OF CONTENTS

LIST OF FIGURES

LIST OF TABLES

ACKNOWLEDGEMENTS

I gratefully acknowledge Prof. C. V. Thompson, my advisor for this thesis, for his guidance and advice, and especially for maintaining his enthusiasm for this project in the face of some initially puzzling and frustrating results. It's much too easy, after years of monitoring every detail for feel overwhelmed by the complexity of a problem. I also thank Prof. Russell and Prof. Rudman for being a part of my thesis committee and whose comments and words of advice were much appreciated.

I also thank my parents who patiently worried about my well being for six long years and who after having raised me to reach for the highest goals possible, would have done anything to take the difficulties in my life away. I thank my sister Hana who remembered to keep in touch when I was too buried in my work to realize just how much time has passed since we last talked.

I'm deeply grateful to Steve, my husband, who was as needed be: my patience, my enthusiasm and my reason.

If there is one MIT experience that will never cease to warm my heart, it was that the more frustrating life became and the more obstacles stood in my way, the more people gathered around me to offer their support and encouragement. I've never before had so many great friends.

Chapter 1:

INTRODUCTION

The stability of fine structures in the form of thin films and narrow lines is becoming an issue of increasing importance to the electronics industry. Thin film stability has long been an important issue in the area of catalysis, where large surface areas of precious metals are needed. Today, fabrication of integrated circuits is increasing in complexity in terms of both processing, including chemical reactions between thin films, and the materials being used. As in catalysts, the thin films and narrow lines used for devices have a very high surface to volume ratio, which produces a large driving force for reduction of surface area. Surface area can be reduced through mass transfer by diffusion. If this diffusion takes place, the thin film or narrow line will change shape and become discontinuous causing the device to fail.

Agglomeration is the decomposition of a thin continuous film into a collection of beads. It occurs in two steps, void formation and void growth. A cylinder evolves into a row of beads through the growth of small amplitude fluctuations in the surface[1]. As will be discussed in Chapter 2, a plane surface does not contain this kind of instability. In other words, while fluctuations in the surface of a cylinder will grow if they are larger than a critical wavelength, small amplitude fluctuations in a plane surface will not grow, regardless of their wavelength. A thin film must therefore decompose by means of fluctuations large enough to penetrate the film.

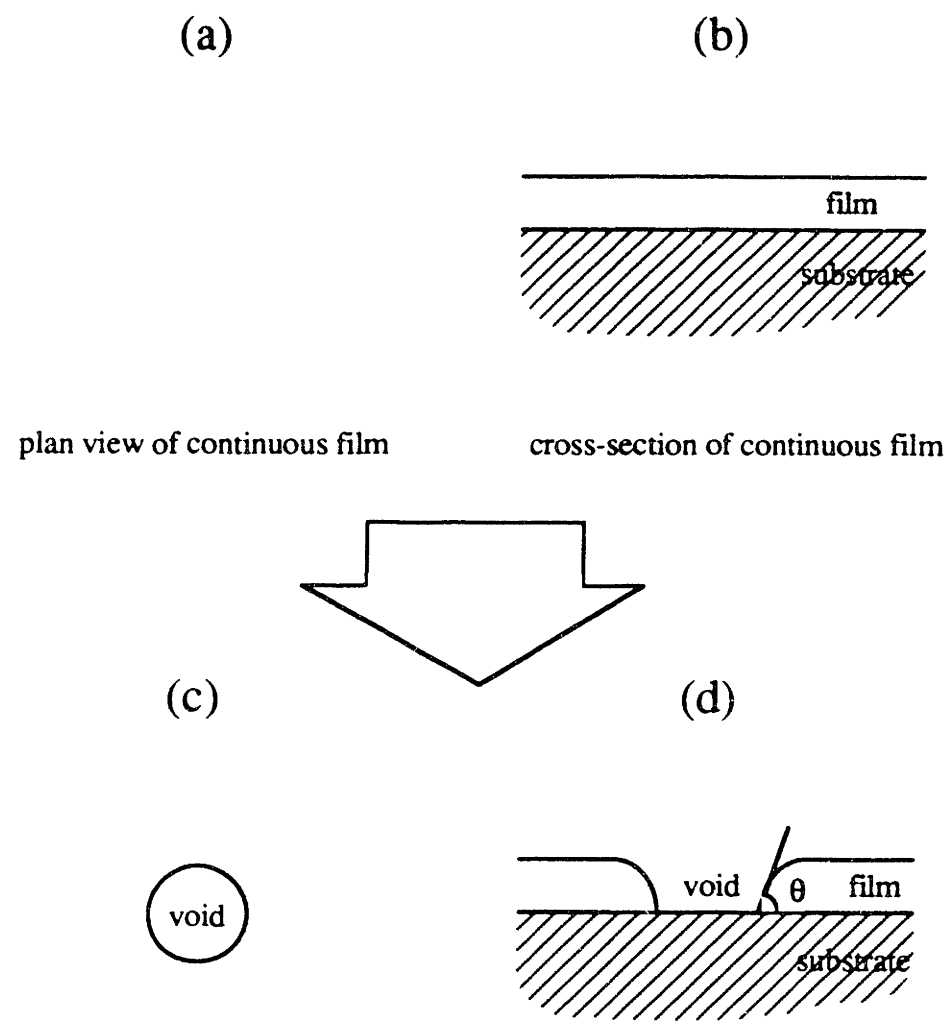

Figure 1.1: Schematic representation of a thin film on a substrate: a) and b) are continuous film, c) and d) are the film perforated by a hole. The film edge created when the hole forms meets the substrate at a contact angle θ.

As soon as a stable void in the film forms, the edge of the film assumes a contact angle with respect to the substrate, resulting in curvature in the film edge profile (Fig.1.1d). The growth of the void is driven by the reduction of this curvature. Figure 1.1 shows a thin continuous film (a and b) and a thin film with a void extending through the thickness (c and d). The film becomes discontinuous when voids impinge and islands of material form. These islands then evolve into equilibrium shapes such as caps or beads. This sequence of events is illustrated schematically in figure 1.2.

As will be seen in Chapter 4, the simple model depicted in figures 1.1 and 1.2 does not fully describe the agglomeration process. The voids that grow do not have the simple shapes described in figure 1.1 and existing models for the morphology and the growth rate of voids in thin films do not adequately predict this behavior.

The experimental work in this thesis consists of two parts. The first part is a detailed study of agglomeration at the microscopic level which lead to the derivation of a new model, and the second part is a quantitative study using gold on fused silica which lead to a verification of the proposed model and determination of kinetic parameters. Two unique approaches made the quantitative study possible. One of these involved the use of laser light transmitted through the sample to measure *in situ* fraction transformed, and the other involved the use of patterned films to simulate a continuous film with holes already formed. This means that nucleation of holes is not necessary for the transformation to take place and the measurements, therefore, contained only the growth component of the transformation. Patterning also provides a simple geometry for analysis (Fig.1.3).

The purpose of the research described in this thesis is to experimentally characterize the rate of agglomeration by studying the kinetics of hole formation and propagation in thin films as a function of temperature and film thickness and to develop kinetic models which will allow the prediction of void growth kinetics. Gold on fused silica is used as the model system in this study.

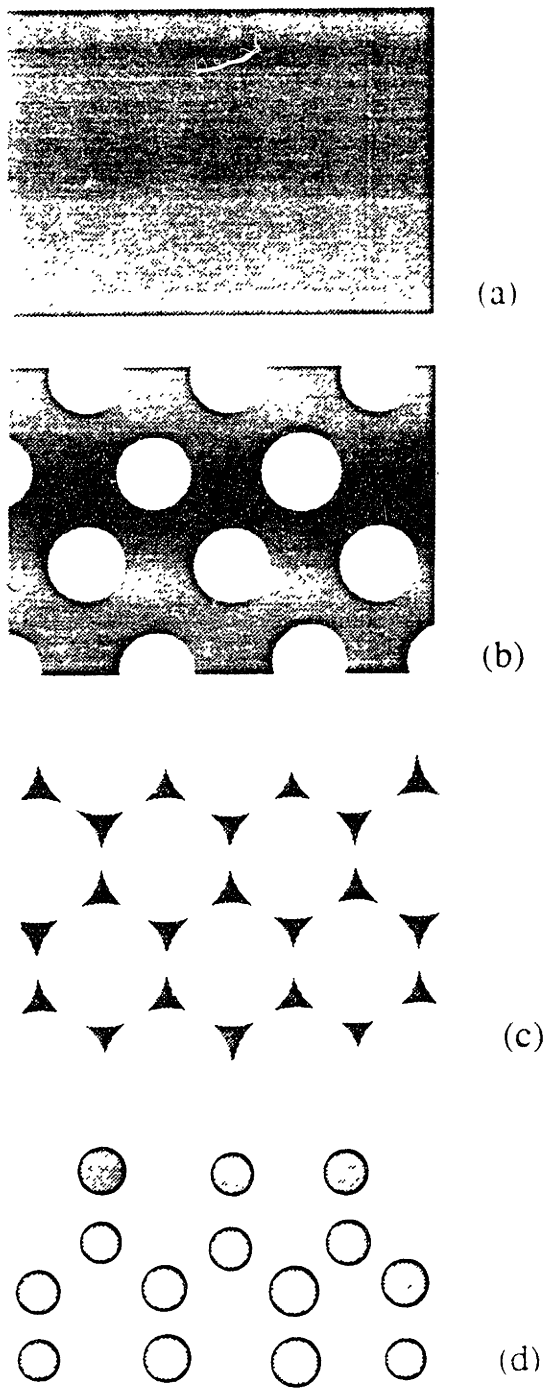

Figure 1.2. Schematic of a thin film in the process of agglomeration showing: a) a continuous film, b) a perforated film after nucleation of voids, c) a discontinuous film as voids impinge, and d) beads.

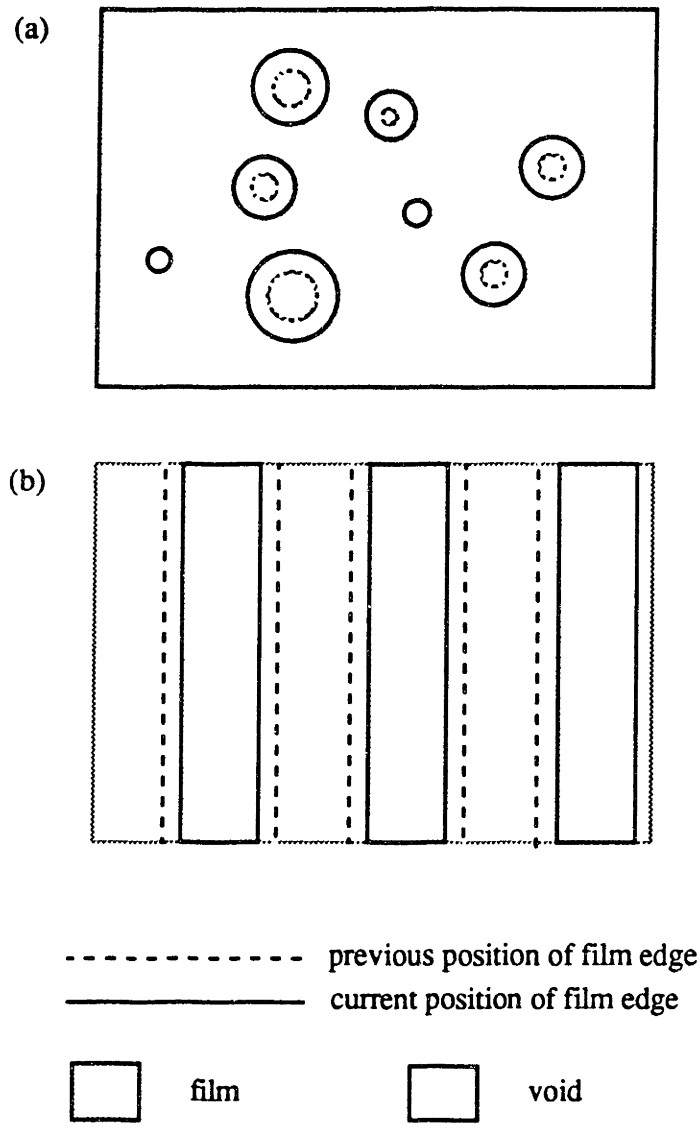

Figure 1.3. Schematic representation of: a) continuous and b) patterned films at two different points in time.

Chapter 2:

LITERATURE REVIEW

Literature Review of Theory

Capillarity Driven Morphological Evolution of a Surface

For a change of shape to occur, there must be a shape available with an overall lower free energy than the current shape. The calculation to determine a final shape can be approached from two directions. The simplest is to subtract the free energy of the initial shape from that of the final shape. This energy difference must be negative for the perturbed shape to be stable. The second way is to apply a perturbation to the surface and determine the range of perturbations whose amplitude will grow and further, determine the perturbation that has the fastest rate of growth. Neither can absolutely predict the final shape. The final shape used in the stability approach must occur through some kind of fluctuation in the surface of the initial shape. The small amplitude fluctuations studied in perturbation analyses do not necessarily yield the critical wavelength that would become stable when the amplitude is large.

Metastability of a thin film to bead or island formation (instability to large fluctuations)

Solutions for the stability of agglomerated configurations have been found for certain geometries. For example, in the case of the infinite cylinder, the critical wavelength found by *comparing the initial and final energy state is* $(9/2)a$. [2], where a is the radius of the cylinder. Srolovitz and Safran[2] compared the energy of a continuous film on a

substrate, to the energy of a film with an array of holes through the thickness and with the energy of beads whose volume was equal to the original volume of film. They found that for holes a certain size and beads of a certain size, this energy difference is negative and so in this size range the perturbed film is more stable than the continuous film. Therefore, if by means of some fluctuation a continuous film develops perturbations within this negative energy range, these perturbations would remain stable against closing and the film would become discontinuous.

Stability of the surface of a solid to small and large fluctuations:

The transformation of a continuous film to beads must begin with some kind of fluctuation in the surface of the film. In the case of the infinite cylinder, studied by Rayleigh, the critical wavelength for a surface *perturbation to grow* was found to be $2\pi a$ [1]where a was the radius of the cylinder (Fig.2.1). Rayleigh also found that the fastest growing wavelength was $4.508 \times 2\pi a$. On the other hand, the behavior of a general plane surface of an isotropic solid was modeled by Mullins[3]. He subjected the plane surface to small amplitude sinusoidal fluctuations and considered four possible ways that capillary forces could cause these fluctuations to grow or shrink: viscous flow, evaporation-condensation, volume diffusion, and surface diffusion. A combination of these processes may be in effect, and the dominant process for mass transfer will change according to the temperature and wavelength of the fluctuation. Under all conditions, the surface decays with time to a flat plane. This means that a plane film can not transform through the growth of small fluctuations in its surface.

Since thin films are metastable with respect to caps or beads, a large fluctuation in the surface, so large as to penetrate the film and expose the substrate, could produce a stable or more stable geometry. Since, in practice, agglomeration occurs, there must be a source of these large fluctuations already present.

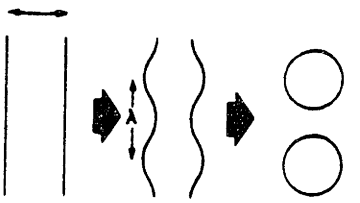

Figure 2.1. A cylindrical solid subject to radial fluctuations of wavelength λ. When the fluctuations are of sufficiently large amplitude, the cylinder breaks up into a line of spheres.[2]

Figure 2.2. Configuration for analysis by Lanxner*et al.*[5]

Morphological Decomposition of a Thin Film

Formation of holes

Although the surface of a film is stable against small fluctuations, once a fluctuation penetrates the film it may be stable and grow. Such large fluctuations can be attributed to grain boundaries and their junctions.

Mullins showed, through a kinetic analysis, that a single grain boundary in an infinite sheet deepens as the fourth root of time[4]. This would mean that if the sheet was a thin film, it would always eventually be penetrated. Srolovitz and Safran [2] considered a *polycrystalline film*, and on the basis of equilibrium considerations and certain assumptions regarding the geometry, concluded that the grain boundary reaches a finite depth, which depends on the diameter of the grains relative to the thickness of the film and on the equilibrium groove angle. For large equilibrium groove angles, the groove depth is large and (for a particular grain size) a much a wider range of film thicknesses is subject to penetration by grain boundaries[2]. Grain boundary triple junctions also have a finite depth, but the critical grain size for penetration is so small that all such vertices reach the substrate.

Criterion for the growth of holes

If the formation of holes in a thin film is treated as a nucleation and growth phenomenon, then there is a critical size beyond which the hole should grow, and below which the hole should shrink. Srolovitz and Safran[2] found, *for a film in contact with a substrate*, that when the value of β, defined as:

$$\beta = \left(\frac{R}{h} \right)^2 (1 - \cos \theta) \qquad (1)$$

where h is the original thickness of the film, R is the distance between holes and θ is the contact angle with the substrate, is more than about 15, then there exists a range of hole sizes which are energetically more stable than the continuous film. This range is preceded

by a maximum in energy change with hole size and so holes that are too small shrink. The range of hole sizes for which the energy change is less than zero can include impingement: the hole size is equal to distance between holes. The geometry of a continuous film being perturbed to spherical caps was treated similarly.

Lanxner *et al*[5] studied single crystal gold films with holes generated upon deposition. These films were lifted off the substrate on microscope grids, and annealed. The *films were thus free-standing*: both the top and bottom of the film exposed to the same ambient. Upon annealing, holes grew or shrank or remained stable. The model proposed to account for this was also based on minimizing energy with respect to hole size.

$$dE = 2\pi(2r - h_o)\,\gamma\,dr \qquad (2)$$

where r is the radius of the hole and h_0 is the thickness of the film. It was proposed that holes grow if $r > h_0/2$ and shrink otherwise (Fig.2.2).

The Rate of Growth of large holes

Two solutions to the rate of growth of holes have been published. Srolovitz and Safran[6] used a small contact angle approximation but the solution was not steady state in profile so an explicit solution for the rate of growth as a function of temperature and film thickness could not be found. Brandon and Bradshaw[7] approximated the surface flux with a simplified geometry and solved for an expression as a function of temperature and film thickness. The two results are discussed below.

Srolovitz and Safran[6] considered two cases for hole growth: hole growth under the action of condensation and evaporation and hole growth under the action of surface diffusion. In the limit of large holes and small slopes in the hole edge profile, the first mechanism yields a steady state profile and:

$$\frac{dr}{dt} = \frac{\text{constant}}{h_o} \qquad (3)$$

where h_o is the original film thickness, and r is the radius of the hole. At small r, the profile is no longer time independent and the velocity is not constant. At very small r they found that the velocity is negative so that the hole fills in and the film becomes continuous (Fig.2.3). The second mechanism, surface diffusion, is governed by an equation derived by Mullins[4] for the velocity of a surface normal to itself, V_n:

$$V_n = - B \nabla_s^2 \kappa \qquad \text{and} \qquad B = \frac{D_s \gamma \Omega^2 \nu}{kT} \; . \qquad (4)$$

Srolovitz and Safran solved the equation for the growth of a round hole, in cylindrical coordinates and in the small slope limit. The solution exhibited a ridge which thickened as the edge receded (Fig.2.4). Behind the ridge was a hollow as in Mullins'[4] simulation of profiles created by surface diffusion. There is no steady state profile for this condition. The ridge increases in size with time and the hollow behind deepens with time. Eventually, the hollow reaches the substrate, the entire thickened edge detaches and the process begins again.

Measuring the *rate* of growth of holes leads to determination of kinetic constants. Brandon and Bradshaw[7] took into account that if matter transfer is effected by surface diffusion, there will be an accumulation of material along the edge (followed by a depression, a second hump and so on, but so highly damped that very little of the secondary features would be visible). They modeled the edge in cross-section simply as a semi-circle, so that the contact angle was 90°, and ignored the depression behind it for simplicity (Fig.2.5). The rate equation is derived by solving for the flux due to surface diffusion in atoms s^{-1} cm^{-1}[4],

$$j_s = - \frac{D_s}{kT} \nu \nabla_s \mu \qquad (5)$$

where D_S is the surface diffusivity in cm^2 s^{-1}, k is the Boltzman constant in ergs K^{-1} $atom^{-1}$, T is the temperature in K, ν is the surface concentration in atoms cm^{-2}, μ is the chemical potential and s is the distance, in units of cm, along the surface. The

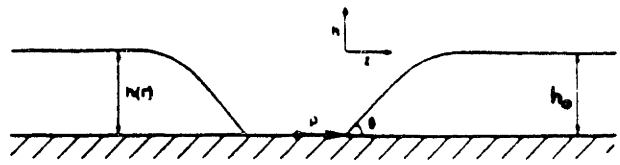

Figure 2.3. Cross-section of a hole of radius r in a thin film of thickness h_o where θ is the equilibrium contact angle. The hole is modelled as growing by condensation-evaporation.[6]

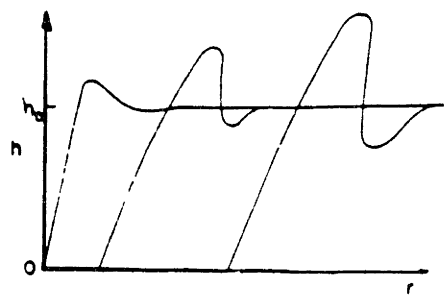

Figure 2.4. Cross-section of the receding film profile caused by surface diffusion.[6]

gradient in chemical potential can be approximated by considering the difference in chemical potential between the curved edge, μ_L, and the flat film beyond the edge, μ_∞:

$$\mu_L - \mu_\infty = -\Omega\gamma_s\left(\frac{1}{r} - \frac{1}{r'}\right)$$

$$= -\frac{\Omega\gamma_s}{r} \qquad r' >> r \ , \tag{6}$$

where r' is the in-plane curvature and r is the radius of curvature of the receding edge (Fig.2.5). Ω is the atomic volume and γ_s is the surface tension. This potential change occurs over a distance of approximately πr. The flux is therefore:

$$j_s = \frac{D_s}{kT}\,\nu\,\frac{\Omega\gamma_s}{\pi r^2} \ . \tag{7}$$

The total volume transferred around the edge of the hole of radius x is,

$$\frac{dV}{dt} = j_s\, 2\pi x\, \Omega, \tag{8}$$

where dV can also be written as,

$$dV = 2\pi x\, r\, dx, \tag{9}$$

Conservation of mass,

$$2\pi x\,\frac{\pi r^2}{2} = \pi x^2 h \ , \tag{10}$$

can be used to solve for r in terms of x, the hole radius, and substituted into equations 7 and 9. The rate, dx/dt, can be expressed in terms of x, the radius of the hole, and h, the film thickness. For the limit of large round holes their result was:

$$\frac{dx}{dt} = \frac{B\, x^{-3/2}\, \pi^{1/2}}{h^{3/2}} \tag{11}$$

$$x^{5/2} = \frac{5\,\pi^{1/2} B\, t}{2\, h^{3/2}} \tag{12}$$

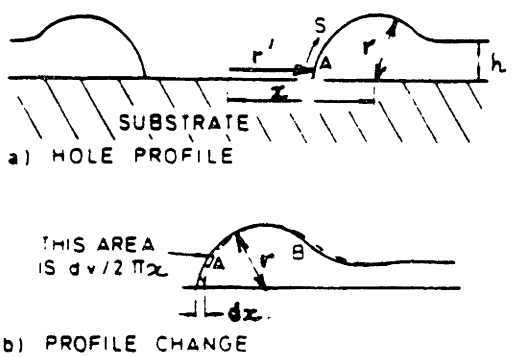

Figure 2.5. Hole growth: analysis of Brandon and Bradshaw.[7]

$$x = \text{constant} \times B^{2/5} t^{2/5} \qquad (13)$$

B contains all the values related to the material properties of the film: the surface diffusivity, surface tension, atomic volume and surface concentration of atoms. Note that the rate, equation 13, is not constant but slows with time.

Presland et al[8] applied the Brandon and Bradshaw formula, equation 12, but in terms of the area of substrate exposed:

$$A^{5/4} = \frac{5\pi^{7/4} B t}{2h_o^{3/2}} \equiv g t \qquad (14)$$

so that:

$$A = g' \frac{t^{4/5}}{h_o^{6/5}} \qquad (15)$$

They observed, from experiment, that there were two distinct values of g and attributed the sharp decrease at longer times to the fact that hole curvature, once islands form, is in the same direction as the curvature of the edge, and the edge curvature is much less at that point in time. This would reduce the driving force.

Summary

In summary, a continuous thin film is metastable relative to an agglomerated film. If there are no stresses in the film the process of hole nucleation cannot take place by means of the growth of small amplitude fluctuations in the surface. Holes must therefore form from large fluctuations already present in the film as grain boundaries and triple junctions. The growth of round holes by means of surface diffusion is accompanied by a thickening of the film edge and in all existing models is characterized by a decreasing rate of growth as a function of time.

The modelling in this thesis (Chapter 5) is motivated by the fact that the morphology and rates of growth of the voids observed in this investigation (Chapter 4) are not correctly described by these models.

Review of the Literature on Experiment

The agglomeration of thin films has been studied by several researchers in silver[8,7,9] as well as gold films[10,11,12] with less detailed studies of lead[13], nickel[14] and tin[15]. The process is described as consisting of four stages:

1. hillock formation due to relaxation of material subjected to thermal stresses and leading to hole formation,
2. hole growth by surface diffusion, caused by diffusion away from an area of high curvature at the edge of the film,
3. island formation as holes impinge, forming a network,
4. equilibration of the irregularly shaped islands from step 3, driven by reduction of surface area .

The purpose of the studies was to characterize the agglomeration process and agglomerated film morphology as a function of the annealing environment or deposition conditions. A model of agglomeration can yield diffusivity constants just as the modelling of the evolution of other shapes does. Other techniques, most commonly used to determine diffusivities, are the grooving of a grain boundary and the decay of scratches, both based on Mullins' models. The results of studies of agglomeration in gold are summarized below.

Kane et al[10] studied 60 to 80 Å thick gold films deposited through a mesh onto a layer of zinc sulphide and capped with a layer of zinc sulphide. The gold formed patterns of 1/16 inch wide strips. They monitored the resistivity of the gold film during anneals in helium in the temperature range 330°C to 480°C. The resistivity of the film increased as the strips agglomerated by hole formation within the strips and growth. They modeled the change in resistivity as a function of the necking down of the connected area between

rectangular voids and calculated an activation energy of 1.8 eV. They interpreted this value as falling between the values for surface and volume diffusion, and suggested therefore that both mechanisms are active.

Hummel et al[11] studied 800 Å thick films deposited on quartz glass slides, in the form of stripes 1.74 mm wide and 16 mm long connected to electrode pads at the ends. The films were annealed in helium at 190, 340 and 560°C. They were compared to films doped with sodium and indium. In the pure gold they observed grain growth and grain boundary grooving. The grain boundary grooving and "blisters" which formed in the film and appeared to "burst" lead to void formation within the stripes. Indium stabilized the films against annealing-induced voids by stabilizing the grain structure, i.e.: there was no apparent grain growth, grooving and void formation under testing conditions of indium doped films.

Zito et al,[12] used a wide variety of techniques to characterize 300 Å thick films annealed at 360°C for 1 hour (pinholes and hillock stage) and at 630°C for 10 min (complete agglomeration). The pinholes did not produce a change in the transmittance of 632.8 nm wavelength light but produced polarization of some of the reflected light at 441.6 nm. The authors characterize the state of agglomeration according to the amount of polarization as a function of scattered angle. At the higher temperature, they observe rods and beads of gold. The rods had a mean width of 0.30±0.07 μm with an arm spacing of 1.0-2.0 μm. Beads had a diameter of 0.68±0.25 μm. 60% of the area was covered by gold estimated to be 500 Å thick. They concluded that the optical integrity of a gold coating is compromised at temperatures above 360°C and used this to calculate the vulnerability to agglomeration of different configurations of solar reflectors.

Summary

In summary, fluctuations in the surfaces of thin films must penetrate the film to produce a stable void in the film which will grow if larger than a critical size. These

fluctuations occur in the form of grain boundaries and triple junctions in the film. The growth of the hole under surface diffusion is accompanied by the thickening of the edge of the receding film which causes hole growth to slow down with time. This has been shown by modeling and by experiment, in the case of equations 13 and 15 on single crystal silver films on mica[8] and polycrystalline silver films on glass[7], respectively. The holes in the single crystal film were round and the material accumulated at the edges as modeled. The holes were finely spaced and impinged while the holes were still round and the accumulation uniform. The holes in the polycrystalline film also impinged at an early stage but in this case the accumulation occurred in hillock areas and the holes were uneven in appearance. The experimental work in this thesis is undertaken to study the morphology and, quantitatively and *in situ,* measure the rate of hole growth as it grows beyond this initial stage and develops a more complicated morphology.

In summary, studies have been initiated by researchers in the areas of catalysis[7,8], electronics[10,11] and optics[12]. Experimental observations of agglomeration in gold and quantitative studies[10,11,12] are very few. Among the limited number of studies in agglomeration, the studies of Presland *et al.*[8] and Brandon and Bradshaw[7] in silver are relatively complete. The possibility of using the agglomeration process to measure kinetic parameters was introduced[7,8,10].

Chapter 3:

MICROSCOPY OF AGGLOMERATION

Objectives

The objective of this thesis is to study the kinetics of the process of agglomeration. In order to derive a model for the rate of mass transfer during agglomeration, the evolution of the receding film edge was studied at the microscopic level. The film edge to be studied is created when a hole forms in a continuous film on annealing, or an edge can be created by patterning the film before annealing.

Both continuous and patterned films were used for this study. Patterned films allow bypassing the nucleation stage of agglomeration. The growth stage is, therefore, isolated for study. *In situ* monitoring of a transformations can sometimes be the only way to determine with confidence how a transformation takes place. To perform the experiments for this thesis, two *in situ* techniques were used. One was a combination of transmission electron microscopy (TEM), with use of a heating stage and video camera/recorder. The second technique, which will be described in detail in Part II, involved a laser probe in combination with a furnace. In Part I, the TEM experiments are described followed, in Chapter 4, by the results of observations made regarding the microscopic, morphological changes which lead to the recession of the film edge.

Experimental Design: *in situ* observation by hot stage TEM

Description

The transmission electron microscope can be used at magnifications high enough to resolve individual void arms and individual grains. In combination with a heating stage, the microscope allows *in situ* observation of dynamic processes such as agglomeration where large amounts of material are moved at elevated temperatures. Video recording is a useful tool in this case because taking still photographs of a moving object, with the exposure times required, can result in blurred images. One way to get sharp photographs is to heat the sample in the heating stage, and at the point of interest in the transformation, lower the temperature to freeze in the structure. Some of the photographs of the film edge in Chapter 4 were taken in this way. Other interesting features of the transformation could only be captured by the video camera. The video recorder has somewhat poorer resolution than a photograph taken under normal circumstances, but it allows us to record the process without interrupting it. The tape can then be examined frame by frame if desired. In this work, a Jeol 100 transmission electron microscope and a Gatan heating stage were used. The video camera was installed directly below the TEM viewing screen. A high resolution tape (3/4" wide) was used for recording.

Substrate requirements and preparation

In order to fit in the heating stage, the samples had to be smaller than about 2 mm in their widest dimension and, for observation, had to be transparent to electrons. The gold films were therefore deposited to a thickness of only 250 Å.

To render the substrate transparent, a commonly used method for creating thin nitride membranes was used. Silicon wafers with about 1000 Å of silicon nitride deposited by chemical vapor deposition on the surface were used to make transparent membranes for the TEM. First the nitride film on the back of the wafer was removed in an array of 2 mm areas using photoresist as a mask and reactive ion etching to remove the

nitride (Fig.3.1.a). The wafer was then chemically etched in a solution of potassium hydroxide, KOH, and water at 80°C, which is an anisotropic etch. In the case of wafers oriented with the 100 crystal direction normal to the surface, lateral etching (Fig.3.1.b) is slow compared to etching through the thickness of the wafer. Silicon nitride etches negligibly in this solution, so that the final structure consists of a thin nitride membrane supported by a frame of silicon wafer (Fig.3.1.b). Since these membranes are very fragile, separating the samples by cleaving the wafer can break the membrane. To minimize this kind of damage, the back of the wafer is scribed after half the required time in the etching solution. The scribe marks expose silicon wafer to the etching solution and a trough is etched into the substrate. This weakens the wafer along the scribe marks and makes cleaving the wafer possible with much less shock to the membranes.

Sample preparation: patterning by evaporation through a mesh

Observations were made on both continuous and patterned films. Continuous films were prepared simply by mounting the substrates and loading them into the evaporator. Patterned films were prepared by evaporation through a mesh. This is done (Fig.3.2.) by placing a mesh on a substrate, depositing the gold and then removing the mesh. The gold is left behind in an array of deposits shaped according to the openings in the mesh.

Evaporation through a mesh is limited in the patterns that can be generated, and the sharpness of the edges, but it requires very little handling both of the substrate before evaporation and of the gold covered sample after deposition, minimizing contamination of the gold interfaces. It can also be applied very easily to small samples such as those used for transmission electron microscopy.

The nickel mesh was purchased as a sheet from Ernest F. Fullam, Inc. It was cut and mounted in the clean room. Dust particles were removed with a nitrogen blow gun. The mesh was not cleaned further because of the difficulty in handling such a thin piece of material. It was assumed that the mesh would not actually come in contact with the gold

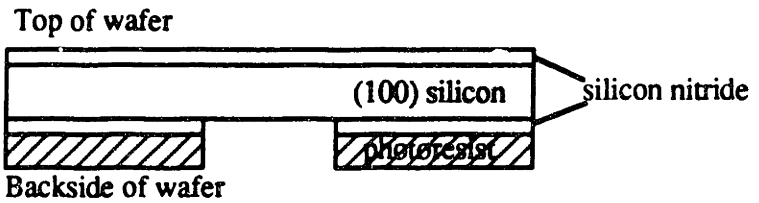

(a) after RIE etching

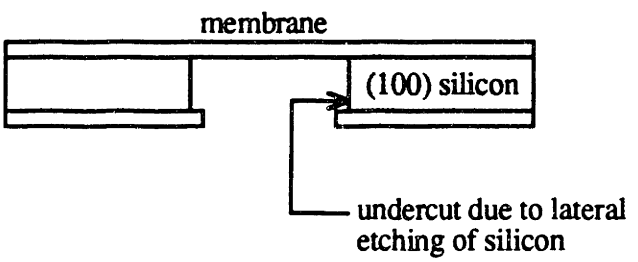

(b) after KOH etch

Figure 3.1. Silicon nitride membrane process:
a) The back side of the wafer is masked with photoresist and reactive ion etched to remove the silicon nitride on the back of the wafer. This exposes silicon in the required areas.
b) The photoresist is removed and the wafer is placed in the etching solution to remove the silicon. This leaves behind the silicon nitride at the front of the wafer which will serve as a substrate for the gold film.

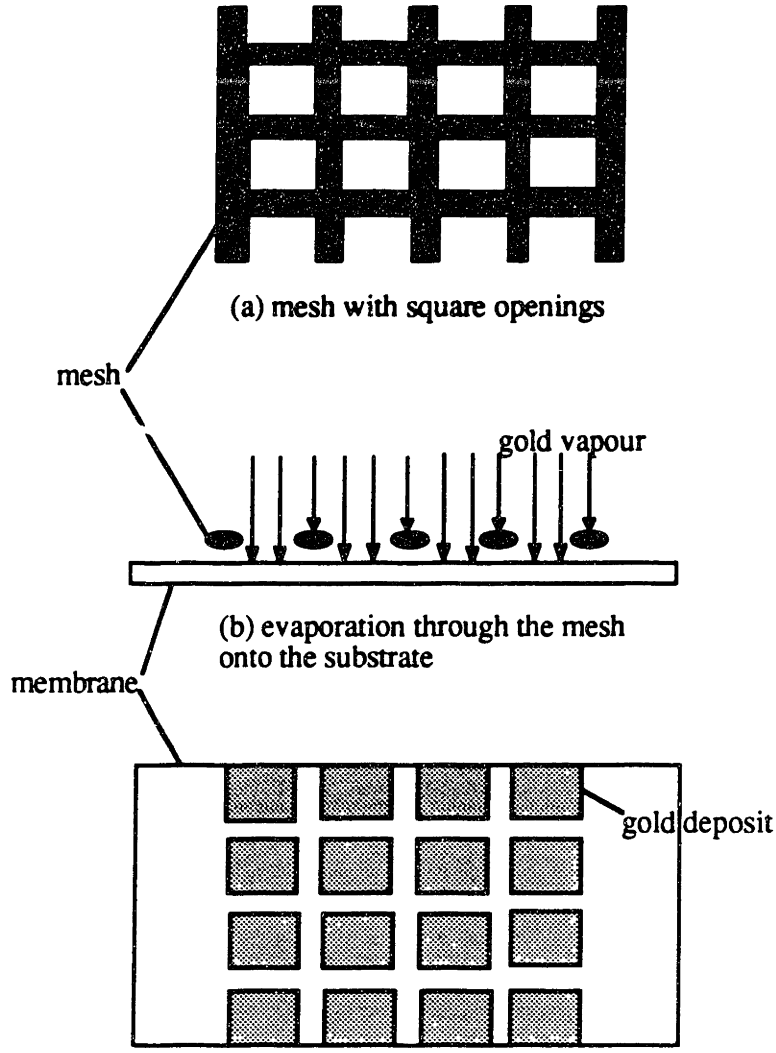

Figure 3.2. Schematic diagram of the process for creating a patterned film by evaporation through a mesh.

deposited. The mesh openings were 50 × 50 μm squares producing a pattern of 50 × 50 μm squares of gold.

Experimental procedure

After membrane preparation and just before loading into the evaporator, the membranes were cleaned in a 5:1:1 bath of deionized water, hydrogen peroxide and ammonium hydroxide (a cleaning solution for oxides used by electronic laboratories) rinsed in de-ionized water and carefully dried with nitrogen from an air gun. The samples were mounted on an evaporation plate and immediately loaded into the evaporator. In the case of patterned films, a mesh glued to the underside of a flat aluminum frame, was clipped down over the substrate, and the substrate loaded into the evaporator.

Gold (99.999% pure) was deposited on the substrate using an electron beam evaporator at a rate 5 Å/s in a system with a background pressure of about 1×10^{-6} torr. Afterwards, the mesh needed only to be removed by removing the clips. Any dust particles would hopefully only affect the areas between the squares where the mesh may have been in contact with the substrate. The gold and its interfaces should have been clean. The samples were loaded into the transmission electron microscope immediately upon unloading from the evaporator. The temperature of the sample was gradually increased until holes formed or the film edge started to recede.

Summary

The receding edge of a thin film can be most effectively studied *in situ*, in a TEM equipped with a heating stage. This study can be accomplished using a membrane created prior to deposition of the gold as a substrate for the thin film. This means that the gold deposition is the last step in the preparation of the sample, minimizing the handling and, therefore, contamination of the sample. Patterning is accomplished by evaporation through a mesh. This method also requires minimum handling of the gold film. The film should

thus be as clean as a high vacuum deposition system and the purity of the gold source allow.

Chapter 4:

RESULTS OF MICROSCOPY

Preliminary examination of continuous gold films on silicon dioxide substrates showed that the morphology of the growing void is not as simple as described in Chapter 1. The movements of the edges of thin films in the process of agglomeration were observed using hot stage TEM. A typical progression was recorded on video tape. The sequential pictures in this chapter were taken from the video tape, as stills, for detailed study. The moving front of the film was also photographed for some special structures by lowering the temperature and freezing in the motion. Observations were also made using scanning electron microscopy (SEM) and optical microscopy of thicker films. The TEM and SEM results show the time evolution of material distribution. It will be shown that contrary to the simple models described in the literature, the film edge becomes unstable and develops a morphology determined by the local film thickness.

Material Redistribution

Optical microscopy, SEM and TEM show that, as the edge recedes, thicker areas develop in the film edge. Figure 4.1.a) is an SEM photograph of a void edge in profile showing accumulation at the edge. Figure 4.1.b) is a still TEM photograph of a void at the stage where there are many grains along its periphery. Thickened areas, such as those marked with an x, appear to be darker, overall, in the photograph. The edge deposit is not continuous or evenly distributed. It extends about one edge grain deep into the film which is about 2000 Å: a distance much greater than the thickness of the film: 250 Å. The built up areas are isolated or separated by areas which appear similar to the rest of the film,

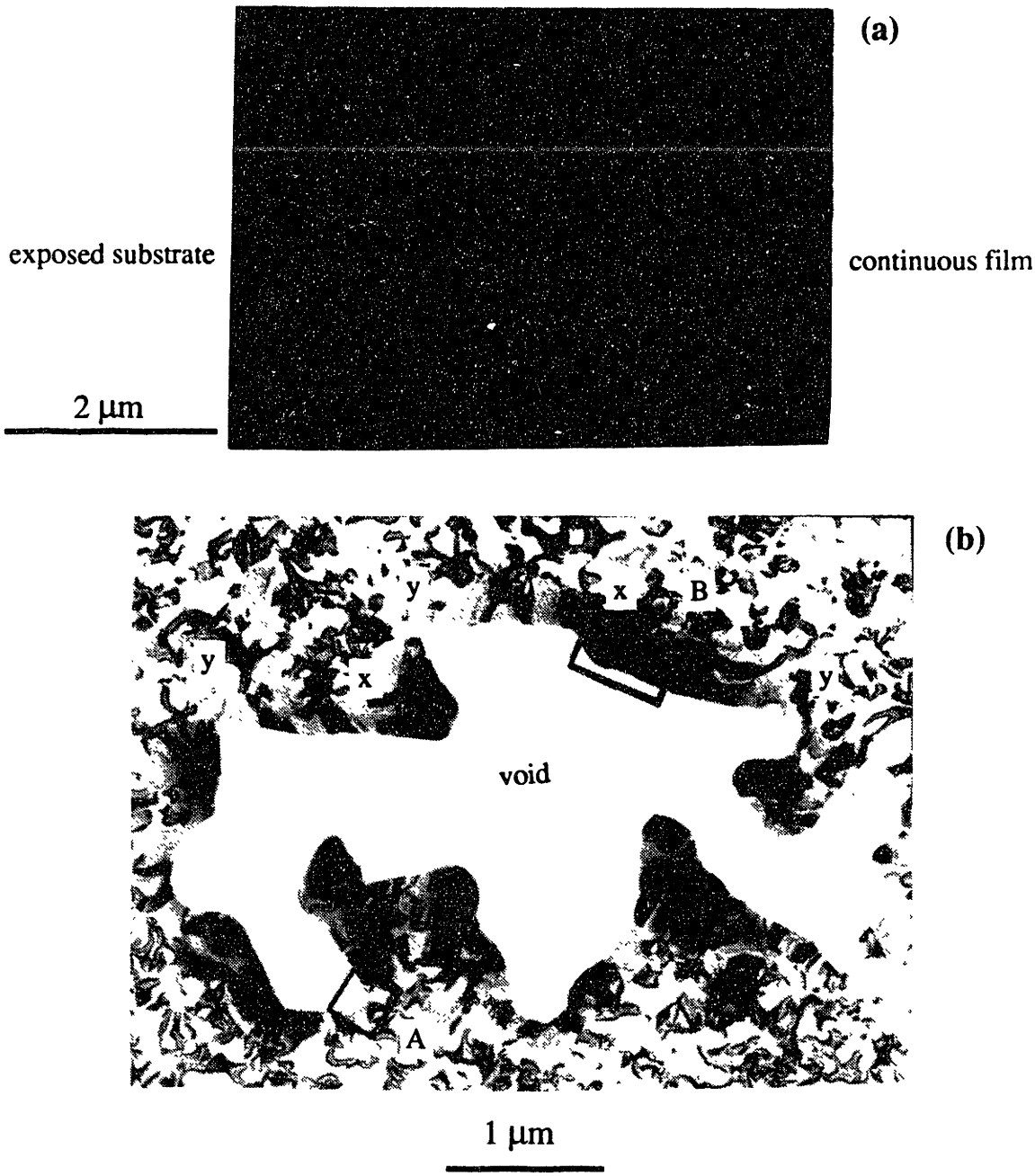

Figure 4.1: The material removed from the substrate as the film edge recedes causes the edge of the film to thicken. This is observed using several microscopic techniques. Here, TEM and SEM examples are shown.
a) SEM photograph of a hole edge in profile. (gold film on fused silica, 800 Å thick, annealed in air at 850°C for 110 minutes)
b) TEM photograph of void. Thicker areas appear darker than thinner areas in transmission. Thicker areas are indicated with an x, thin areas with a y. (gold film on silicon nitride membrane, 250 Å thick, annealed in the TEM heating stage by gradually increasing the temperature)

examples are marked with a y in figure 4.1.b). Here the void protrudes into the film, rather then vice versa. This indicates that the fastest moving part of the the edge is that part where build-up is minimum.

Because material accumulates unevenly at a receding edge, and the edge recedes fastest in the thinnest areas of the film, the void develops arms and channels that move around any built up areas. This is illustrated in the sequence drawn in figure 4.2. Figure 4.2.a) is the initial shape of the void arm where the film is thick to the right and above the void. Figure 4.2.b) is a superimposed trace of several pictures taken from the video tape showing the progression of the void. The void arm moves slightly up then proceeds sharply to the left where the film is thin. Figure 4.2c) is a photograph showing the final shape of the void arm in the sequence.

Interactions Among Void Cusps and Grain Boundaries

The overall appearance of the void, at the stage where there are many grains along its periphery, is facetted. The facets often have their cusps at grain boundaries and it might be expected that the meandering aspect of the void arms is due to the fact that the cusps follow grain boundaries. However, the facetting along the edge of the void does not necessarily coincide with grain boundaries. From a closer view of area A in figure 4.1.b) shown in figure 4.3, we can see that one or two void cusps can be included within the grain as the void propagates. The grain boundaries that intersect the void edge may move toward the void cusps because grain boundary area may be reduced in this way. The final result is that the cusps end up at least temporarily at the grain boundaries.

In figure 4.1.b), the thick areas contain only larger grains (Fig.4.4, area B). This occurs because grain boundaries parallel to the void edge where the film is thick can reduce their area by moving into thin areas of the film and are thus pushed ahead of the receding, thickening edge. This is illustrated in figure 4.5. Figure 4.5.a) is the photograph of the initial extent of the void in the sequence of figure 4.5b). In figure 4.5.b), the adjacent

Figure 4.2. Exerpt from the video tape showing a void propagating preferentially through the thin areas of the film to the left and not to the right and above where the film is thicker.

a) initial morphology,

b) superimposed outlines of void edge as it propagates, time increasing in the direction of the arrow; the numbers indicate stills from the video tape representing the morphology after the following time intervals since the point in time in (a):

1: t = 0,

2: t = 4 seconds,

3: t = 8 seconds,

4: t = 10 seconds,

6: t = 14 seconds;

c) morphology at the end of the sequence.

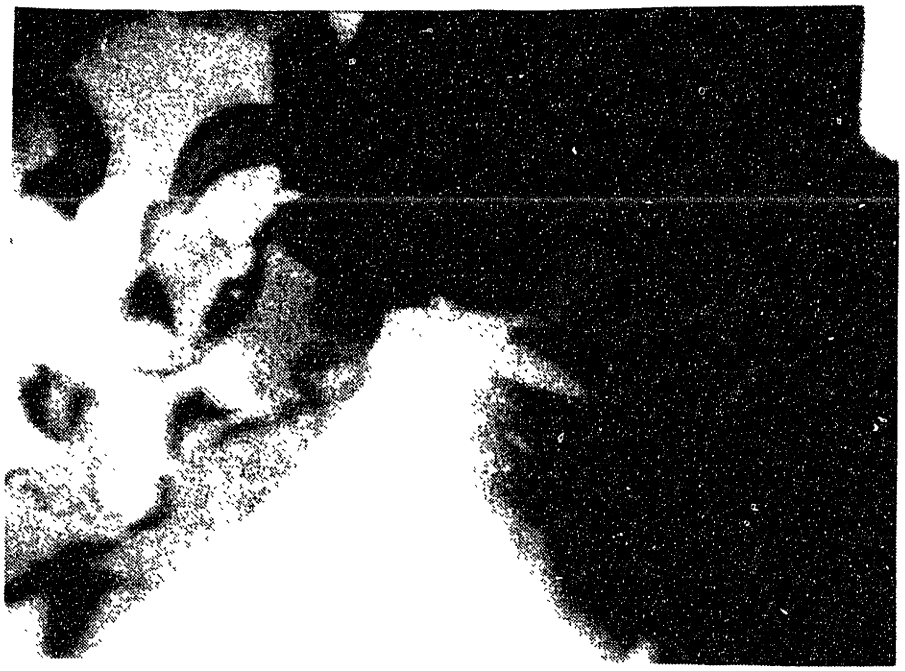

(a)

0.1 μm

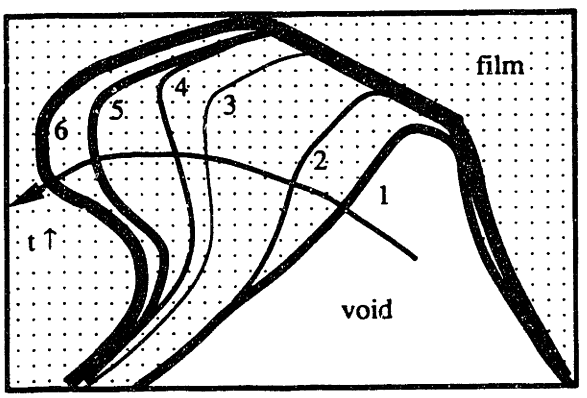

(b)

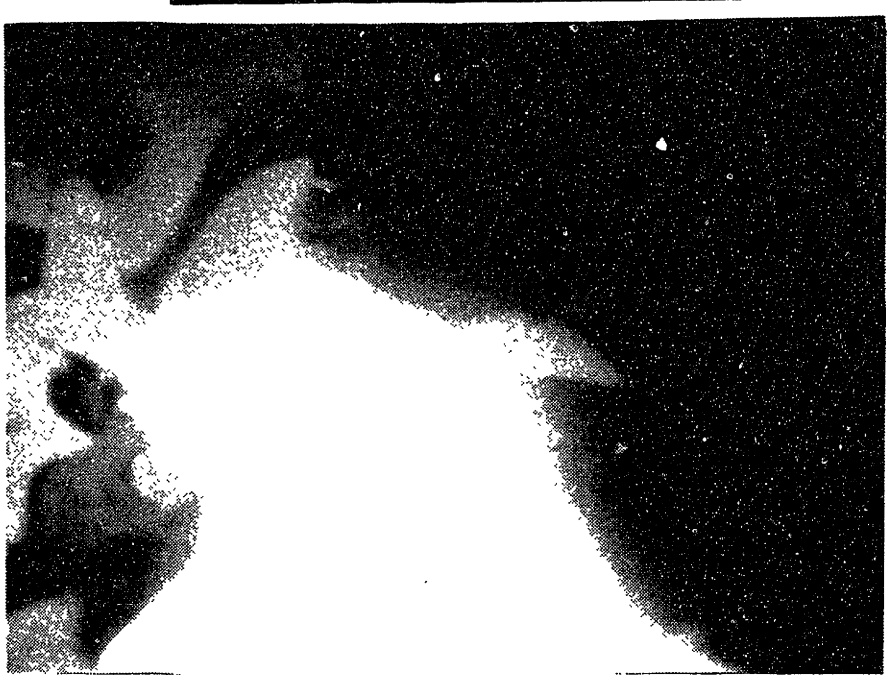

(c)

0.1 μm

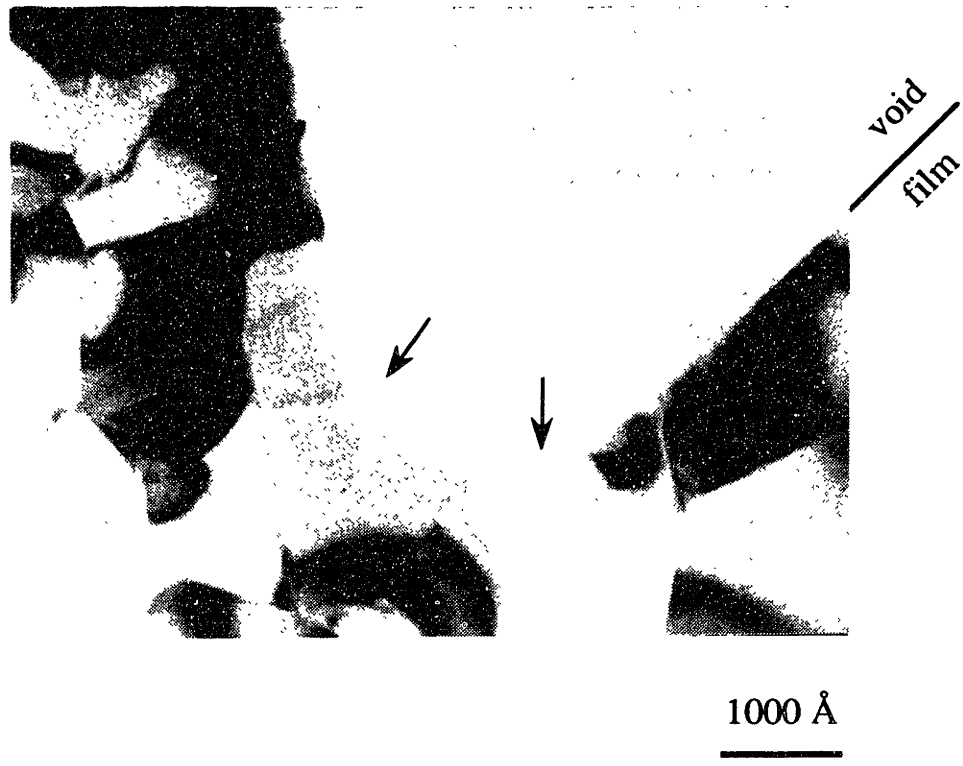

Figure 4.3: An example of a void cusp (facet) within a grain. This is a close-up picture of part of the void in figure 4.1b).

Figure 4.4: This is a magnified view of the thickened part of the edge in figure 4.1b), areaB. It illustrates that thick areas at the edges contain only large grains.

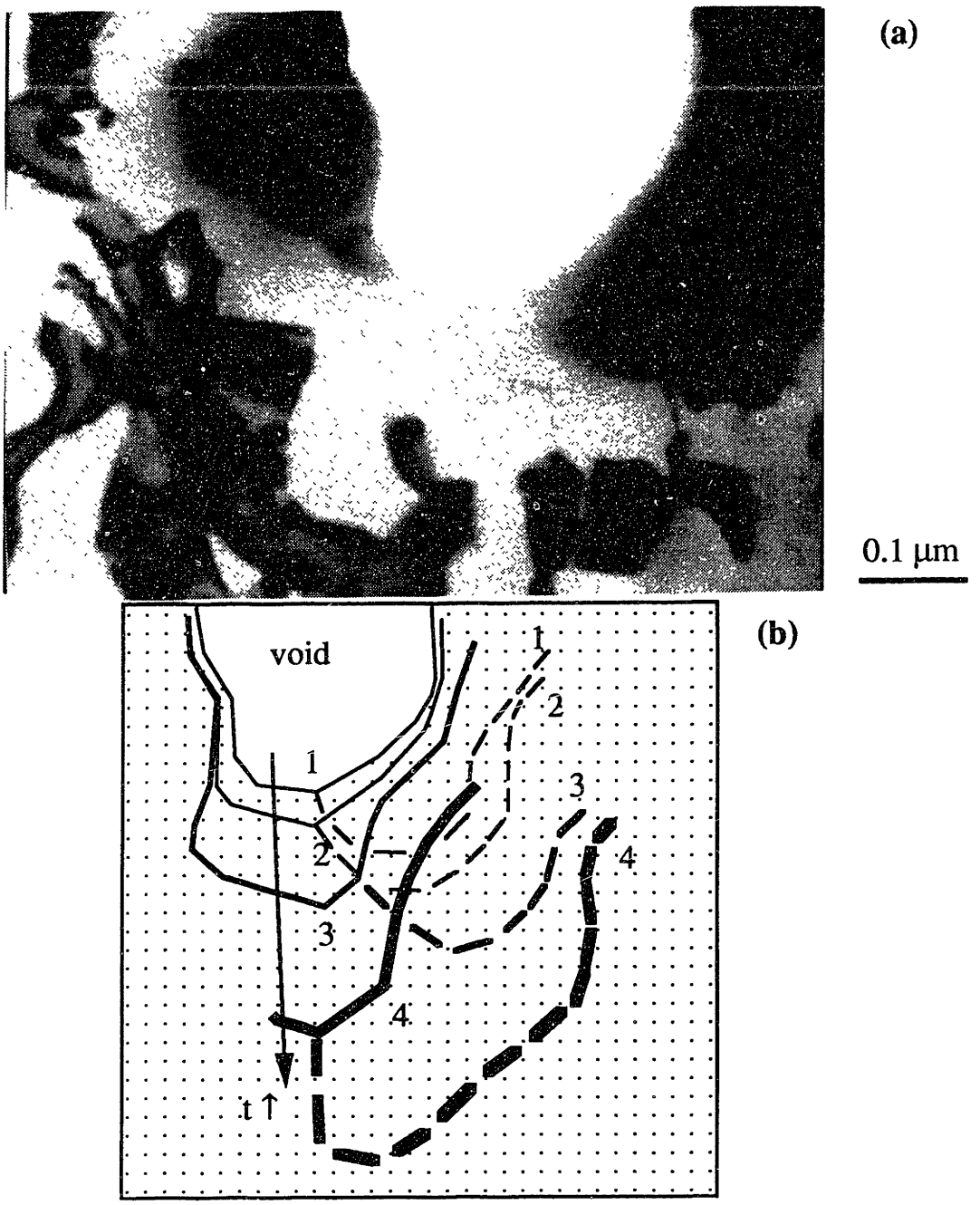

Figure 4.5: Excerpt from the video tape showing that the grain boundary is pushed ahead of the thick edge: a) initial morphology, b) position of film edge (solid line) and grain boundary (dashed line) as a function of time.

grain is consumed by a thick grain in the last step of the sequence, eliminating a grain boundary perpendicular to the edge. This results in only large grains in the thickened edge.

A great deal of activity among the grain boundaries related to the *approaching* of the void was observed. In particular, it was observed that a grain boundary parallel to the approaching void in the thin area of the void disappears suddenly once the grain becomes narrow due to the advancement of the void. Figure 4.6 shows schematically how grain structure might responds to the growth of the void. The grain boundaries in an equilibrium structure meet at triple junction at 120° angles. The grain boundary area for boundaries intersecting the void edge in grain *a* can be reduced if they intersect the edge at 90°. But, as the edge grain becomes very thin, these conditions produce a large curvature in the grain boundaries which causes the grain boundary parallel to the edge in the thin grain, *a*, to move into the void.

The Morphology of the Receding Edge

Mullins[3] showed that a planar solid surface subjected to a sinusoidal fluctuation will flatten under the influence of capillarity. In the case of a terminated film, a similar argument can be applied to the edge itself. If the edge does not thicken, then the problem should be a two dimensional analogue of Mullins' analysis and the same stability conclusions may be drawn: the fluctuation will disappear into the edge. In a successful theory, therefore, a *three dimensional picture of the edge, ie build-up at the edge, must be presented* to explain the instability.

Figure 4.1.b) shows that build-up of material along the edge is not uniform and so thick and thin areas develop. Once the edge starts to thicken, it becomes susceptible to a Rayleigh instability. Consider the geometry of Brandon and Bradshaw in figure 2.5, where the edge of the film is rounded with a radius of curvature that increases with time. This configuration approaches a half cylinder as the radius increases. This half cylinder would be subject to the same fluctuations as a whole cylinder of the same radius. The fluctuation

Figure 4.6. A schematic drawing of how grain structure responds to the approaching void edge.

a) Grain boundaries intersect the film edge at 90°. The dotted lines indicate the honeycomb shape of the grain boundary structure in the places where the grain boundary deviates from it. This creates curvature in the grain boundary.

b) As the edge recedes, the edge grain *a* becomes very small and the curvature becomes very large.

c) The curvature can no longer be supported and the edge grain *a* is consumed by grain *b*. This is accomplished by migration of the *a-b* grain boundary into the void.

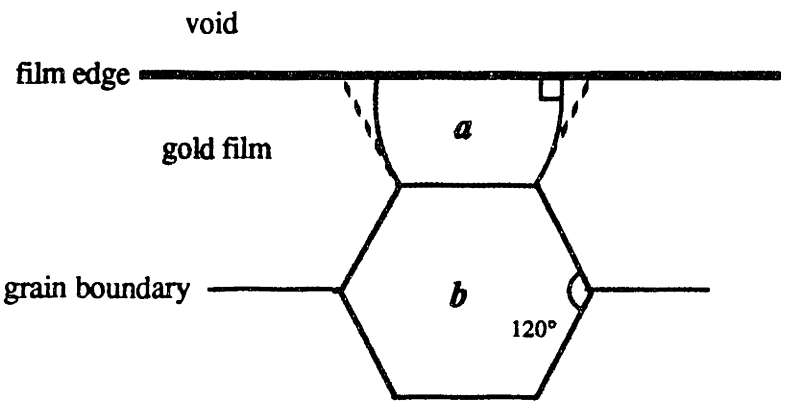

(a)

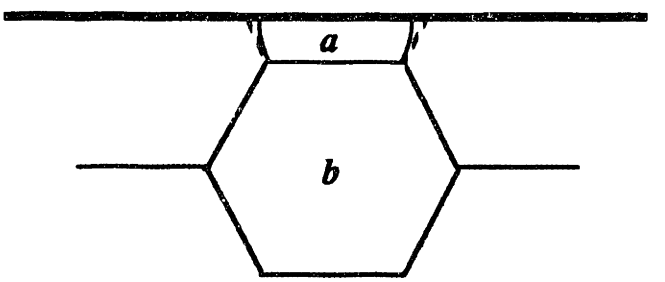

(b)

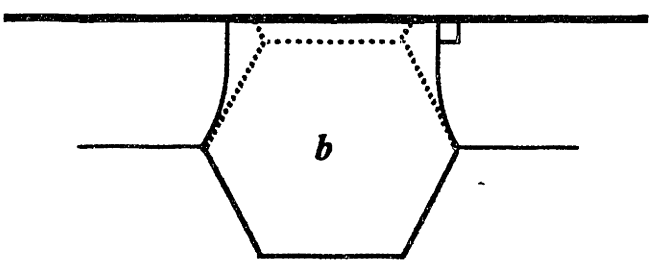

(c)

that leads to decomposition produces gradients in curvature along the length while the perimeter of the cylinder remains circular in cross-section. Since diffusion occurs in response to these gradients, material will be displaced along the length of the cylinder. Then, since, as a result, parts of the half cylinder become thinner, the void edge may penetrate through these into the rest of the film. Therefore, Brandon and Bradshaw's configuration could eventually become unstable along its length, developing thicker and thinner areas and leading to a cellular morphology (Fig.4.7).

The edge, modeled as a cylinder, would tend to evolve into a row of beads. In practice, this kind of break down appears to govern the morphology rather than the penetration behind the thickened edge that Srolovitz and Safran[6] predict. Figures 4.7 and 4.8 are SEM micrographs. Figure 4.7 illustrates the cell-like nature of the receding edge of a gold line and figure 4.8 the morphology of the beaded film. Because of the instability in the thickened edge, the build-up around the edge of the void is not evenly distributed and the void can penetrate the thickened edge. The void propagates much faster through the thinner areas. This is similar to the phenomenon of constitutional undercooling where solute builds up at a solidification front. A fluctuation that penetrates the build up protrudes into liquid that is undercooled and therefore grows faster than the rest of the front. Solidification thus occurs in a cellular or dendritic pattern. In figure 4.9 the receding front is drawn schematically based on this analog.

Void arms impinge to form islands. If this happens while the film is relatively thin, there is movement of grain boundaries in the neck region and the region of the bead. In figure 4.10, a grain boundary in the bead near the neck region migrates into the base of the bead. The neck first thins then disappears completely into the two masses it connected. The grains inside the bead disappear as the bead becomes thicker (darker) and smaller in plan view. Eventually, the bead will consist of only one grain. When void arms impinge, part of the edge breaks away from the film, it may be one grain or often a strand of grains that are subject to further agglomeration as the beads at the ends grow large and eventually

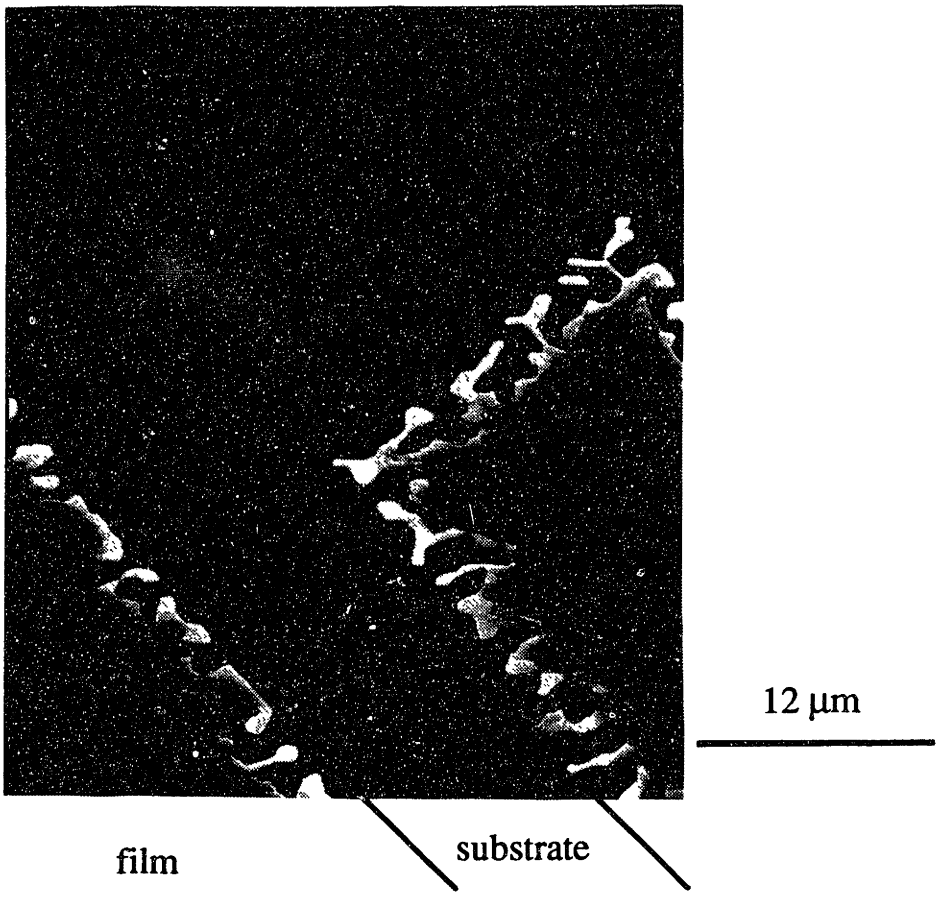

Figure 4.7: SEM photograph illustrating the cell-like morphology of the receding void edge. (patterned gold film on fused silica, 500 Å thick, annealed in air at 675°C for 20 minutes)

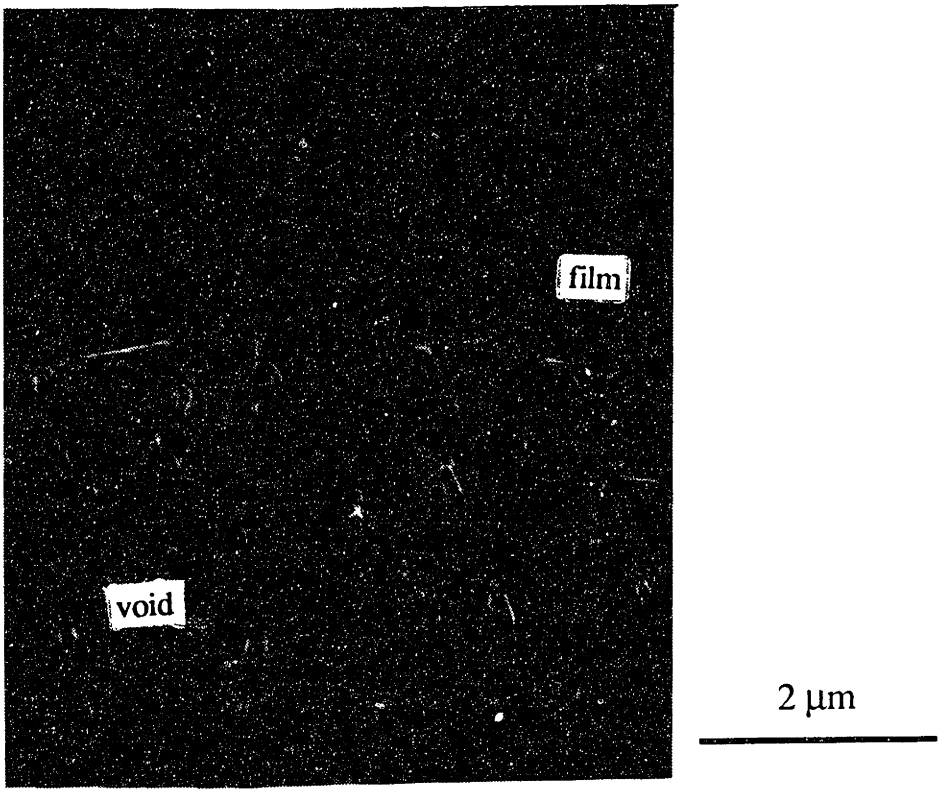

Figure 4.8: SEM photograph of the morphology of a beaded area of continuous film. (same sample as 4.1a)

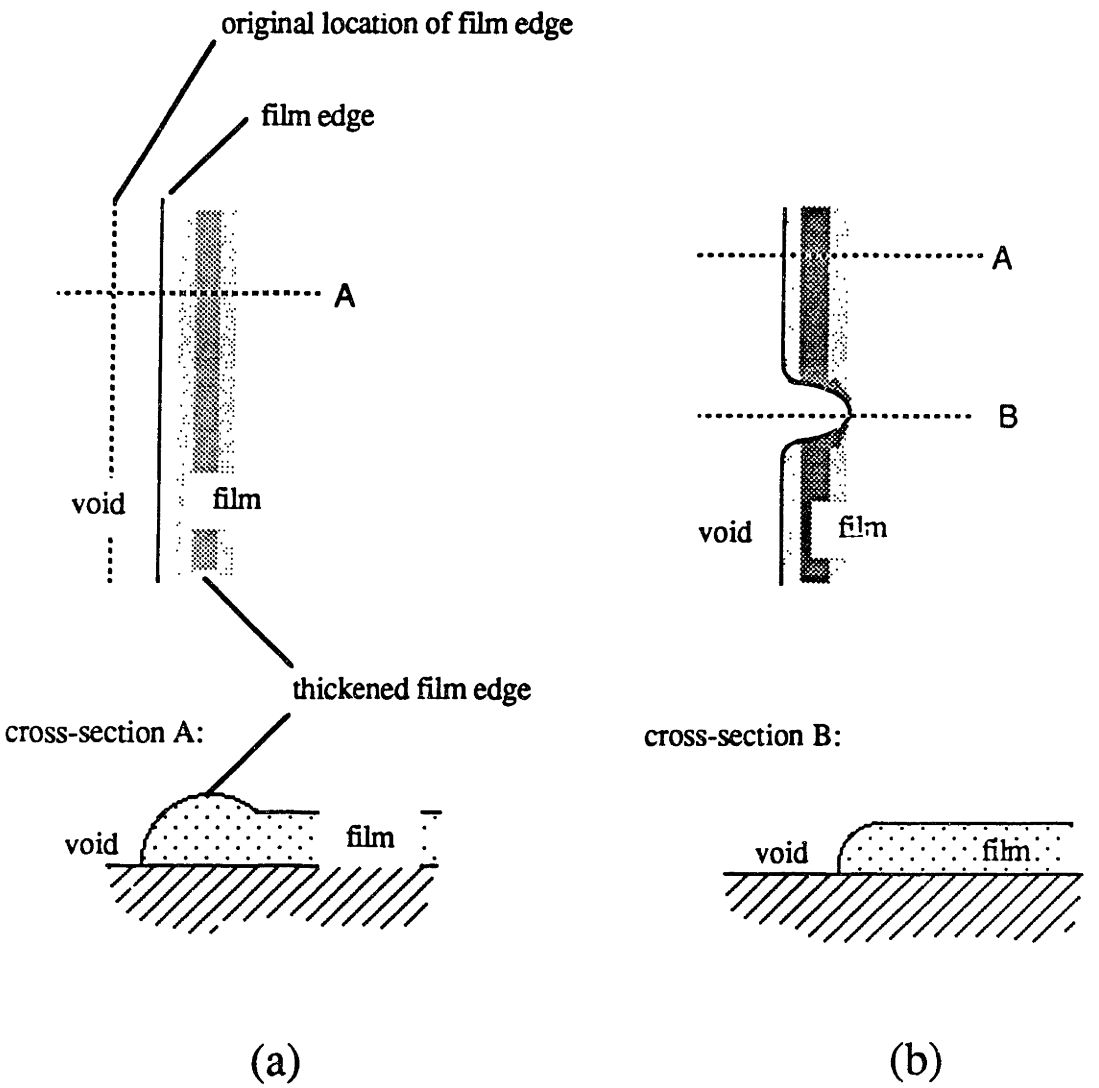

Figure 4.9. Schematic of cell or dendrite formation in analogy to constitutional undercooling where mass build-up at the edge corresponds to solute build-up at the interface.

a) The edge thickens as it recedes, slowing down,

b) a fluctuation penetrates the build-up and thus grows faster than the rest of the edge.

continued next page..

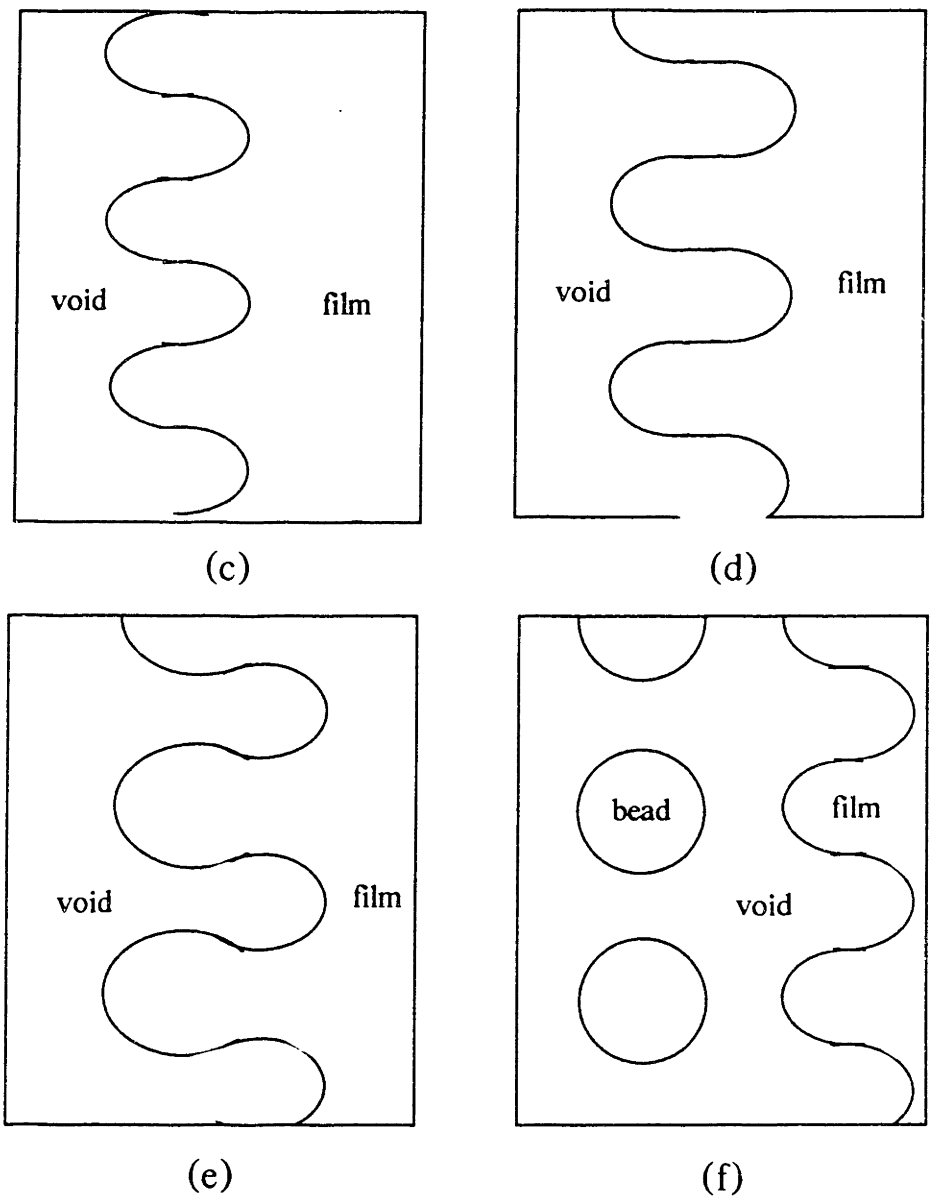

Figure 4.9. continued....

c) A series of fluctuations which have penetrated the thickened edge.

d) Fingers of gold are left behind by the growing void cells.

e) The fingers lower their surface area by rounding off and thickening.

f) The thickened tip detaches forming a bead.

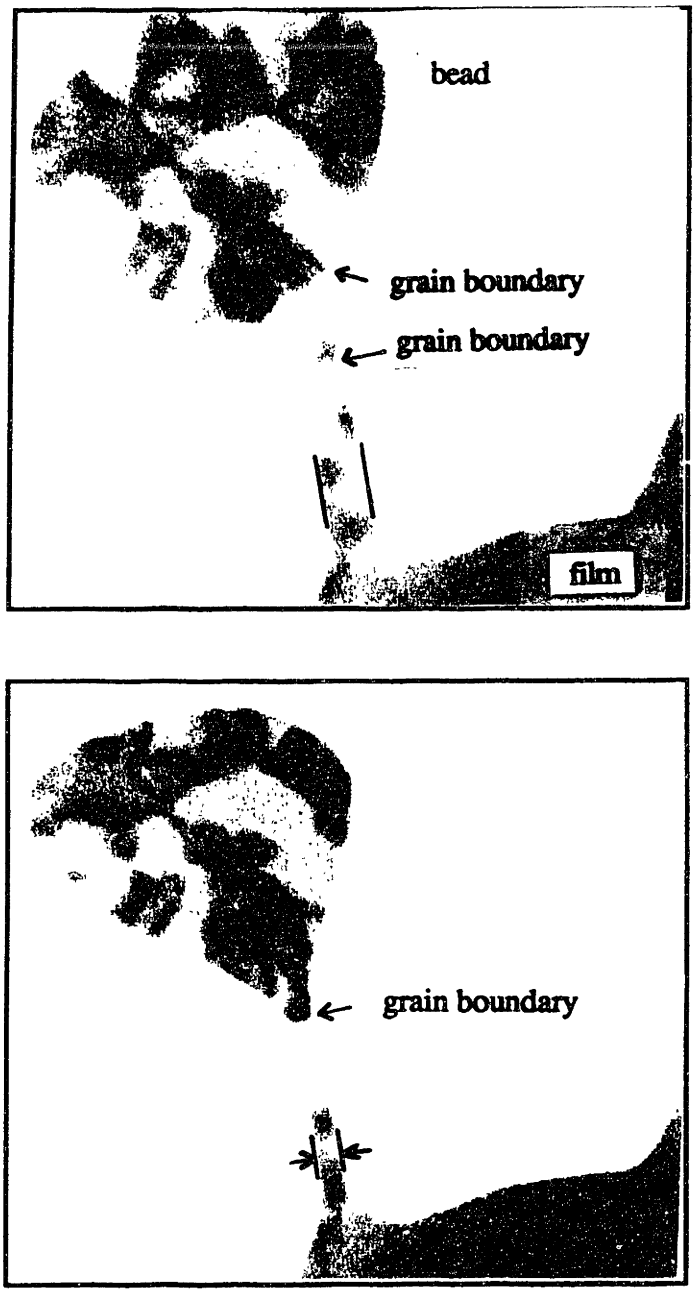

Figure 4.10: Separation of a bead from the film edge as two void dendrites impinge: (b) is at a later time than (a). The neck eventually fails by thinning and separating approximately half way between the film and the bead.

dissociate from the main strand, or as the whole strand becomes subject to decomposition similar to Rayleigh's infinite cylinder[1]. Figure 4.11 is a high magnification image, showing void propagation through thin areas of film. The thickened edge in this case is separating as a strand.

Summary

The microstructure of the polycrystalline film is affected by the advancement of the void. Grain boundaries are pushed ahead of a thicker build up or absorbed into the void in thin areas. The advancement of the void removes grain area and causes growth of grains in the film ahead. Thus the grains that comprise the beads are much larger than the grains in the original film, and the spacing between the beads is much larger than the size of the original grains.

Figure 4.9 illustrates, schematically, the process of agglomeration. When a hole is created in a thin film, the edges of the hole retract and the material removed from the area of the hole is deposited around the periphery, thickening the edges as they recede. The thickened edge becomes unstable and certain parts of the edge become thicker than others. Therefore, as the hole continues to expand it is able to penetrate into the thin areas of the film and since it propagates much faster there, a non-planar front develops.

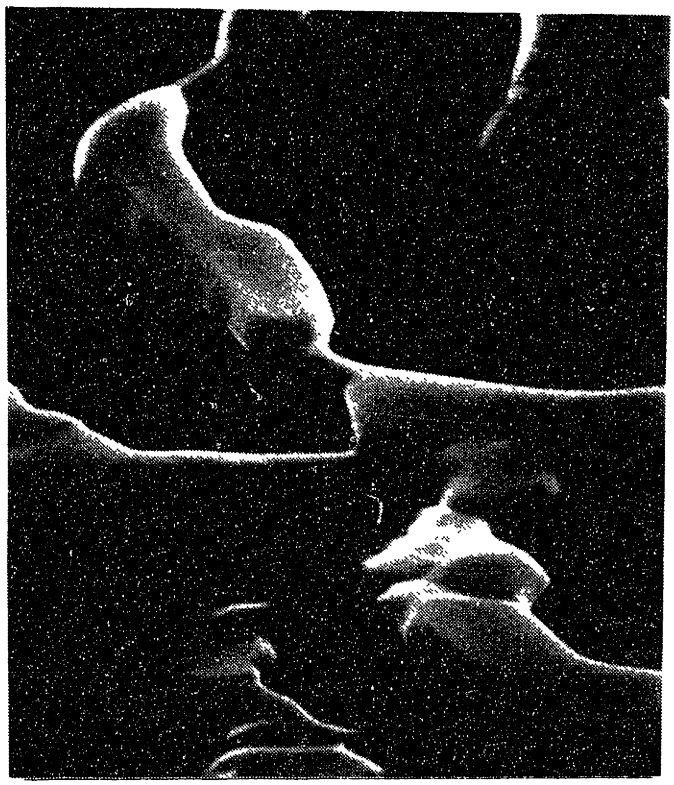

Figure 4.11: SEM photograph of the progression of the void through thin areas and around built-up areas (same sample as 4.1a).

Chapter 5:

MODELING OF AGGLOMERATION

Agglomeration in a continuous film occurs through the formation and growth of holes. In chapter 4, the growth of holes was investigated using continuous and patterned films. While holes in a continuous film must first form, then grow, holes in a patterned film, with its artificially created edges, are already present and patterned films agglomerate immediately on heating.

Previous models[6,7] described the edge deposit as uniform around the periphery of the hole. The resulting rate equations give the growth velocity as decreasing with time. Although the film edges studied in chapter 4 did thicken as they receded, the deposit was not uniform. The void penetrated the thickened edge by means of thickness instabilities in the edge and propagated by spreading through the thin areas of the film.

The purpose of this chapter is to model the agglomeration process by first deriving an expression for the rate of growth only (which is equivalent to describing agglomeration in patterned films), incorporating the fact that holes propagate through the thin areas of the film. Next an expression for the transformation curve of a continuous film is derived, which includes a nucleation component as well as a growth component. It will be seen that the growth rate in this model is not time dependent as previous models indicate.

Modeling of hole growth.

In order to analyze void propagation in real systems,we have modified the Brandon-Bradshaw model (Fig.5.1a). The receding front was modeled as level with the film thickness (Fig.5.1b), taking into account the fact that the void propagates only through

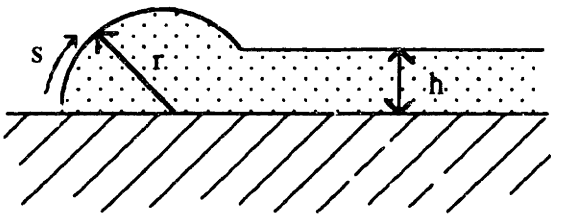

(a)

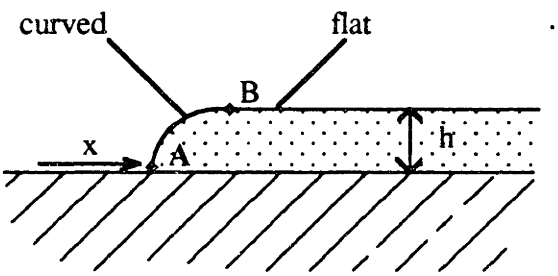

(b)

Figure 5.1. Profiles of the receding edge according to: a) Brandon and Bradshaw[7] and b) the proposed model based on observations in this thesis.

thin areas of the film. This implies that the material removed from the substrate is deposited at stationary areas to either side of the moving tip of the void. Such a situation is drawn schematically in figure 5.2. Figure 5.2b) is a close-up of one of the cells penetrating the line edge in 5.2a). The cross-hatched areas indicate thicker areas in the film, the dotted areas indicate film of as deposited thickness and the void tip, the moving part of the void, points towards the thinnest areas of the film. The atoms move from the area of the tip to the built-up areas to either side of the moving tip. To simplify the geometry, it will be assumed that the in-plane curvature, r', is large compared with the curvature of the cross-section, h, so that the maximum driving force for diffusion will be the difference in chemical potential between the small curvature of the tip cross-section and the flat plane beyond. The atoms would, therefore, move from the curved edge, A, to the flat plane, B. Following the example of Brandon and Bradshaw, the equation governing the time, temperature and thickness dependence of the process is derived below.

The driving force for agglomeration is the reduction of surface area. The model assumes morphological changes are due to surface diffusion driven by surface energy minimization. Figure 5.2 shows the agglomeration of gold patterned into a wide line. The thickness of the film is "h" and the edge of the film can be described by a quarter circle of radius equal to the film thickness. As in the Brandon and Bradshaw model[7], the edge is modeled as contacting the substrate at a ninety degree angle. Atoms will flow from this curved surface so that the net flux away from the edge is[4]:

$$j_s = - \frac{D_s}{kT} \frac{\partial \mu}{\partial s} \nu , \qquad (16)$$

where D_S is the surface diffusivity, $\partial\mu/\partial s$, is the chemical potential change over an element of arc length and ν is the surface concentration of atoms. The chemical potential change between the curved portion, with edge curvature h and an in-plane curvature r', and a flat

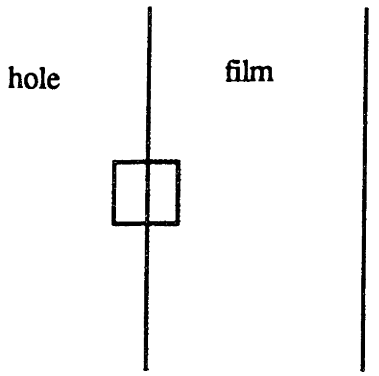

(a)

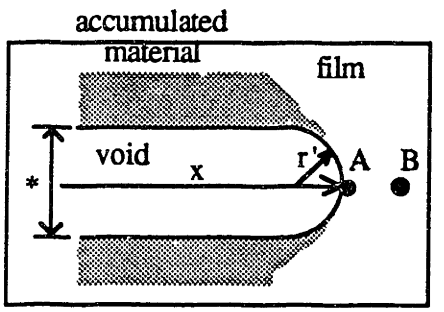

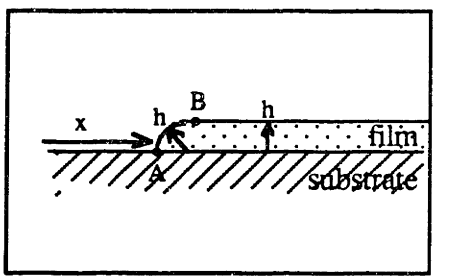

(b) (c)

Figure 5.2. The film in (a) is patterned into a line. An area of the line edge, schematically represented as a square in (a), is represented in top view in (b) and in cross-section through the moving tip in (c). The distance indicated by * represents approximately the moving length of the tip. This distance times the number of moving tips represents the length of the moving interface.

area of the film, which has a radius of curvature of infinity, is given by the following expression:

$$\mu_A - \mu_B = -\Omega \gamma_s \left(\frac{1}{h} - \frac{1}{r'} \right), \qquad (17)$$

where Ω is the atomic volume and γ_S is the surface tension. It will be shown in chapter 7, that r' can be very large compared with h, so that

$$\Delta\mu = -\frac{\Omega \gamma_s}{h} \qquad r' >> h . \qquad (18)$$

The distance along the surface over which this change occurs, Δs, is in our case $\pi h/2$. The rate of volume transfer of material is equal to the surface flux times the total length of advancing interface, *l*, (which correspond approximately to 2r' times the number of cells) times the atomic volume:

$$\frac{dV}{dt} = j_s \, l \, \Omega . \qquad (19)$$

The velocity of the interface dx/dt is then equal to the rate of volume transfer divided by the length of the moving front and by the thickness of the film:

$$\frac{dx}{dt} = \frac{\Delta x}{\Delta t} = \frac{1}{hl} \frac{\Delta V}{\Delta t} . \qquad (20)$$

Substituting for $\Delta V/\Delta t$ in equation 20 using equation 19:

$$\frac{\Delta x}{\Delta t} = \frac{j_s}{h} \Omega . \qquad (21)$$

Equation 16 can be substituted in 21 for j_S with $\Delta\mu$ given by equation 18 and Δs given by $\pi h/2$:

$$\frac{\Delta x}{\Delta t} = \frac{D_s}{kT} \frac{\Omega^2 \gamma_s}{\pi} \frac{2}{h^3} . \qquad (22)$$

The material removed from the substrate is assumed eventually to be deposited to each side of the moving tip. Equation 22 is independent of tip width because, it was assumed, atoms diffuse first in the direction of the moving tip. In this case, the tip width is not included in

the derivation. Once at point B in figure 5.1, however, the diffusing atom must move out of the way of the moving tip fast enough to prevent accumulation. In this second step, if the tip width becomes significantly large it may have to be taken into account in the analysis.

In terms of the kinetic parameters, $\Delta x/\Delta t$ is expressed as follows:

$$\frac{\Delta x}{\Delta t} = 2\frac{D_o \gamma_s \Omega^2}{kT\pi h^3} \exp\left(-\frac{Q_s}{kT}\right) \tag{23}$$

$$= \beta \frac{\exp\left(-\frac{Q_s}{kT}\right)}{kT\, h^3}, \tag{24}$$

where β in equation 19 is equal to $2D_o\gamma_s\Omega^2/\pi$. This equation predicts that the *growth rate* of the hole is *constant* in time. The slope of an Arrhenius plot of $(\Delta x/\Delta t)\, kT$ versus $1/kT$ would be Q_s, the activation energy of diffusion, and the intercept can be used to determine D_o, the pre-exponential of diffusivity. Equation 24 also gives the thickness dependence of the rate as inverse cubic.

Defining a transformation curve for agglomeration

In a continuous film, a hole must first form. The above result can be applied to continuous films, by accounting for the nucleation of holes in the film. The number of voids forming in a time interval between τ and $d\tau$ is $I^a A^c d\tau$, where A^c is the area of unagglomerated film and I^a is the nucleation frequency per unit area of film. Each of these voids will have an area at time t of:

$$a_\tau = \pi \quad u^2 (t - \tau)^2 , \tag{25}$$

where u is the velocity of the interface and equal to $\Delta x/\Delta t$ in equation 24. If there is no impingement and all the nuclei form at once, then the total area of the transformed region is:

$$A_{void} = N_h\, A\, \pi \left(u\ (t-\tau)\right)^2, \qquad N_h \neq f(T) \tag{26}$$

where τ is the time when nucleation occurred, N_h is the number of nuclei per unit area and A is the total area of the film. Figure 5.3a) shows that the resulting curve of fraction transformed vs time is a flat line at zero and a parabola with its minimum at time τ. As long as the holes are large enough to develop the steady state morphology of cells or dendrites, u can be substituted with $\Delta x/\Delta t$. Considering only the part of the curve after nucleation and substituting for u with $\Delta x/\Delta t$ from equation 24, the area exposed varies with temperature and film thickness as follows:

$$A_{void} = N_h\, A\, \pi \frac{\beta^2 \exp\left\{\frac{2Q_s}{kT}\right\}}{(kT)^2 h^6}\ (t-\tau)^2. \tag{27}$$

If N_h is not a function of either time or temperature, this would be the time dependence observed. The activation energy can then be determined from an Arrhenius plot of $(kT)^2 A_{void}$ vs 1/kT, for a fixed time since nucleation, the slope of which will be $-2Q_s$, or by extracting $\Delta x/\Delta t$ and plotting these values on an Arrhenius plot to obtain the effective activation energy .

If impingement of the voids takes place, equation 26 and 27 overestimate the area transformed. This overestimated area is called extended area. The ratio of void area change, dA^v, to extended area change, dA^v_{ex}, is given by the ratio of untransformed area, $A-A^v$, to total area, A[16]:

$$dA^v = \left(1 - \frac{A^v}{A}\right) dA^v_{ex}, \tag{28}$$

where the superscript v refers to area occupied by voids. Equation 28 can be integrated to solve for the extended area,

$$A^v_{ex} = -A \ln\left(1 - \frac{A^v}{A}\right). \tag{29}$$

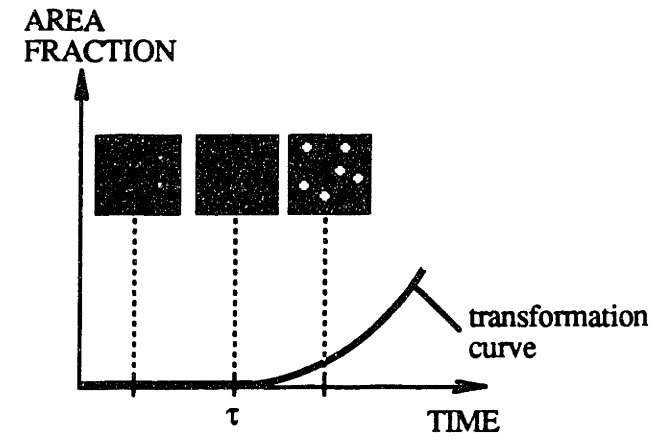

(a)

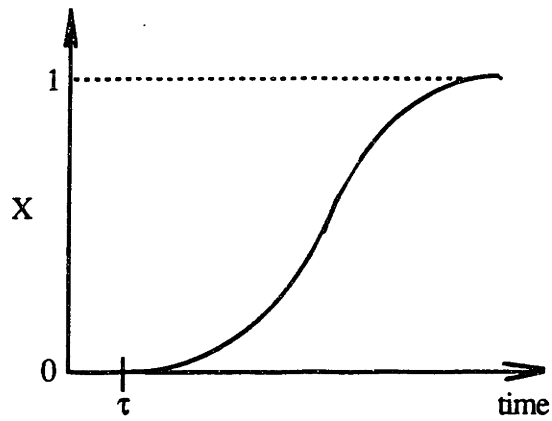

(b)

Figure 5.3. Transformation curve for a continuous film where all the nuclei formed at time τ.

a) parabolic time dependence of area transformed

b) X vs t for a parabolic time dependence in ln(1-X).

Substituting for the extended area, A_{void}, of equation 27 with the expression for extended area of equation 29, gives:

$$-\ln\ (1 - X) = N_h\ \pi\ u^2\ (t - \tau)^2, \qquad (30)$$

where X is the area fraction transformed, A^v/A.This defines a transformation curve, X vs t, which levels off as the available film area is consumed by voids, and the transformation stops (Fig.5.3b).

Summary

The thickness and temperature dependence of the agglomeration front velocity for the agglomeration of lines, $\Delta x/\Delta t$, can be described by equation 24, with β equal to $D_o\Omega^2\gamma_s\nu/\pi$. Contrary to previous models, this equation predicts a velocity which is independent of time. The agglomeration of thin, continuous films is treated as a two dimensional phase transformation with a constant growth velocity, $\Delta x/\Delta t$. If all the nucleation occurs at once, then the transformation curve, X vs t, is defined by equation 30. Since patterned films require only the growth component to agglomerate, the transformation of patterned films can be used to determine $\Delta x/\Delta t$, and from this the diffusivity. The transformation of continuous films can also be used to determine $\Delta x/\Delta t$ if the nucleation frequency is known, or to determine the nucleation frequency if $\Delta x/\Delta t$ is known. The latter may be used to determine the type of defect responsible for the nucleation of holes.

Chapter 6:

LASER ASSISTED MEASUREMENT OF FRACTION TRANSFORMED

Experimental Objectives

The objective of this thesis is to study the kinetics of the process of agglomeration. This can be accomplished experimentally by measuring the rate of the transformation from a continuous film to beads or islands, as a function of temperature and film thickness. Measurement of a rate as a function of temperature allows calculation of an effective activation energy and diffusion coefficient.

Since the process of agglomeration is made up of nucleation of voids and growth of voids, two different configurations were used. In order to study the growth component only, and thus directly obtain the transformation rate, gold patterned into "wide" lines was used. "Wide" is used to describe a stripe many times wider than its thickness, so that it simulates a continuous film with voids already formed in it (at the edges) and approximates certain structures in electronic devices. The agglomeration front then moves in from the edges of the stripe. Information about nucleation of voids can be obtained by then studying fully continuous films.

The substrate is heated in a furnace with a controlled atmosphere in the chamber. The rates were measured *in situ* using transmitted laser light through the sample to measure the area of transformed film. In Chapter 7, this transmittance vs time measurement is translated into the rate of void propagation derived in terms of time, film thickness and material constants in equation 24.

Experimental Design: Laser assisted, *in situ* measurement of transformation curves.

Description of the laser system

A low power laser is used as a probe to detect agglomeration in the films. Figure 6.1 shows schematically the equipment used. The laser light is directed at the sample from below and picked up by a detector located above the sample: the upper detector. The intensity of light at the upper detector is related to the amount of substrate not covered by gold, which can in turn be related to the amount of gold film that has not agglomerated. This apparatus permits continuous monitoring of the transformation during the annealing of the sample in the furnace.

The laser signal was generated by a Jodon HN-7 laser at a wavelength of 3.39 μm. The gold films used were nearly opaque to this wavelength. The laser beam was chopped (turned on and off periodically by blocking the light from passing through the chamber) to distinguish it from similar radiation being emitted by the furnace at the annealing temperatures. The laser light is focused by a calcium-fluoride lens onto a lead-selenide detector. The detector produces current in response to the light, so that the change in transmitted laser light intensity is transformed to a decrease in the voltage drop across a resistor. This voltage drop, in the form of a square wave due to the chopping of the beam, is sampled by the computer and the amplitude recorded against time.

The annealing chamber is constructed using seals and valves designed for vacuua of 10^{-6} torr. The chamber is opened using a 1.5 inch o-ring seal. The thermocouples are 1/16 inch in diameter to fit through two 1/16 inch bored-through CAJON fittings. The thermocouples extend to almost the bottom of the cold chamber as they expand when heated. They are in contact with the chamber wall near the point in the furnace where the sample is located. The sample rests on the floor of the chamber, which is located at the center of the furnace. One thermocouple is connected to the temperature controller and the other to the data acquisition board in the computer. The computer records the intensity of

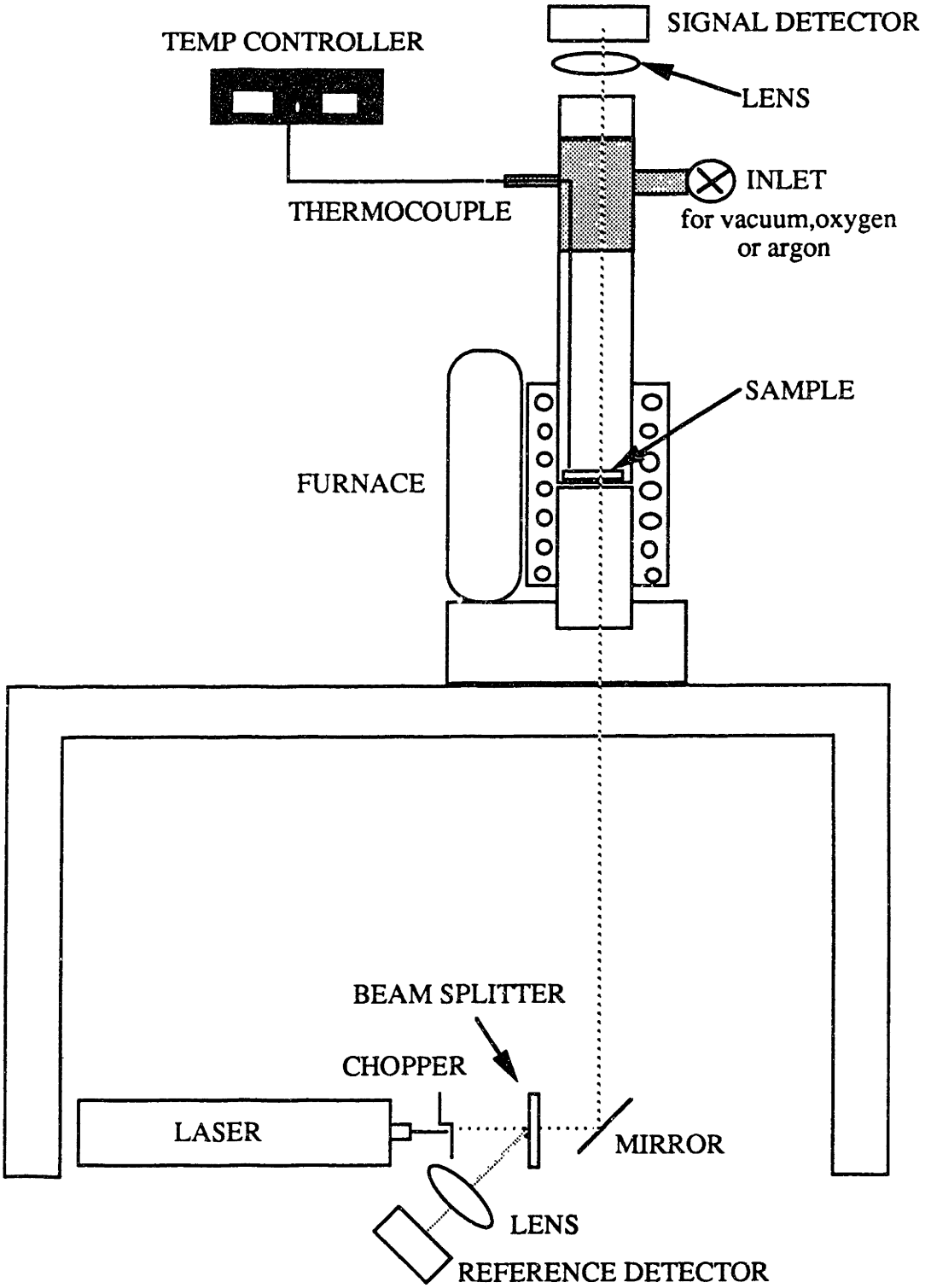

Figure 6.1: Schematic drawing of experimental set-up for laser probe experiments.

the laser light transmitted through the sample and the temperature of the chamber. The cold junction compensation signal in the terminal board is also recorded.

Sample output from laser experiments

Figure 6.2 is a sample trace from an experiment with a continuous film. When a continuous film is used, the initial signal at the detector is very small but finite and increases as the film develops voids and as the voids grow. The traces level off when the whole film is agglomerated and rise again at a much slower rate as the fragments left behind by the void front break-up further. The photographs illustrate the state of agglomeration associated with a particular value of the laser signal.

If wide lines are used, figure 6.3, the signal at the beginning includes light shining through between the lines and the increase represents, in most cases simply the recession of the gold front. The front starts at each edge of the line and the two fronts meet in the center of the line. Because the front is invariably uneven, the termination of the transformation is not sharp, but tapers gradually as the two uneven fronts impinge.

In some cases, the total change in laser signal for the complete transformation is different from a preceding experiment. This is due to changes in total laser power from one experiment to the next. These changes are related to differences in beam alignment. The measured agglomeration rates (proportional to the slopes on the laser trace) are corrected for this amount using the total change in signal between unagglomerated and fully agglomerated film. The rates can then be compared. The scaling of signals from continuous films will be described in Chapter 7.

Substrate requirements

The laser experiments were carried out in transmission, which required the substrate to be transparent to the wavelength chosen at the temperatures used. The fused silica substrates used were polished mechanically so that the surface had the fewest and shallowest scratches possible on one side. A rougher polish caused agglomeration to start at scratches in the substrate and the results for continuous films were not reproducible from

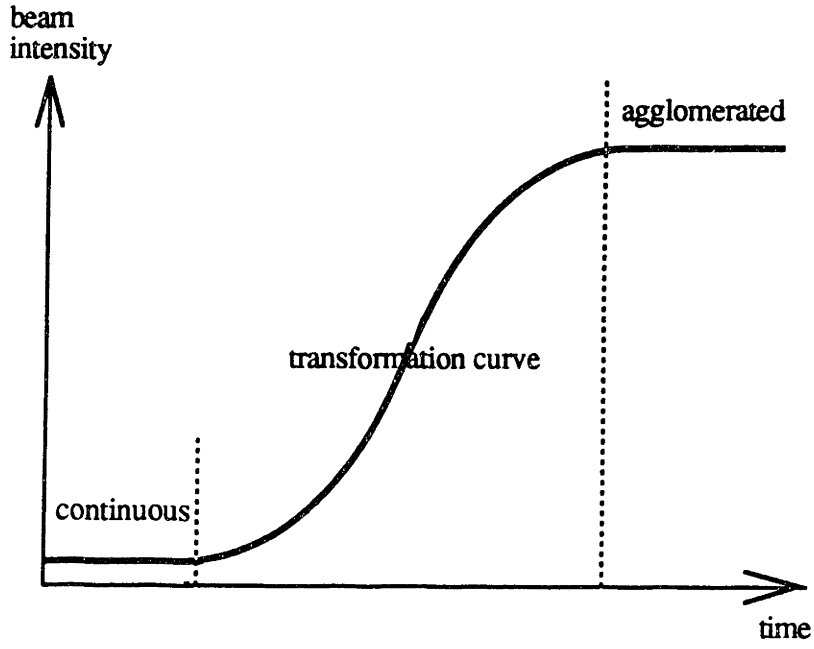

(a)

Figure 6.2: Sample trace from continuous film:
a) ideal trace and
b) actual trace including photographs at three different stages of agglomeration (next page).

continued...

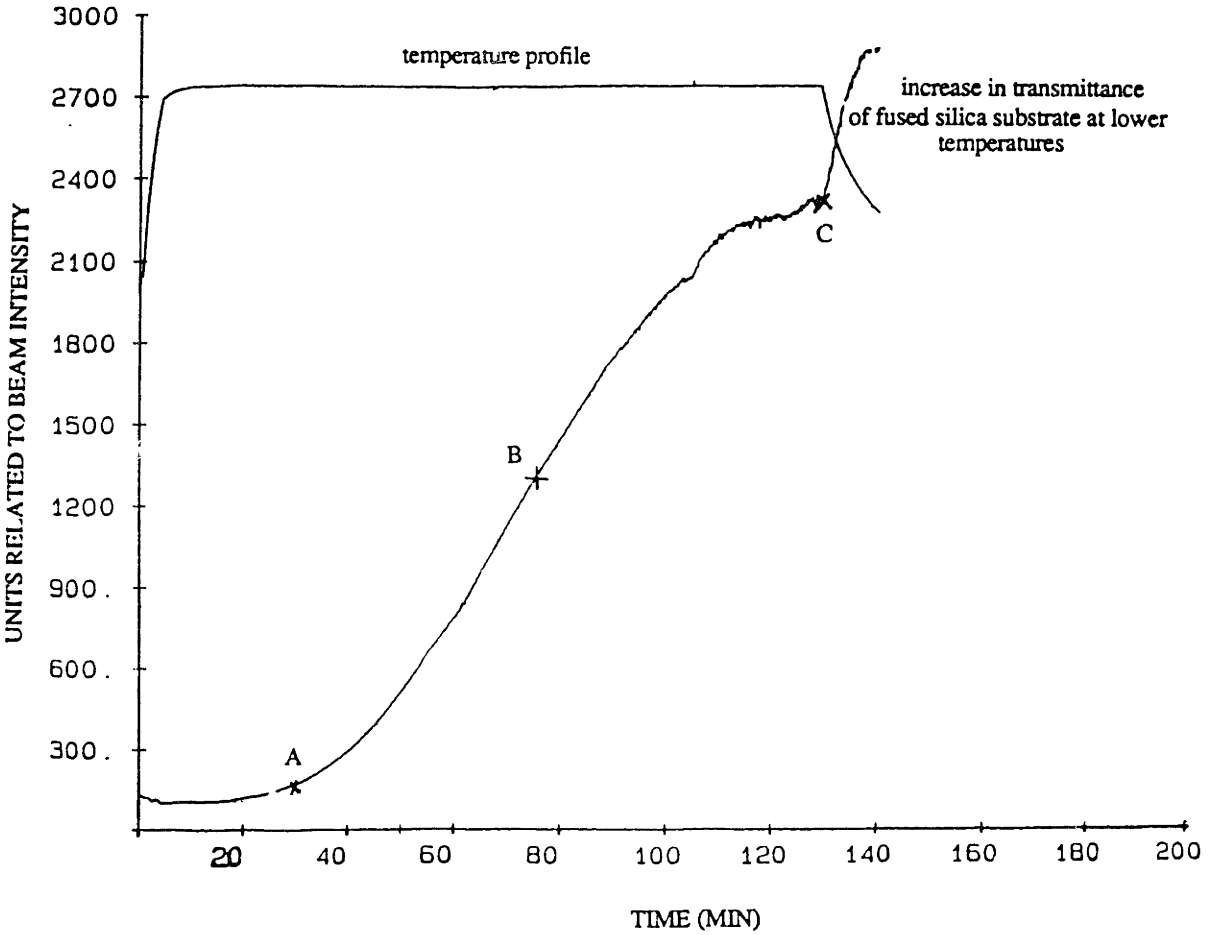
3000
2700
2400
2100
1800
1500
1200
900 .
600 .
300 .
UNITS RELATED TO BEAM INTENSITY
temperature profile
increase in transmittance
of fused silica substrate at lower
temperatures
A
B
C
20
40
60
80
100
120
140
160
180
200
TIME (MIN)

A

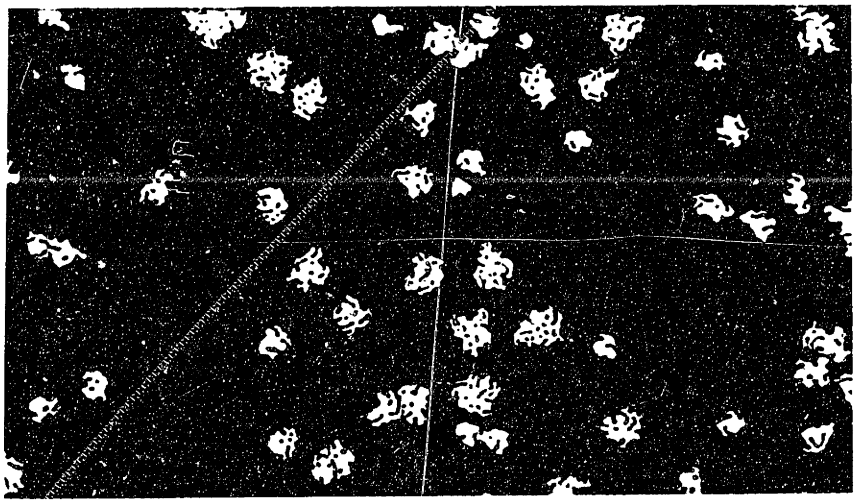

100 µm

B

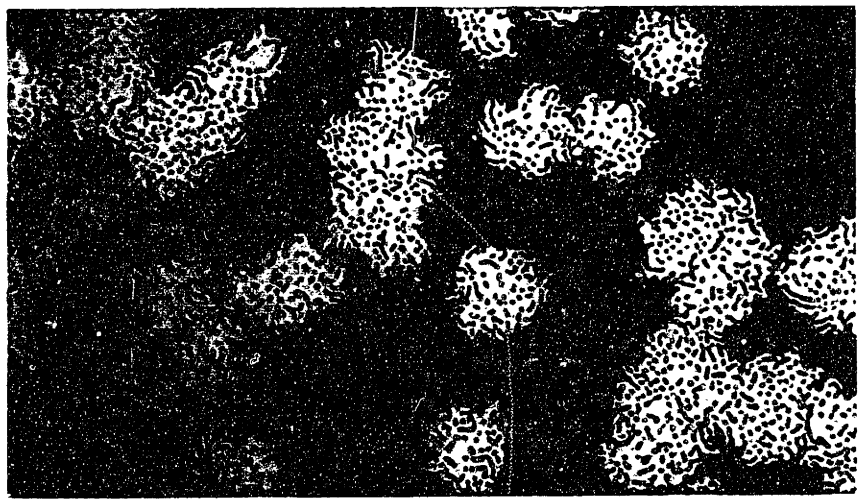

100 µm

C

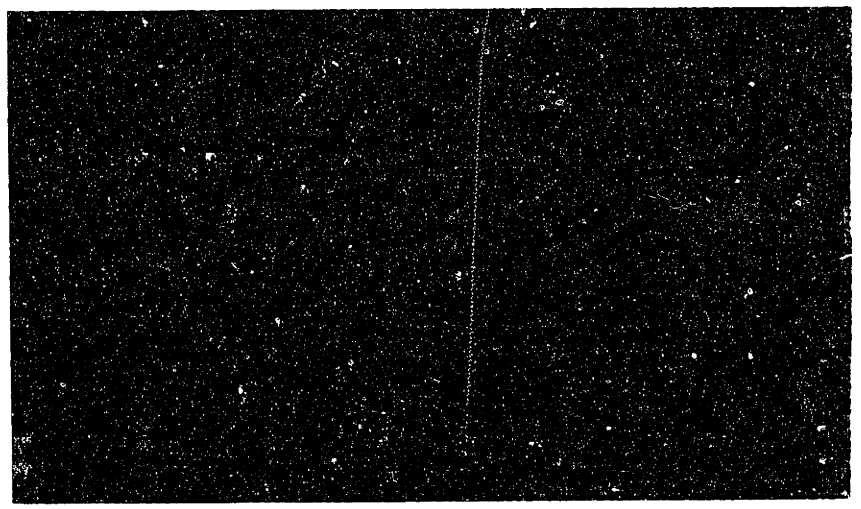

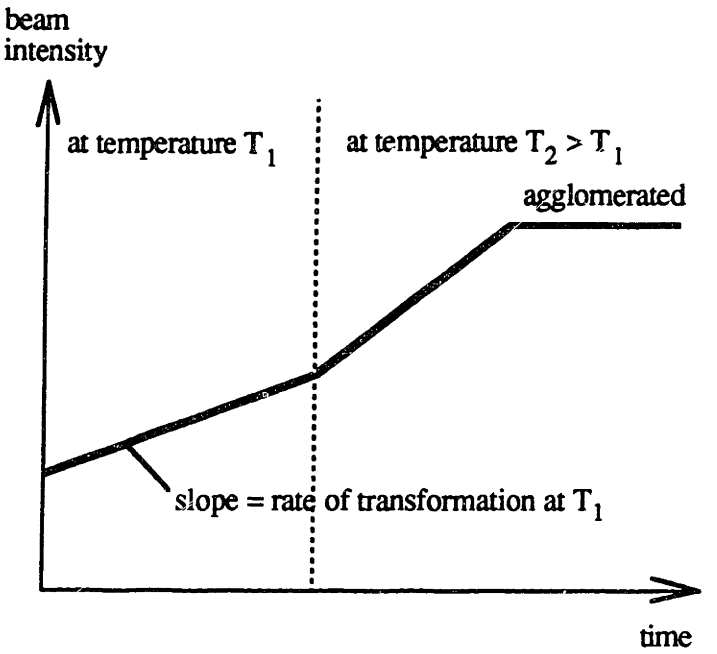

(a)

Figure 6.3. Sample trace from agglomerating lines:
a) ideal, illustrating the change of slope associated with a change in temperature,
b) photographs, in transmission, of lines at different stages of agglomeration:

A: before annealing,

B: partially agglomerated,

C: fully agglomerated.

continued...

A

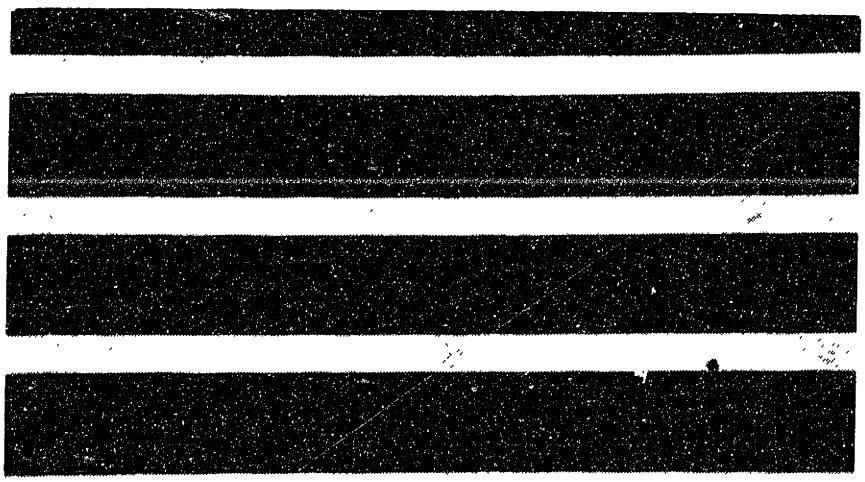

50 µm

B

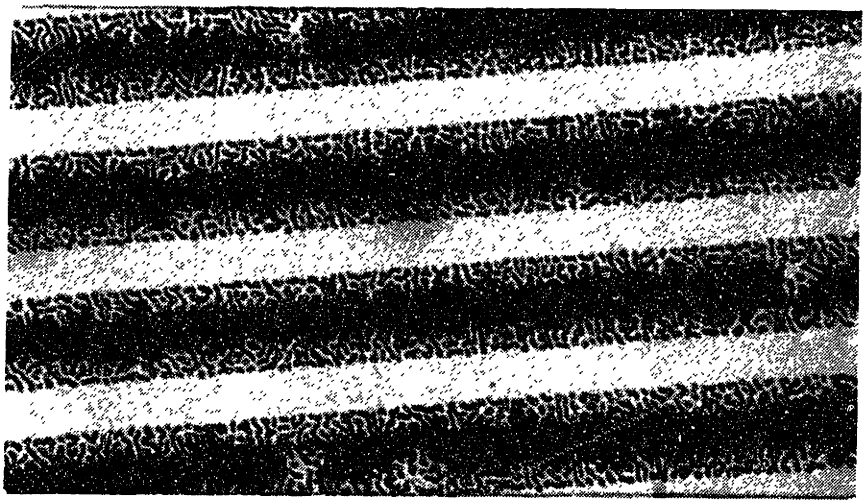

50 µm

C

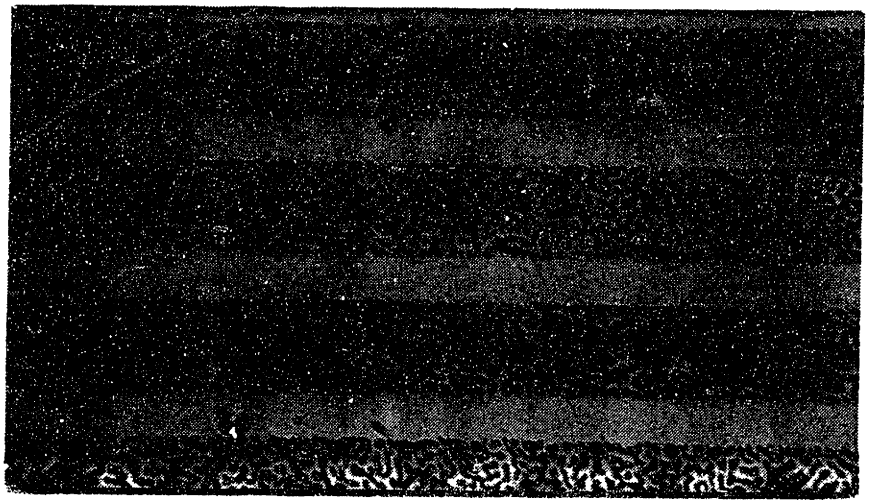

sample to sample. The finer polish produced a more uniform agglomeration pattern but discrepancies in number of nuclei were still present. The discrepancies were taken into account in the interpretation of the results, as will be described in Chapter 7.

Experimental procedure

After the films were deposited, testing of all the samples was initiated and completed in as short a time as possible to minimize contamination of the surface. For the same reason, the samples were annealed at temperatures chosen to keep the experiments short. While one sample was being annealed, the others were kept either in a vacuum desiccator or in sample trays. It was assumed that the desiccator reduced contamination from the air, but repeated pumping and venting might be expected to cause particles to circulate in the desiccator more vigorously than in a closed tray and might then lead to possible surface damage. The trays, on the other hand, being teflon, produce contamination of their own at a very slow rate. The difference between samples from the two storage facilities was negligible, compared with samples which had been stored for long periods, such as several days, where a large effect was seen (Fig.6.4).

Substrates annealed after being stored for several days in clean room air (Fig.6.4b), developed bulges in the film which appeared to be quite smooth. Since the observed roughness of the annealed film is due to grain boundary grooving, the blistered part of the film would appear smooth if it consisted of very large grains. Small dark spots which might be holes could be seen on some of the blisters. There were also large grain areas adjacent to holes in the film which leads to the conclusion that they are blisters which developed a hole that opened up and allowed the bulge to collapse. These blisters were occasionally seen, using the optical microscope, in a freshly annealed film but they were much smaller and very few in number.

For experiments carried out in oxygen or argon, a small mechanical pump was used, prior to annealing, to repeatedly pump down and flush the chamber with argon. In both cases, the sample was brought to temperature in argon and pumped down again once

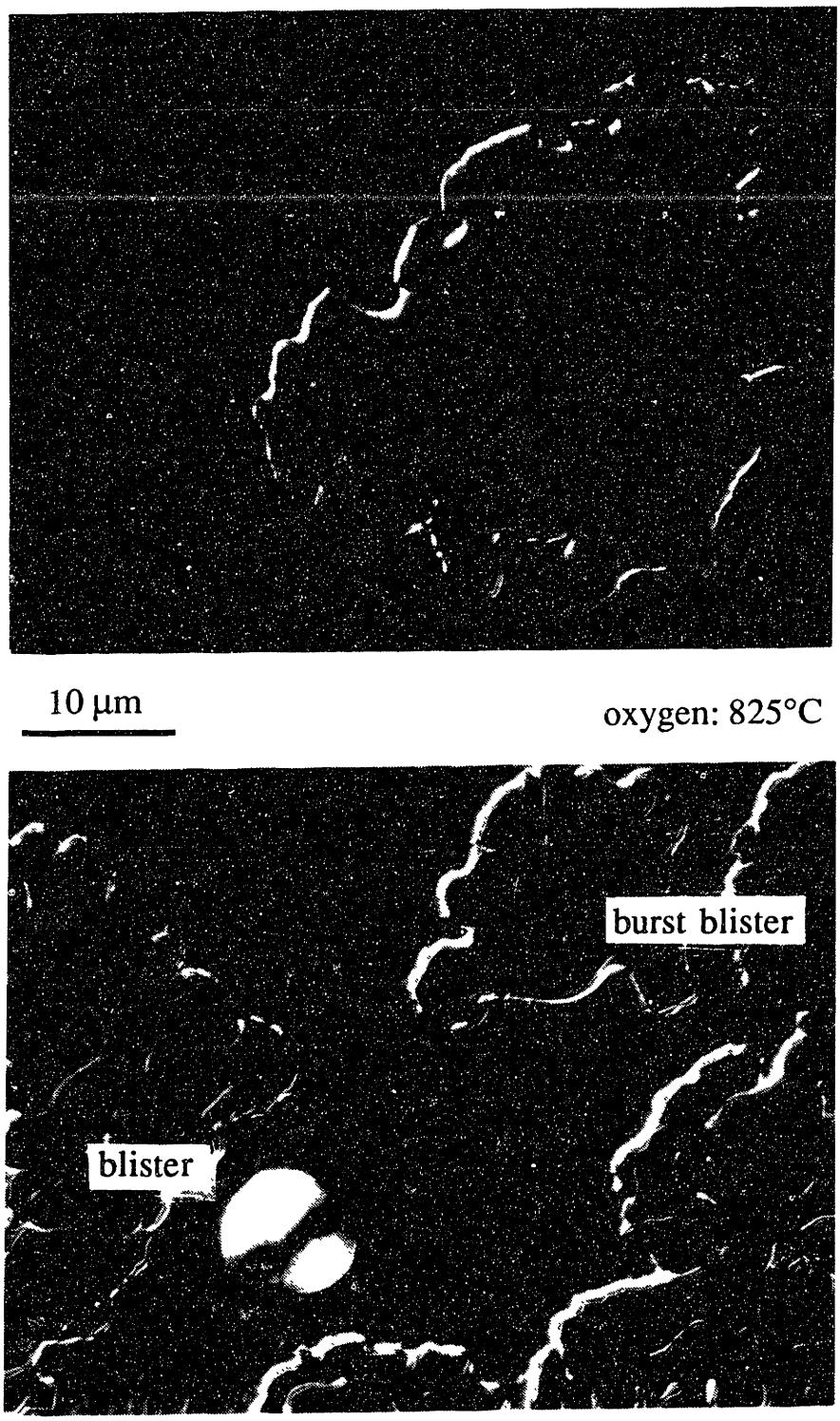

Figure 6.4: Photographs of continuous films partially agglomerated in oxygen at 825°C: a) within hours of gold deposition and b) after four days exposed to air in a class ten clean room.

the annealing temperature was reached. Then the chamber was backfilled with either oxygen or argon to one atmosphere. Figure 6.5 shows a trace from an experiment in which the patterned sample was first annealed in argon and then in oxygen.The transformation appears to be slower in argon than in oxygen and so heating in argon permits reaching higher temperatures before the film fully agglomerates. A bubbler in the gas line was used to maintain a constant positive pressure as the sample was heated, annealed and cooled.

Sample preparation

Substrate Cleanliness

The driving force for agglomeration is reduction of the surface and interface energy of the film and the expected mechanism for agglomeration is surface diffusion. Therefore, the samples were prepared and handled to minimize contamination at both the atmosphere-film interface and the film-substrate interface.

The substrates were prepared with a thorough cleaning. The cleaning of oxides has been thoroughly researched by the electronics industry where contamination must be controlled to control the properties of the devices produced. The fused silica wafers used for this study were cleaned by procedures developed to clean oxide substrates. They were placed in teflon boats and first placed in a beaker of detergent and hot de-ionized water. A silicon wafer with a thermal oxide was added to the boat. The beaker was then placed in a bath equipped with ultrasound for 15 minutes. The boat was removed and rinsed in hot de-ionized water. Next the boat was placed in a bath of 5:1:1 de-ionized water, ammonium hydroxide and hydrogen peroxide at 80°C for 20 minutes. The boat was rinsed again in hot de-ionized water and submerged in a bath of water de-ionized to a resistivity of 18 mega-ohm-cm, which also acts as a solvent, for at least 30 minutes or until the next step could be performed.

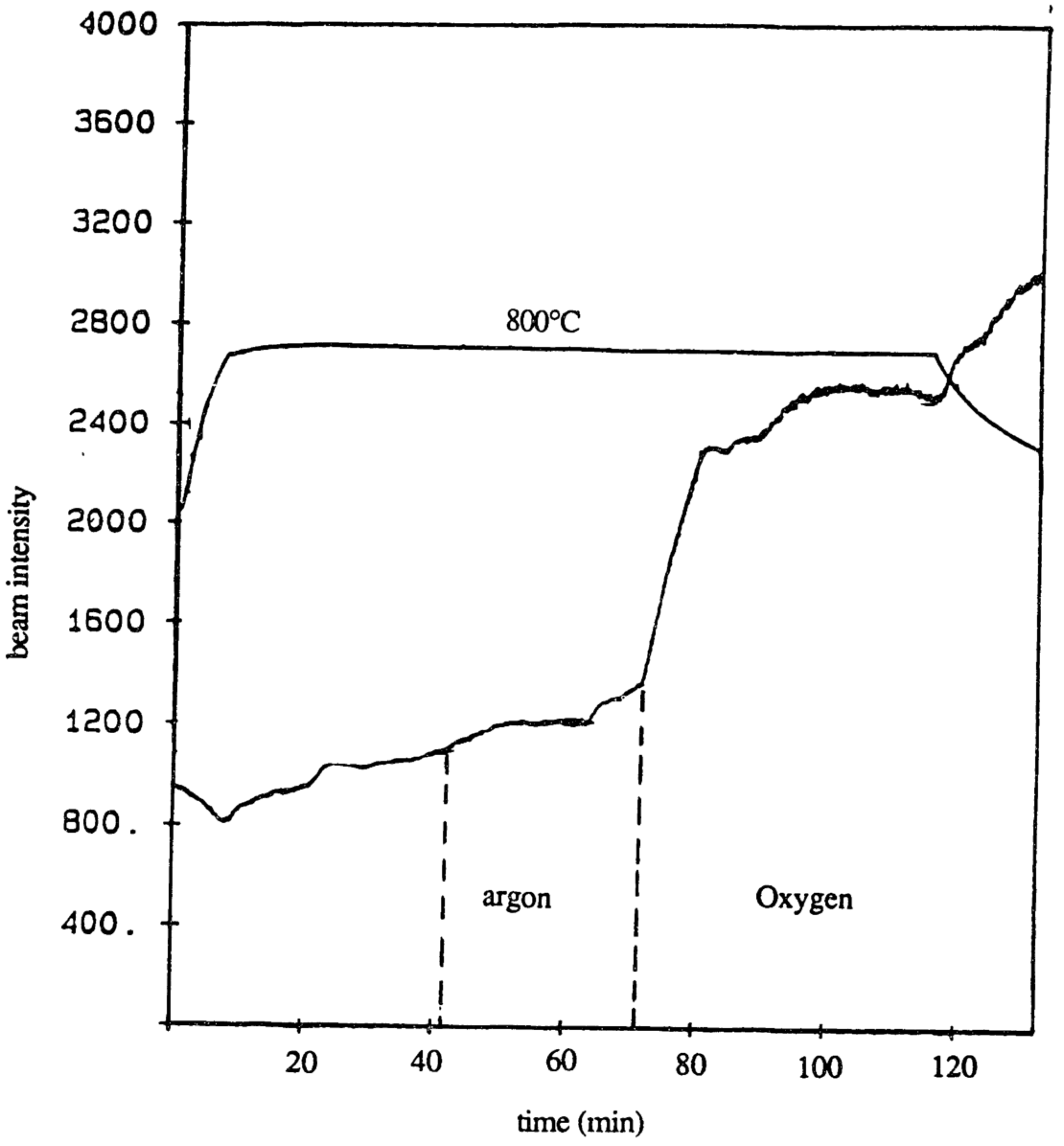

Figure 6.5: Comparing the rate of agglomeration in argon and oxygen by changing the atmosphere during the annealing of a patterned sample.

In order to dry the wafers, a careful procedure was followed. Since the wafer is placed vertically in the boat, water collects at the bottom of the wafer when it is removed from the bath. This causes a water mark on the wafer which is not visible but affects the agglomeration in that area. For this reason, after a wafer was removed the boat was immediately returned to the bath. The wafers were removed and dried one by one in this manner, then spin dried to remove water quickly and uniformly from the upper surface. The bottom surface was dried by leaning the wafer against a glass slide on a hot plate.

To check for cleanliness the steam nucleation test was used. This test applied to surfaces which are hydrophilic when clean, such as oxides, and involves holding the surface of interest above a source of steam: the deionized water bath, and then observing the pattern formed on the surface. If a uniform thin layer of water forms, the wafer is clean. This layer can easily be identified because it forms a color pattern due to the interaction of light with this very thin layer of water as it evaporates. If the surface is contaminated the contaminated areas will cause droplets of water to nucleate on the surface and the surface will appear gray. In the case of fused silica, the substrates are transparent and these patterns are impossible to see. The steam nucleation test was therefore performed on the oxidized silicon wafer that was cleaned simultaneously with the fused silica. If the substrates are contaminated they will contaminate the silicon wafer as well, if they are clean so should be the silicon wafer. If at this point the monitor wafer failed the test, the uv-ozone cleaning was carried out to remove residual organic contaminants, and the steam nucleation test was repeated until the monitor wafer was clean.

If continuous films were required, the next step after cleaning was mounting of the substrates for evaporation.

Electron Beam Evaporator

Substrates were mounted for evaporation using a specially designed plate which holds the one inch diameter substrates so that any clamping is done on the back of the sample (Fig.6.6). The plate has one inch holes machined through all but the top 1/16 inch,

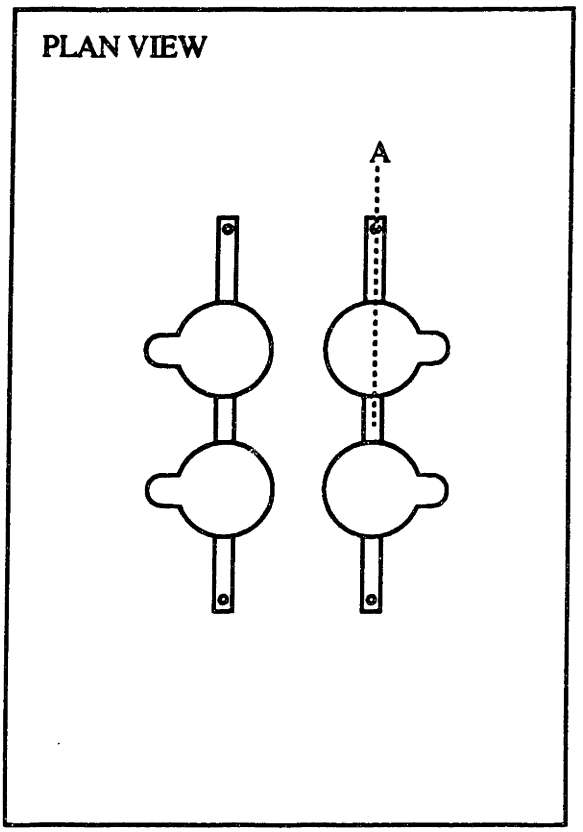

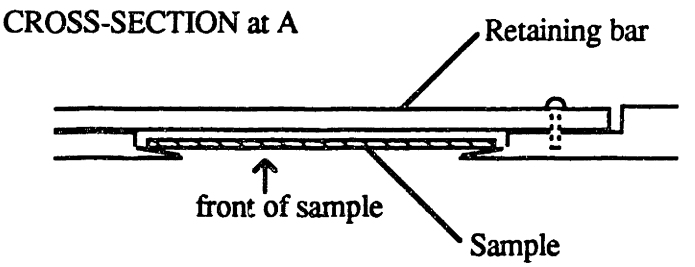

Figure 6.6. Evaporation plate designed to minimize handling of the substrate by clamping the substrate from the back.

and a smaller opening through the rest. The lip that forms is machined to be tapered. A hole through the thickness is made to one side of each large hole to allow for the insertion of wafer tweezers. The substrates are secured from the back with a narrow bar.

Gold (99.999% pure) is deposited on the substrate using an electron beam evaporator at a rate 5Å/s in a system with a background pressure of about 1×10^{-6} torr.

Generating Patterned Films: Photolithography

Lines or gratings of gold can be made by several techniques. The most common way involves the patterning of the continuous gold film. (Fig.6.7) A coating sensitive to a particular wavelength, in this case ultraviolet, is applied to the film, and a mask is used to cover this photoresist. When a positive photoresist is used, the mask has the required pattern in opaque materials (chromium). The mask is made of flexible glass, and is brought into contact with the photoresist by a vacuum created between it and the substrate (Fig.6.7a). When exposed to UV radiation, the areas of the photoresist under the transparent areas of the mask are exposed and the bonds in the photoresist broken. The exposed photoresist is then chemically washed away and the photoresist left behind can in turn serve as a mask for the gold etchant (Fig.6.7b). After the pattern is etched into the gold film, the photoresist is removed (Fig.6.7c).

In the present case, the above technique could not be used because the continuous film readily flaked and peeled off the substrate in the developer or etchant. An alternate patterning technique, referred to as lift-off (Fig.6.8), results in the gold being deposited already in patterned form. 5000 Å resist is applied directly onto a clean substrate treated with a solution of hexamethyldisilasane (HMDS), an adhesion promoter (Fig.6.8a). It is then exposed and developed as described above. After a short uv/ozone exposure to remove any resist residue, the gold is evaporated over the pattern (Fig.6.8b). Because the walls of the resist are steep, and an overhang develops as the gold is being deposited, the gold on top of the resist is separated from the gold between the resist lines. The smaller

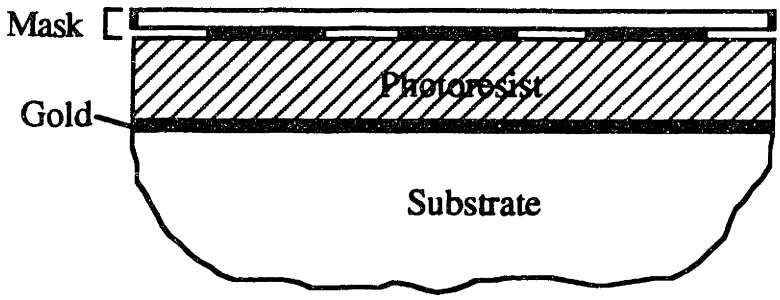

a) Exposure of the resist

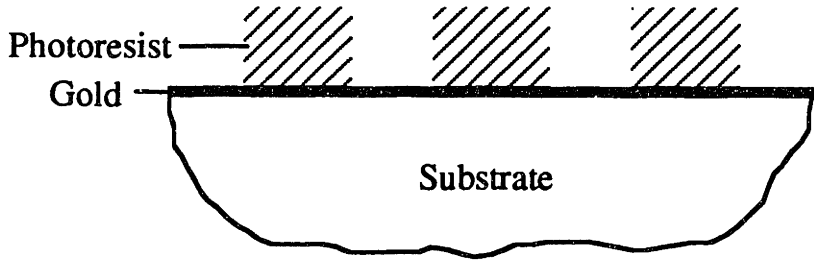

b) Developing of the resist

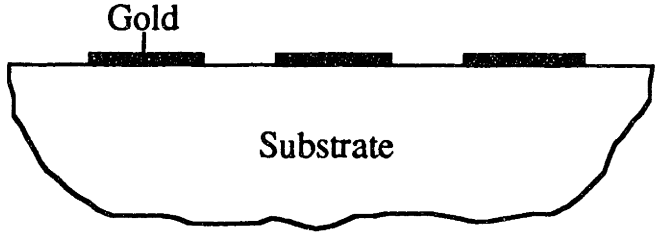

c) Etching of the gold

Figure 6.7: Schematic diagram illustrating a typical photolithography procedure.

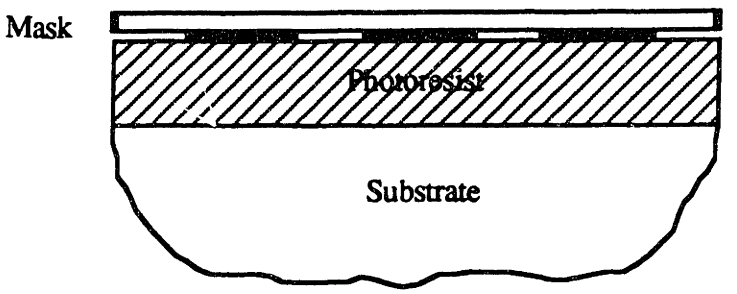

a) Resist exposure.

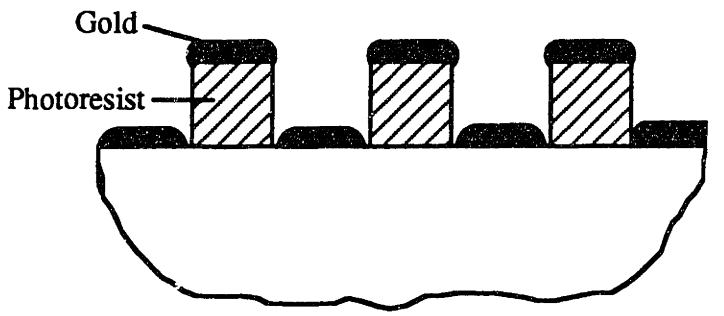

b) After development and gold. deposition

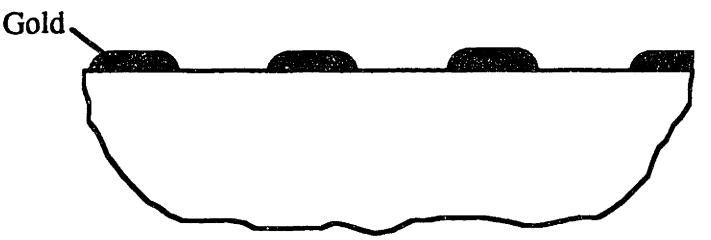

c) After lift-off.

Figure 6.8: Schematic diagram illustrating a lift-off procedure for patterning a thin film.

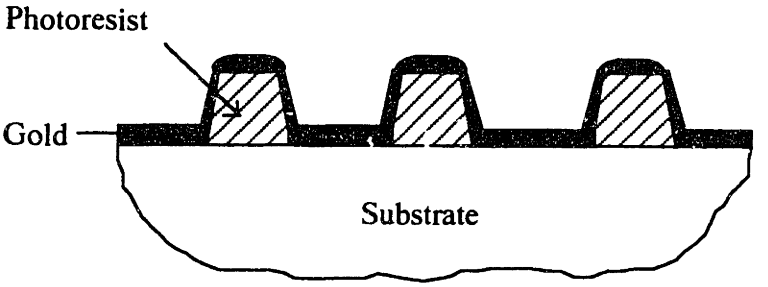

Figure 6.8d) : Illustration of poor contact leading to slanted sidewalls and continuous coverage. The resist in such a sample could not be successfully removed.

structures are under less stress and the resist can be removed in solvents without the lines flaking or pealing off the substrate. Left behind is a gold pattern which is a negative of the mask that had been used (Fig.6.8c).

Although this method proved to be successful, it does require very careful work. If the mask is not in perfect contact with the photoresist, usually as a result of dust particles on the substrate, film, resist or mask, exposure does not produce straight side-walls on developing (Fig.6.8d). In this case, the deposited gold could be continuous and lift-off would become difficult, spotty or impossible.

While the first method involving etching produces a sample with a very clean gold-substrate interface it results in resist being applied to the gold surface and possible contamination of the gold surface. Lift-off introduces possible contamination at the gold-substrate interface while the surface of the gold is only exposed to solvents.

Summary

The experimental objectives are to measure the temperature and film thickness dependence of the agglomeration process. The agglomerating edge were studied at high magnification and the results reported in Chapter 4. The purpose of the experiments described in this chapter was to quantitatively measure the rate of agglomeration.

The measurement is accomplished by means of two novel approaches. One of these is to use patterned substrates to simulate a continuous film in the process of agglomeration. Since nucleation of voids is not required, the growth component of the transformation can be isolated from nucleation effects. A pattern of lines is the simplest geometry for the study and can be produced using photolithography techniques. The pattern is produced on the substrate by lift-off.

The second novel approach is to use laser light transmitted through the sample to measure of the amount of substrate exposed. This requires a combination of wavelength substrate and film so that the substrate is transparent to the radiation and the film

significantly more opaque. Fused silica was therefore used as a substrate for the gold films. The light transmitted through the sample is directly proportional to the area of agglomerated film. The characteristic trace for a patterned film in the process of agglomeration from the edges is a straight line with slope related to the temperature of the anneal. The characteristic trace for a continuous film is a sigmoidal curve showing an incubation time required for the nucleation of holes and a growth curve which gradually diminishes as the holes impinge. Results and analysis of both continuous and patterned films will be discussed in Chapter 7.

Chapter 7:

RESULTS AND ANALYSIS FOR GOLD LINES AND CONTINUOUS FILMS IN OXYGEN AND ARGON

This chapter is divided into two parts: the first part presents the experiments and their analysis for the agglomeration of gold lines and the second part presents the experiments and analysis for the agglomeration of continuous films. Each section contains a list of the experiments, details of data manipulation, and a presentation of the reduced data so that transport coefficients and trends can be extracted. Samples were annealed both in argon and in oxygen. Anneals of gold lines in argon are discussed in Appendix A. The presentation of the reduced data is based on the model proposed in Chapter 5.

Lines Annealed in Oxygen

In order to study the dependence of the void growth rate on temperature and film thickness, lines of gold, 25 μm wide and separated by 10 μm spaces, were patterned on fused silica substrates . Rates were measured for six thicknesses of gold: 400, 500, 600, 700, 800 and 900Å, and measurements were performed at temperatures ranging from 625°C to 850°C. Because agglomeration proceeds much faster at a given temperature in thinner films than in thicker films, it was necessary to use lower temperatures for the thinner films and higher temperatures for the thicker films to maintain agglomeration rates at measurable levels.

To demonstrate reproducibility in the data some anneals were performed two or more times. Each thickness was deposited separately. To demonstrate reproducibily from

one evaporation to the next, two evaporations were carried out for 500, 600 and 800 Å thick films.

The experiments performed are summarized in Table I. The entries are grouped by film thickness and samples from the same evaporation are listed together. The last column lists the temperatures at which each sample was annealed.

Interpretation of transmitted signal intensity vs time

A sample trace of signal intensity, S, as a function of time, t, is shown in figure 7.1. Note that beyond an initial transient during which the film is heated and oxygen is added to the chamber, the slope of S vs. t is constant. The *rate* of agglomeration, $\Delta S/\Delta t$, is determined from this slope. These rates, plotted as $\Delta S/\Delta t$ kT vs 1/kT (based on equation 24), for all samples tested, are shown in figures 7.2a) through f).

Figure 7.3 shows schematically the advance of the cellular void front in a line of unit length, *l*, and width, w. The transmitted beam intensity, S, is proportional to the area of agglomerated film, A, as follows:

$$S = A\ s_v \tag{30}$$

where s_v is the signal per unit area of transformed (agglomerated) film. Because the rate is constant, a change in S, ΔS, over a period of time Δt, can be written in terms of a change in the agglomerated area, ΔA, as follows:

$$\Delta S = (\Delta A)\ s_v \tag{31}$$

The change in area can be rewritten in terms of the advance of the interface, Δx, so that equation 31 becomes:

$$\Delta S = 2(\Delta x) l\ s_v\ . \tag{32}$$

When $\Delta x = w/2$, the line is fully agglomerated and ΔS has its maximum value of ΔS_{total}.

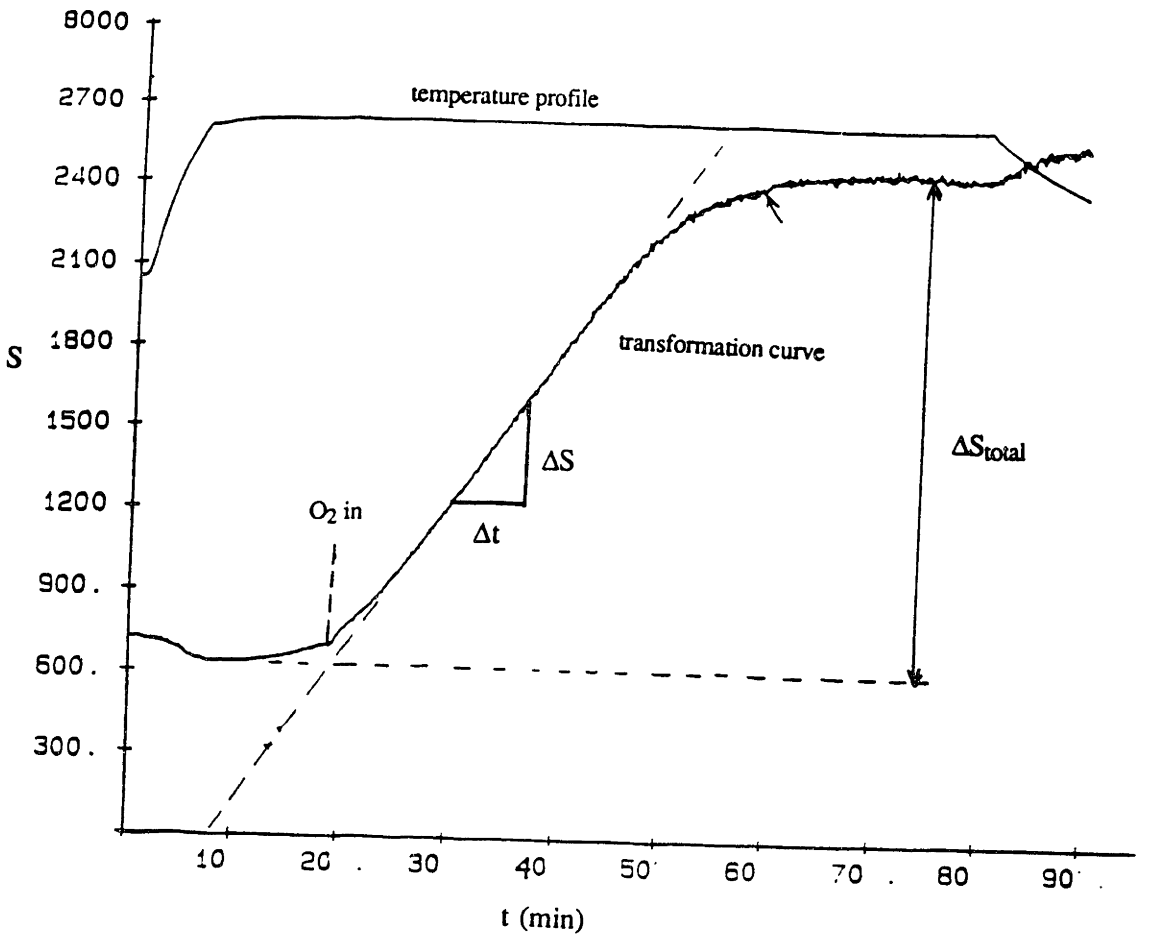

Figure 7.1: Sample trace, S vs t, from line experiments: 500Å thick film annealed at 725C. The vertical axis is signal intensity, S, which is the amplified voltage drop across the resistor in the detector circuit..

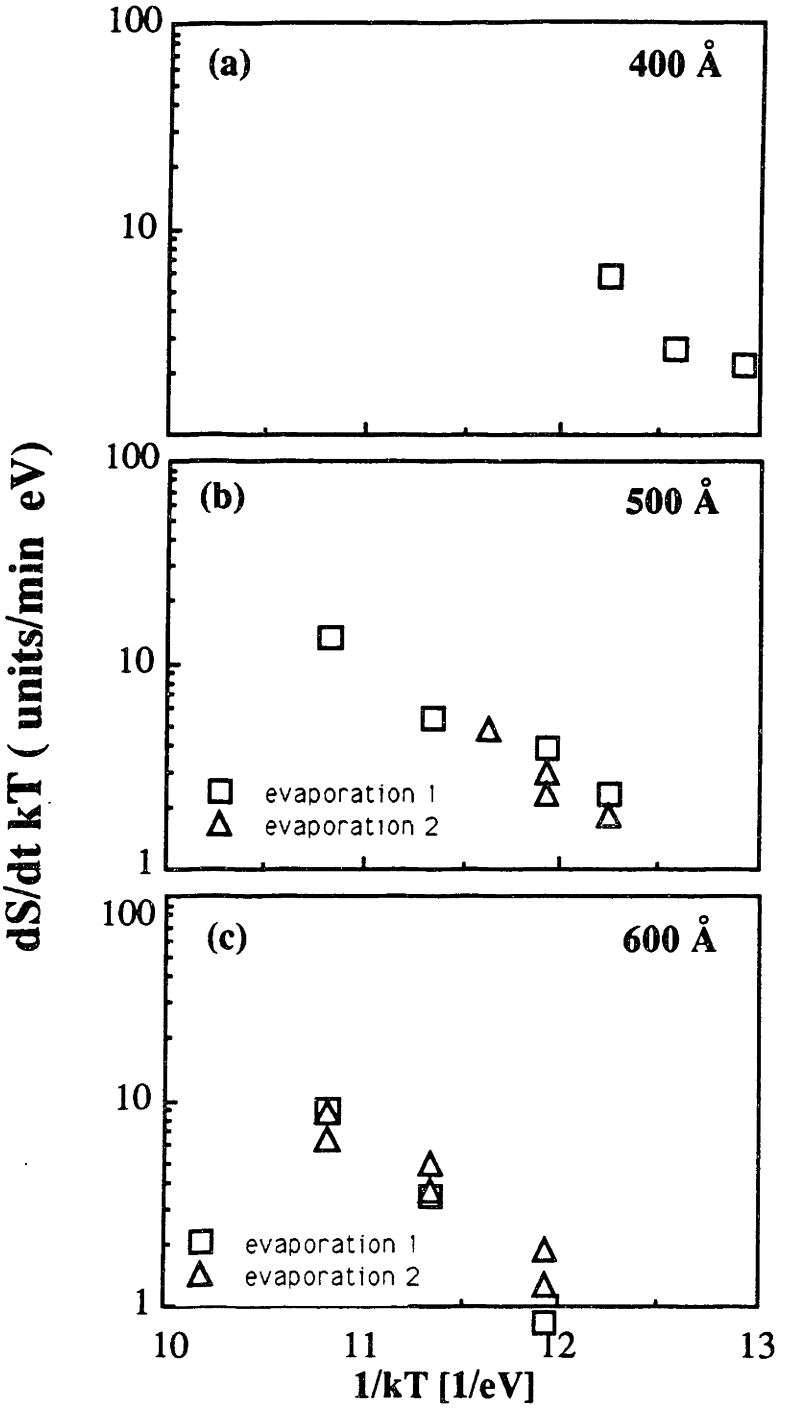

Figure 7.2: Rate of agglomeration, dS/dt, of patterned films in oxygen, plotted against 1/kT. Each thickness is plotted on a separate graph. All samples were lines of gold with a 35 μm period and a 25 μm line width. These are raw data: they have not been scaled for changes in laser power. a) 400 Å, b) 500 Å, c) 600 Å.

continued...

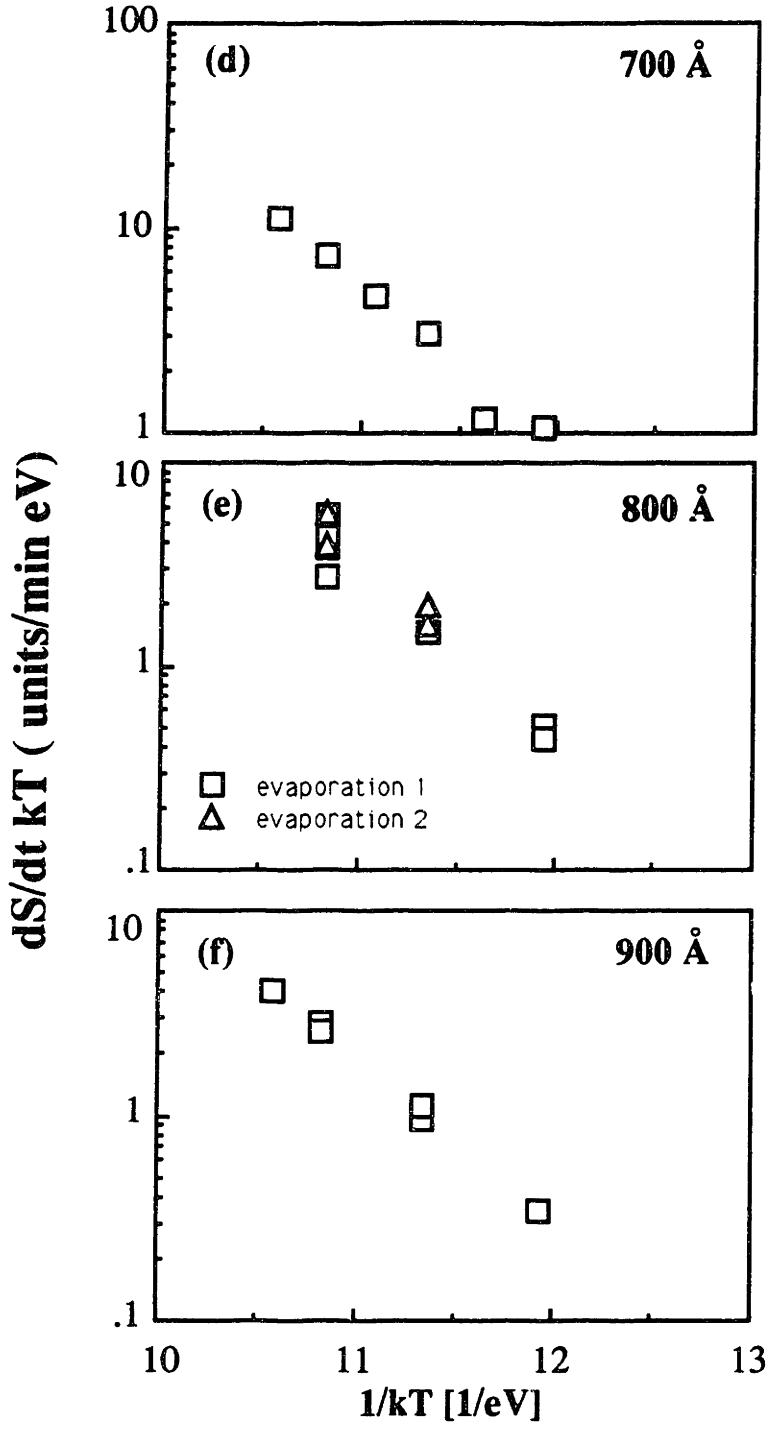

Figure 7.2: (continued from previous page)
d) 700 Å, e) 800 Å, f) 900 Å.

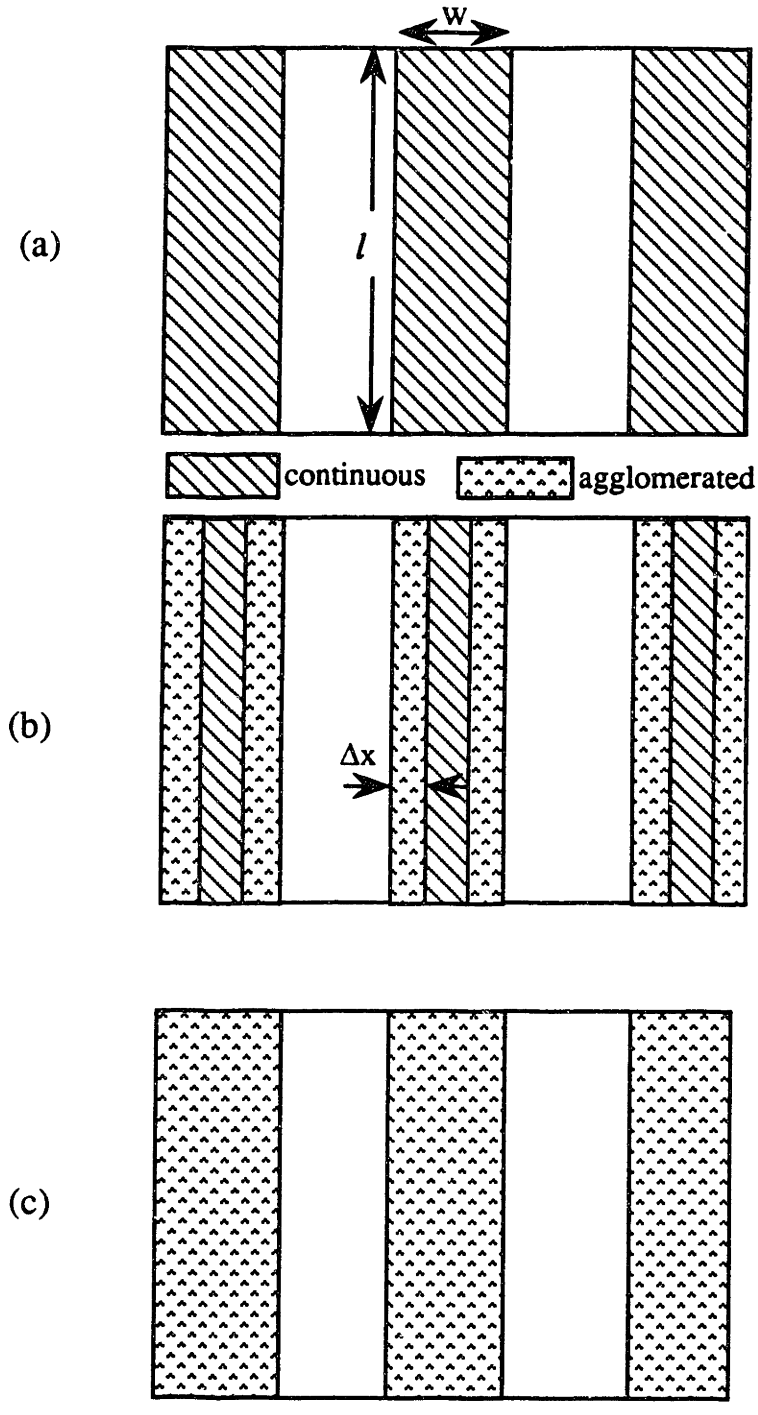

Figure 7.3: Schematic drawing of a line agglomerating:
a) fully continuous line of width w and unit length *l*
b) partially agglomerated, i.e. the area of the agglomerated phase per unit length of line is: $2\,\Delta x\,l$
c) fully agglomerated line.

Thickness (A)	Sample set	Temperatures (C)
400	#1	625 650 675
500	1 2	675 and 700 750 and 800 675 725
600	1 2	700, 750 and 800 700, 750 and 800 700, 750 and 800
700	1	700, 750 and 800 725, 775 and 825
800	1 2	700, 750 and 800 700 and 800 750 800
900	1	700, 750 and 800 750, 800 and 825

TABLE I: Anneals performed on patterned films (oxygen).

which is defined in figure 7.1:

$$\Delta S_{total} = \Delta A_{total}\, s_v = w\, l\, s_v \,. \qquad (33)$$

If the lines are annealed until they fully agglomerate, then ΔS_{total} is known. In order to solve for the rate of advance of the interface itself, $\Delta x/\Delta t$, equation 32 can be rewritten as follows:

$$\frac{\Delta x}{\Delta t} = \frac{\Delta S}{\Delta t}\,\frac{1}{2 l s_v} \qquad (34)$$

and since ΔS_{total} equals $w l s_v$,

$$\frac{\Delta x}{\Delta t} = \frac{\Delta S}{\Delta t}\,\frac{1}{2\, l\, s_v}\,\frac{w\, l\, s_v}{\Delta S_{total}} \,. \qquad (35)$$

From equation 35, $\Delta x/\Delta t$ can be expressed simply in terms of $\Delta S/\Delta t$, which is measured from the slope of the S vs. t trace, and in terms of w, which is also known, as follows:

$$\frac{\Delta x}{\Delta t} = \frac{\Delta S}{\Delta t}\,\frac{w/2}{\Delta S_{total}} \,. \qquad (36)$$

This relationship is intuitively true since the termination of the transformation defines a distance of w/2 travelled by the agglomeration front formed at each side of the line. The termination point also defines a total change in signal ΔS_{total}. If the change in signal for the total agglomeration of lines is, for example, 2300 units, and the lines are 25 μm wide, then the slope of the trace, dS/dt, at temperature can be converted to $\Delta x/\Delta t$ in μm min^{-1} by:

$$\frac{\Delta x}{\Delta t} = \frac{\Delta S}{\Delta t}\,\frac{12.5}{2300} \,. \qquad (37)$$

Application of the model to the data: lines

To determine the activation energy for agglomeration of gold on fused silica, based on equation 24 (Chapter 5) rewritten as follows:

$$\frac{dx}{dt}\,kT = \frac{\beta}{h^3}\exp\left(-\frac{Q_s}{kT}\right) \qquad \text{where } \beta = D_o\,\Omega^2\,\gamma_s\,\nu\,\frac{2}{\pi} \qquad (38)$$

the results for lines were plotted on an Arrhenius type graph in figure 7.4. In this figure the data from figures 7.2a through f has been averaged so that there is only one point per thickness and temperature. The lines represent the best fit of equation 38 to the data. The slope of the line is related to the effective activation energy, Q_S, for the agglomeration of gold of a given thickness. From the intercept of the line, the value of D_o, the pre-exponential for surface diffusion, can be calculated to the level of accuracy that the material constants (Ω, γ_s, and ν) are known.

The effective activation energies, listed on figure 7.4, increase with increasing film thickness. The activation energies, with error bars representing the standard error, are plotted in figure 7.5a). The lowest energy data, data for 400 and 500Å films, contain a relatively small amount of points. In particular, the data set for 400 Å films has a standard error of ± 0.5 eV, in a Q_S value of 1.3 eV. This was taken to indicate that the 400 Å data, in particular, does not contain, on its own, enough data points to represent the temperature dependence correctly. However, in combination with the other data points, it may make a valid contribution. Therefore, assuming that the range in activation energy is due to scatter in the data, data from all thicknesses is combined in one plot: (dx/dt) kT h^3 vs 1/kT. From equation 38 this plot should have a constant slope. The best fit for the data yields the value:

$$D_s = 0.18\exp\left\{-\frac{1.4\text{ eV}}{kT}\right\}\ \text{cm}^2\,\text{s}^{-1}, \qquad (39)$$

so that the effective activation energy is 1.4 eV and where the values of the material constants were taken to be:

Ω = atomic volume = 1.7×10^{-23} cm^3/atom [17],

ν = surface concentration of atoms = $\Omega^{-2/3}$ (if surface concentration does not differ much from bulk) = 1.5×10^{15} atoms/cm, and

γ_s = surface tension = 1450 erg/cm^2 at 1000°C [18].

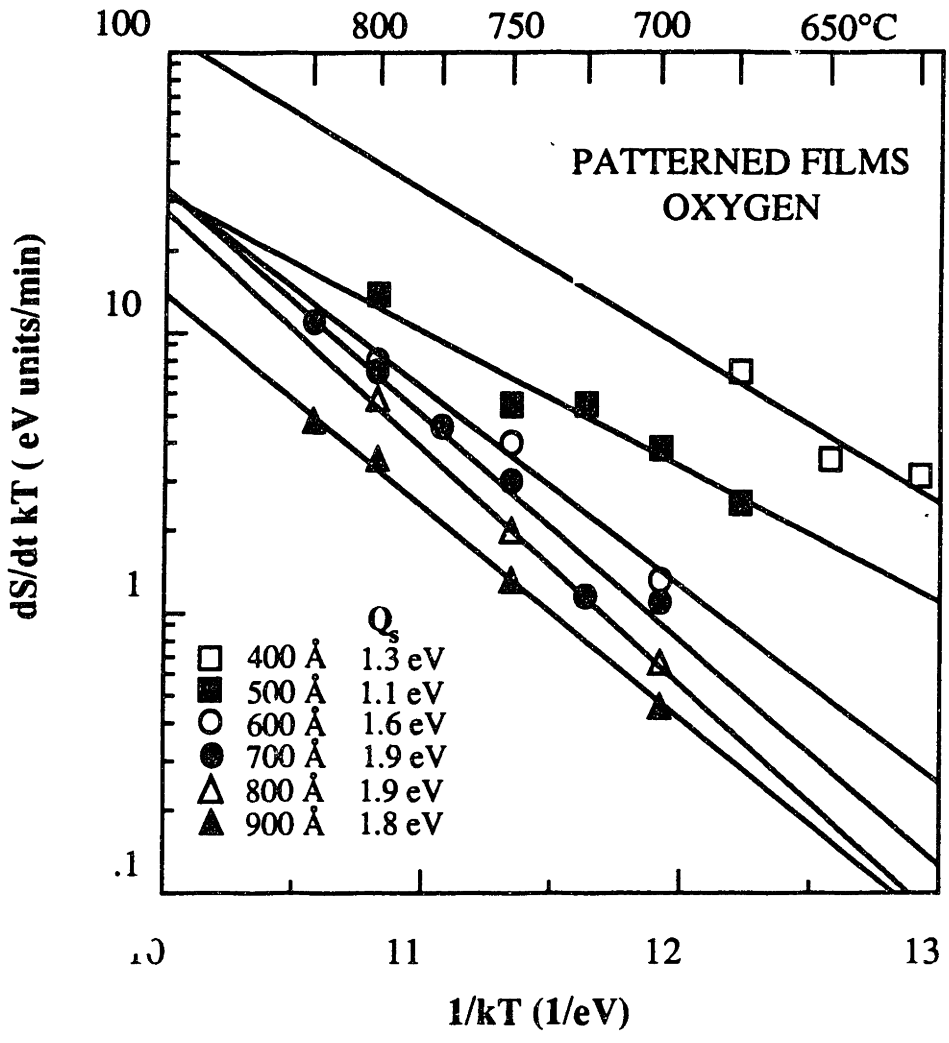

Figure 7.4. Arrhenius plot agglomeration rate dS/dt (units/min), of patterned films annealed in oxygen. These are averages of the multiple readings in figures 7.2e-f so that there is only one point for a thickness at each temperature.

The data from 400 Å thick films are all above the line fitted to figure 7.6. If this is not simply due to scatter in the data, then it may be an artifact of an approximation in the model (Chapter 5). An important assumption made regarded the effect of diffusion in the lateral direction. Since it was assumed that r', the in-plane curvature (see figure 5.2a) is large, a film with a fine cell structure (small r') may be strongly affected by this approximation. The cell period can be inferred from the bead density along the edge of an agglomerated line. For comparison, the bead density was plotted against film thickness in figure 7.5b), directly below the plot of activation energy dependence on film thickness in figure 7.5a). The bead density is approximately constant for thicker films but increases suddenly for 500 Å thick films and it nearly doubles in 400 Å thick films. Since taking into account lateral diffusion changes the geometry of the model, the effect should appear in the pre-exponential of equation 38 and may affect the thickness dependence of the model. However it is not clear how this should introduce a thickness *dependence* into the *slope* of the Arrhenius plot. Because the effect of a thickness dependent morphology is extremely complicated and because the apparent effect on activation is not clear, all data will be included, as a single set, in the analysis and conclusions of this chapter.

The thickness dependence can be determined from the slope of the data on a log(dS/dt) vs log(h) plot. The data are plotted for each temperature in figure 7.7a). Figure 7.7b) shows all the data combined into one curve. According to equation 38, the slope of this plot should vary as -3 so that the actual value of -3.1 agrees well with the model.

In summary, values measured from this set of data are:

1. an activation energy of 1.4 eV
2. a pre-exponential value of the diffusivity of 0.18 $cm^2\ s^{-1}$,
3. a thickness dependence of $h^{-3.1}$.

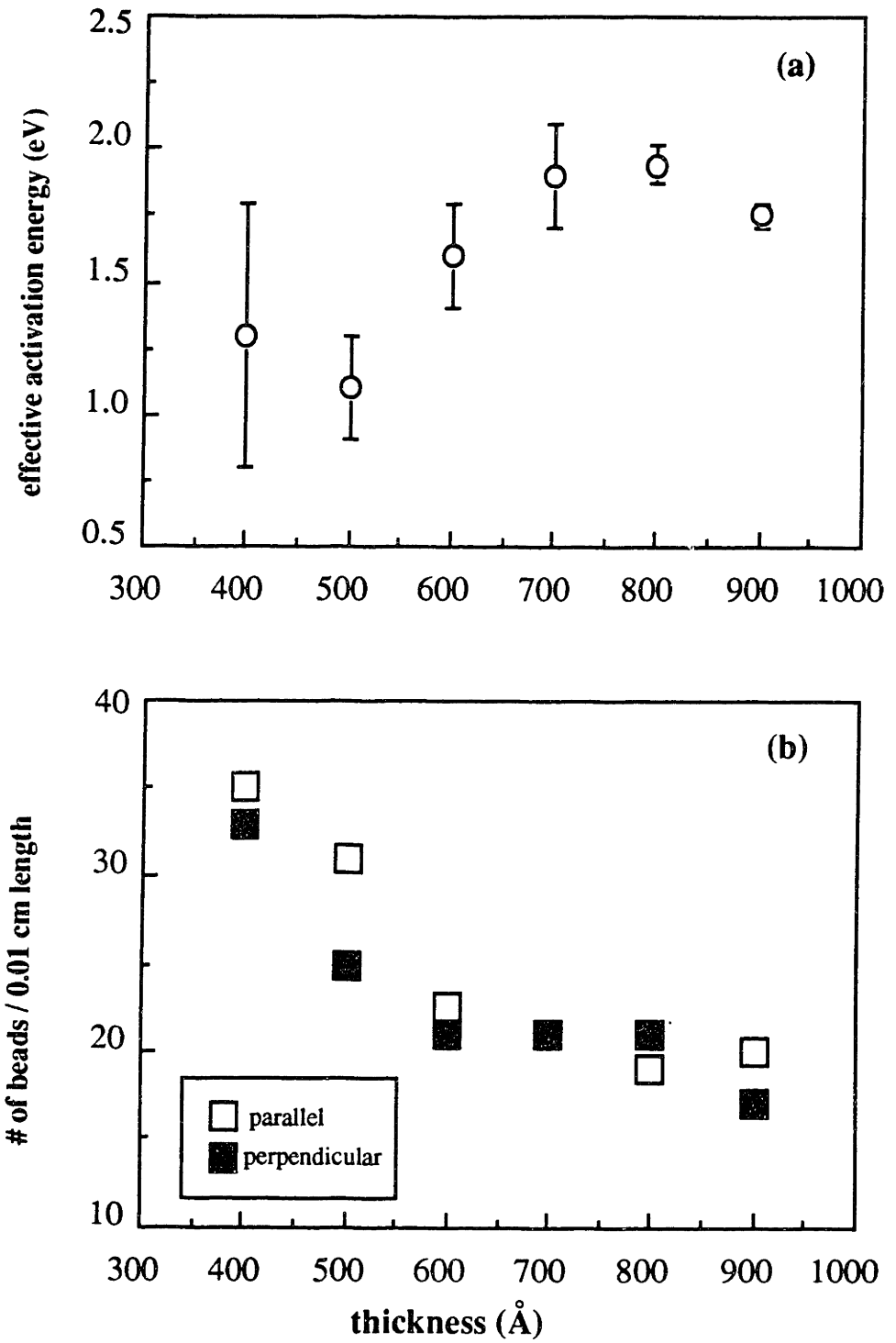

Figure 7.5: Comparing the apparent dependence of activation energy on film thickness with the dependence of bead density on film thickness.
a) Apparent activation energy for diffusion (from Fig. 7.4) with error bars representing the standard error.
b) Number of beads per 0.01 cm length: parallel to the line (along the line edge) and perpendicular to the line (across the width of the line).

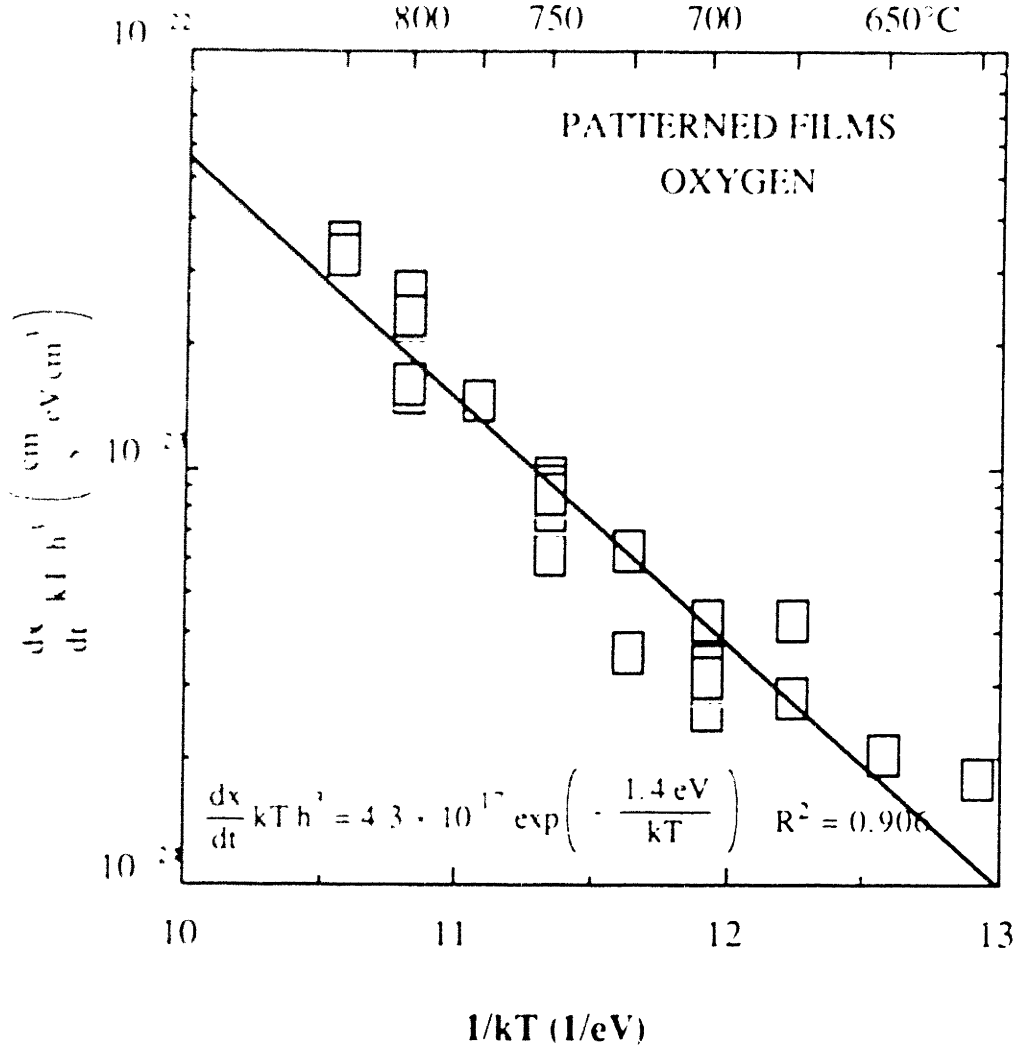

Figure 7.6. Data from all thicknesses combined to allow extracting activation energy and pre-exponential of surface diffusivity according to equation 38.

Continuous Films

The data presented here for continuous films annealed in oxygen is the result of three evaporations of 600Å thick films, each film having been annealed at a single temperature. The temperatures used were 750, 775, 800, 825 and 850°C. The data for films annealed in argon is based on four evaporations of 600 Å of gold and the annealing temperatures were 750, 775, 800 and 825°C. Table II is a summary of these experiments. It was found that the density of nuclei varied from sample to sample. In order to analyze the nucleation frequency for each sample, the anneal was terminated while individual nuclei were still distinguishable: before the sample was about 20 to 30 % transformed.

Interpretation of the transmitted signal intensity vs time

Since the power of the laser varied from one anneal to the next, a method for comparing the traces had to be found. As for lines, if the full transformation curve is recorded, the difference in the signal between the untransformed film and the fully transformed film can be used to compare curves from different samples. In this set of experiments, because the number of nuclei had to be determined, the anneals were stopped before the samples were fully transformed. Figure 7.8a) illustrates this partial transformation curve. Since the endpoint of the transformation is not available, a different method has to be used to compare the samples. If the transmittance of the beam through a fully transformed sample is given by S_{beaded} and the transmittance through a continuous film by $S_{cont's}$ (Fig.7.8a), then the transmittance through a partially transformed sample S_{sample} is:

$$S_{sample} = S_{cont's} \ (1 - X_f) + S_{beaded} \ X_f \qquad (40)$$

where X_f is the area fraction transformed at the end of the anneal. To calculate X_f, equation 40 can be rewritten as:

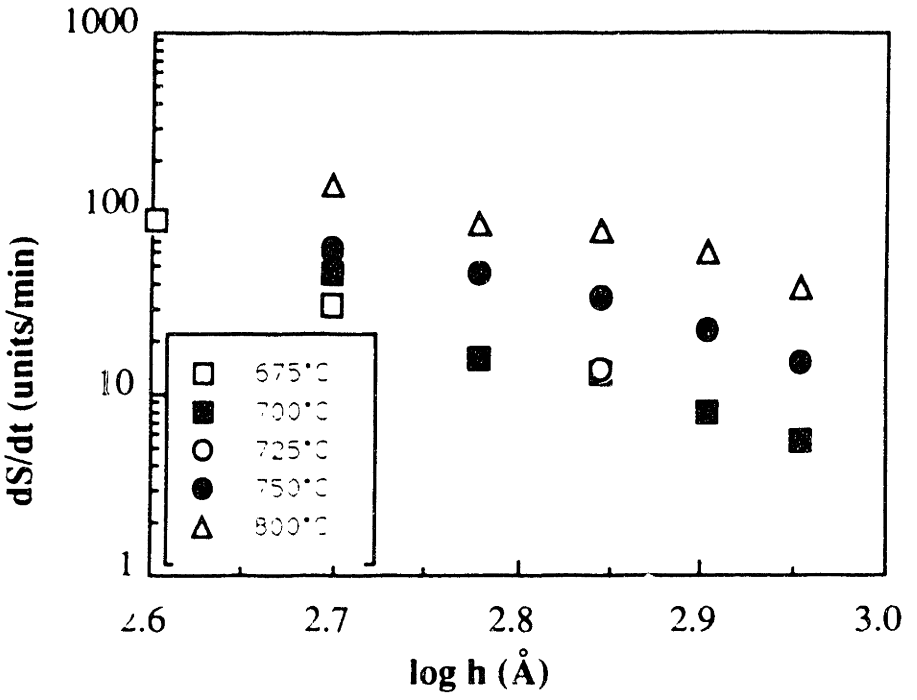

(a)

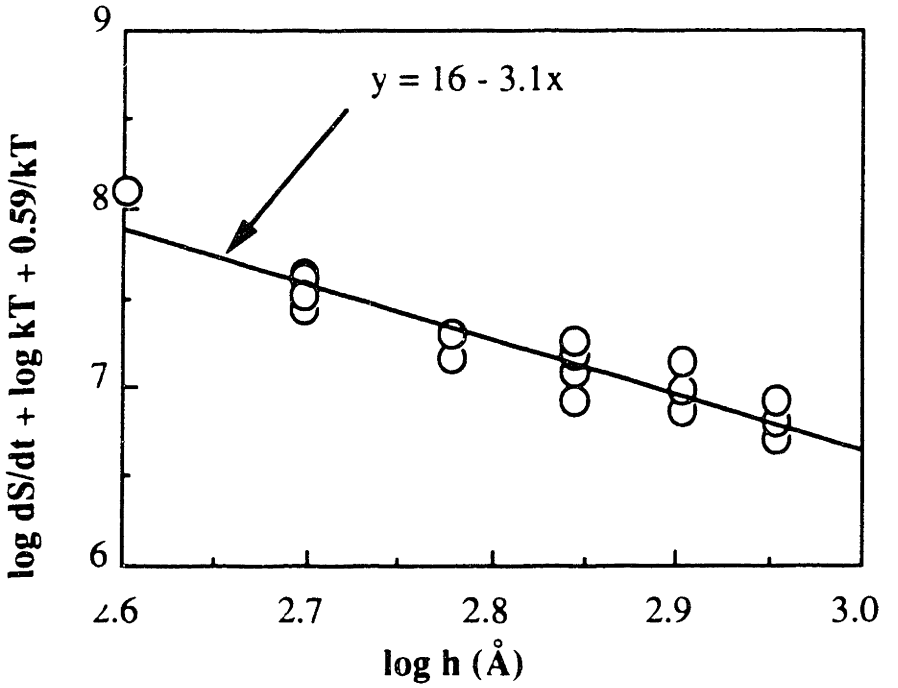

(b)

Figure 7.7: Thickness dependence of agglomeration front velocity:
a) data from all temperatures plotted separately for each temperature,
b) data from (a) plotted so that one line may be fitted to all the points.

Sample #	Sample set #	Ambient	Temperature (C)
1.1	1	argon	800
1.2		oxygen	800
1.3		oxygen	750
2.1	2	oxygen	775
2.2		argon	775
3.1	3	argon	825
3.2		argon	750
4.1	4	argon	825
4.2		argon	825
4.3		argon	825
5.1	5	oxygen	825
5.2		oxygen	850
5.3		oxygen	750

TABLE II: Continuous film anneals performed.

$$X_f = \frac{S_{sample} - S_{cont's}}{S_{beaded} - S_{cont's}} \quad . \tag{41}$$

Therefore, from S_{sample} of each sample, the area fraction, X_f, of beaded area to total area at the end of the anneal can be calculated. Table III lists values of voltage measured using an oscilloscope connected to the detector circuit. Measurements were made on two different occasions to verify the measurement. The table lists first the values obtained for S_{beaded} and $S_{cont's}$. The S_{sample} values follow.Since the power of the laser signal did not change during the course of these particular measurements, the traces can be scaled relative to each other. The difference between the signal at zero film area transformed, $S_{cont's}$, and the signal at the point where cooling of the sample started, $S(t_{anneal})$, is scaled to correspond to the fraction transformed, X_f (Fig.7.8b). Although further agglomeration might have occurred on cooling, quenching to about 650°C takes only a few minutes and at these temperatures the agglomeration rate is quite slow.

The nucleation frequency.

The signal vs time curve must also be individually scaled depending on the number of voids that formed. In some cases this is straight forward as in figure 7.9a where all the voids are about the same size. This can only occur if all the voids exhibit the same growth rate and if they all form at once. In other cases (Fig.7.9b), there is a distribution of void sizes at the end of the experiment. Although the edges of the voids are uneven, the voids are approximately round in shape except as they impinge. This indicates that the rate is the same in all directions and would not be expected to vary from void to void. This, therefore, indicates that the spread in the void size distribution is due to a time dependent nucleation frequency of the voids. Figure 7.10 is a list of histograms of void size distributions at the end of each anneal for those samples where it was possible to distinguish individual voids. The voids counted were often impinged so that a large void might be indistinguishable from

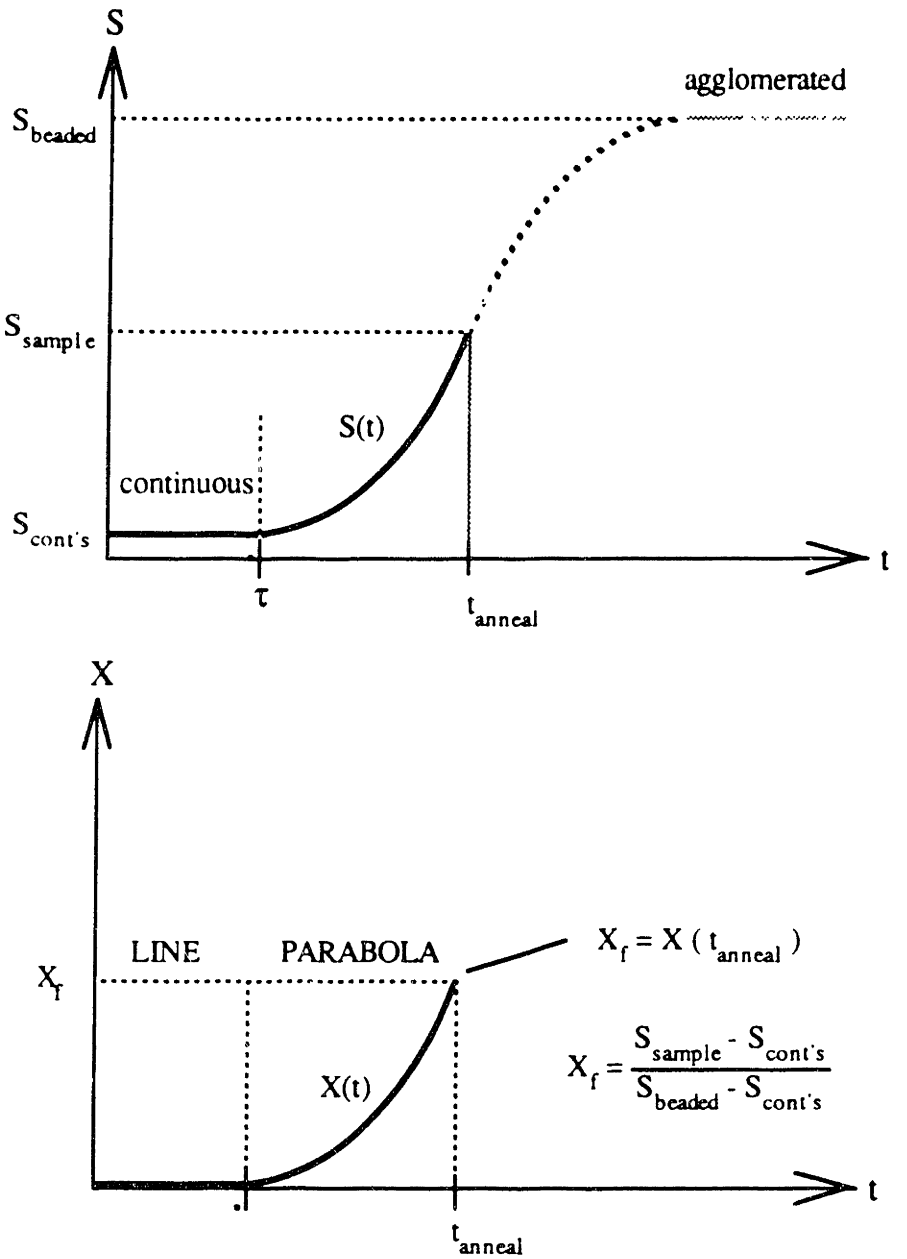

Figure 7.8. Schematic of a trace due to a film that had been partially agglomerated. The area fraction transformed at the end of the anneal can be obtained using equation 41. The terms used in this equation are defined by the drawing.
a) S vs t and
b) X vs t.

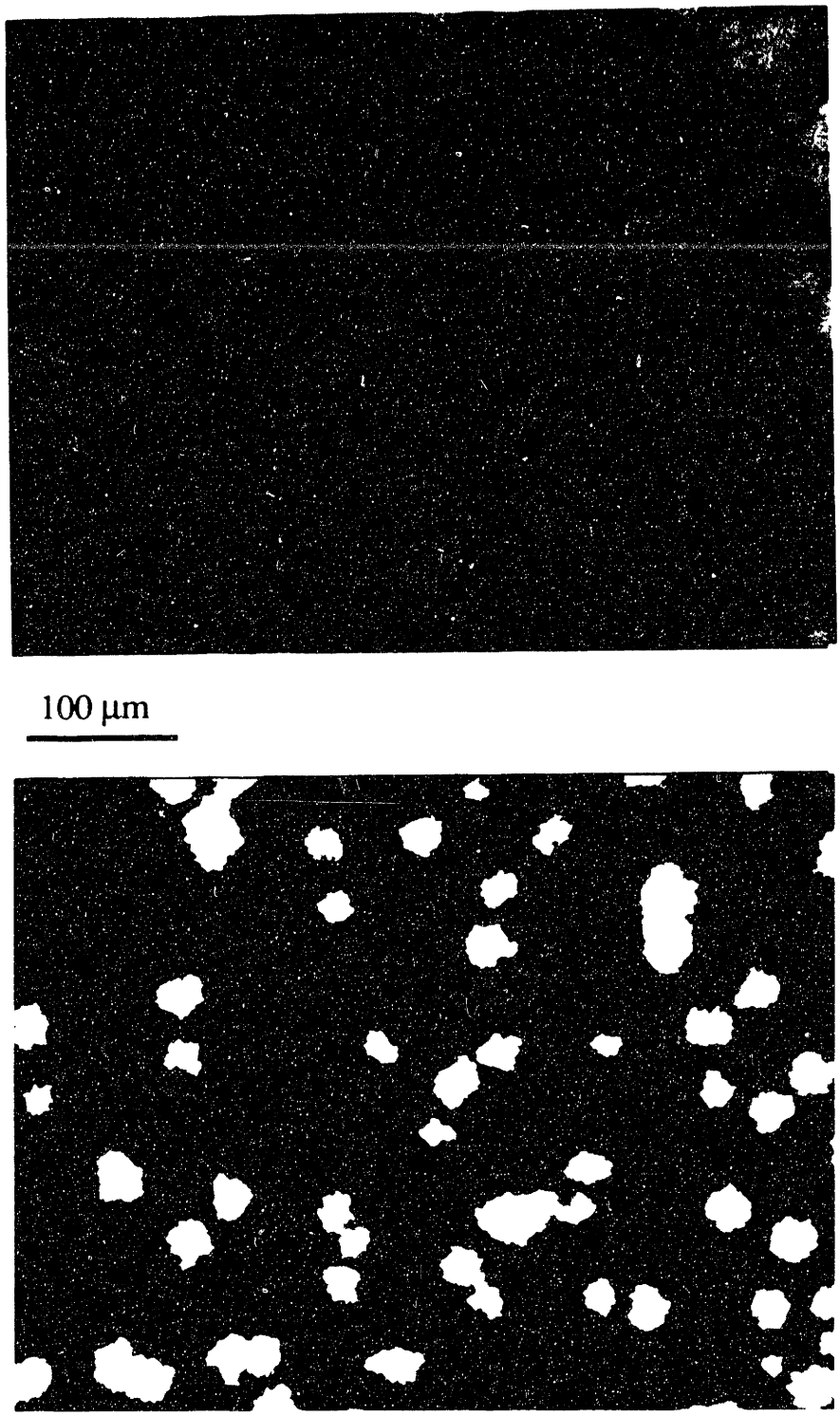

Figure 7.9: Initially continuous films annealed in oxygen: a) voids are the same size and b) voids vary in size from 30 to 80 μm in diameter

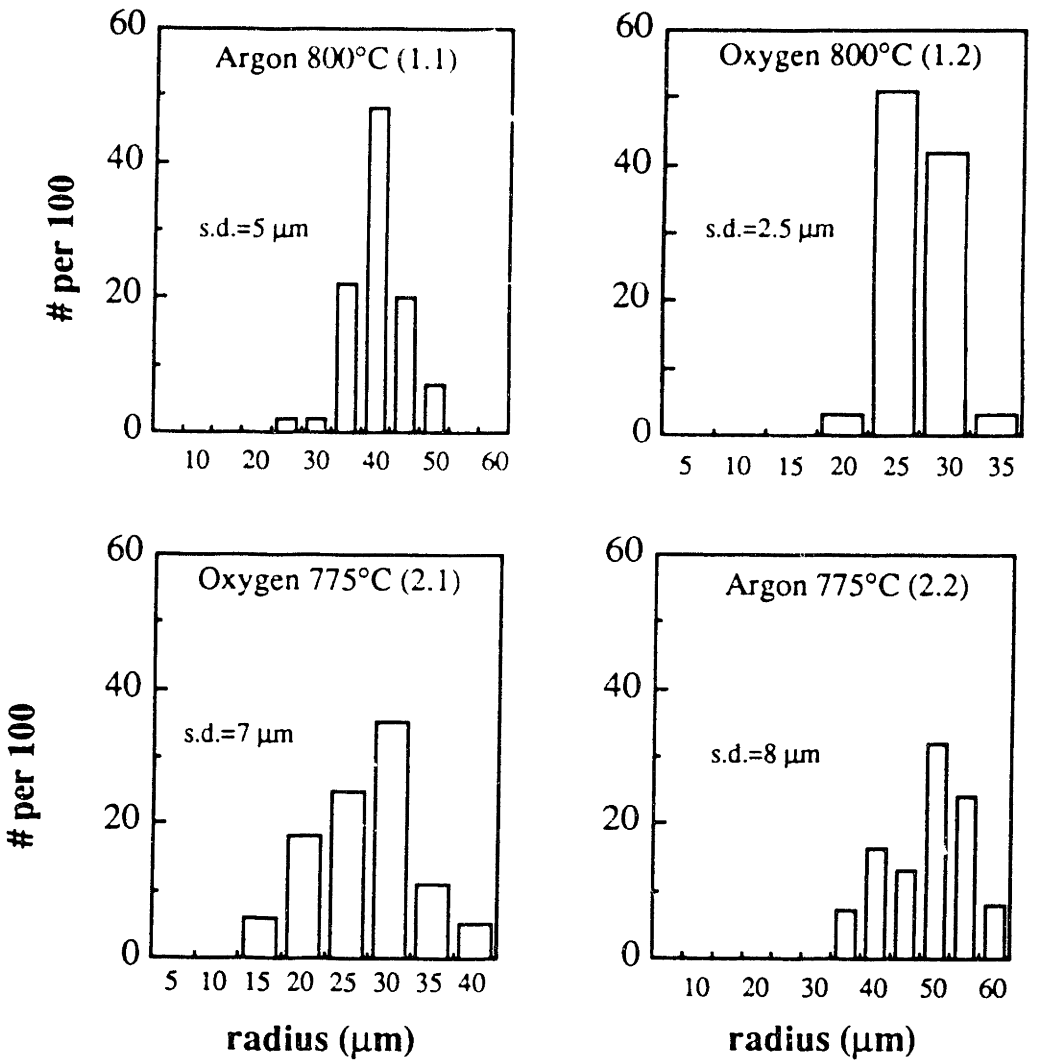

Figure 7.10 : Distributions of void sizes for each of the samples in Table II for which individual voids could be distinguished. The range for the horizontal axis was chosen so that it would include voids formed over the duration of the experiment. The beginning of the range would represent voids formed close to the end of the anneal. Large voids were formed close to the beginning of the anneal.

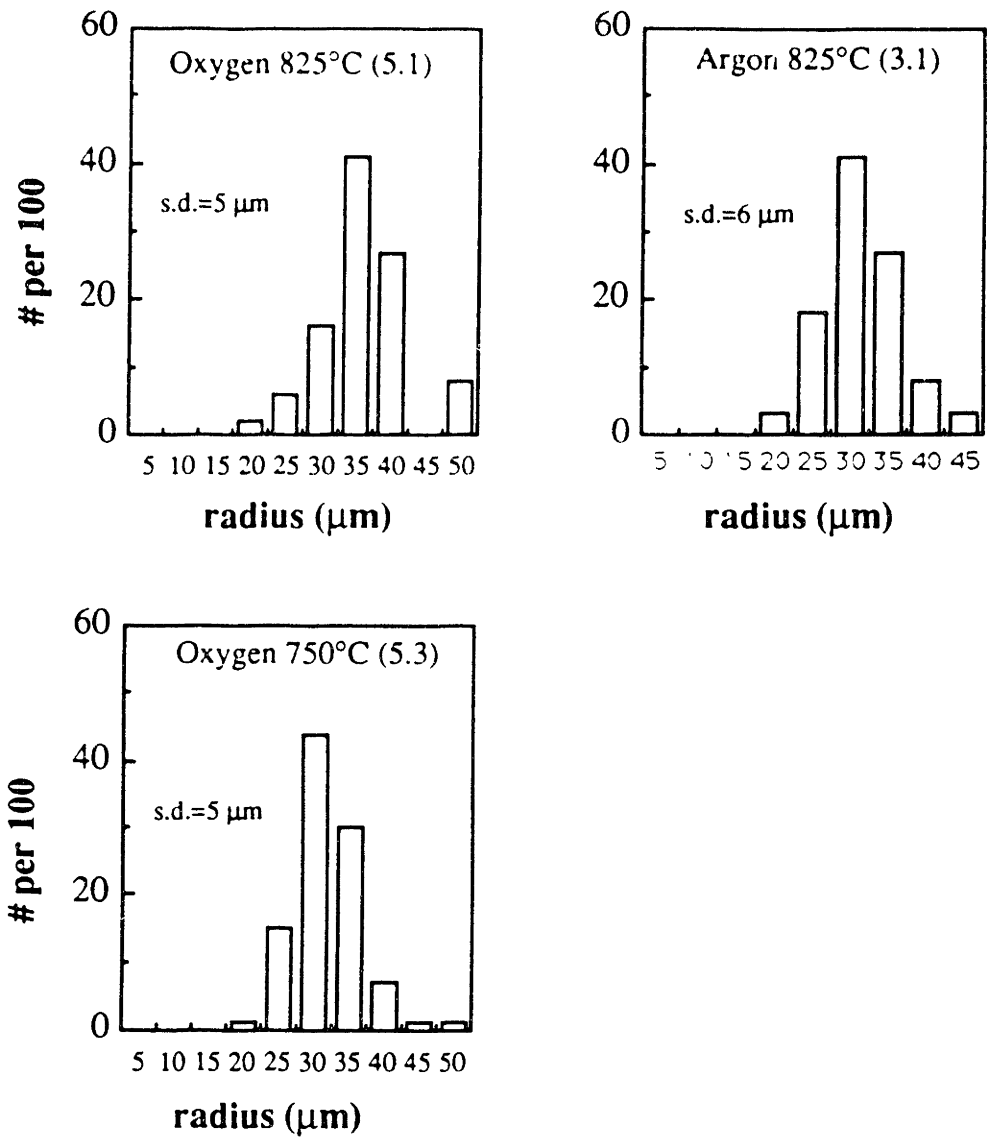

Figure 7.10 : (continued)

Sample	Measurement #1	Measurement #2	X_f
Standards			
$S_{cont's}$	.05	.03	
S_{beaded}	1.35	1.30	
S_{sample}			
2) $S_{5.3}$	.26	.28	.18
3) $S_{2.1}$		.19	.11
4) $S_{1.2}$		.33	.22
5) $S_{5.1}$	.24	.26	.17
6) $S_{5.2}$	.33	.31	.20

TABLE III: Transmittance at the end of the anneal of samples annealed in oxygen.

two smaller ones that had nucleated near each other. Clusters of nuclei were also very difficult to count, so that the distributions may be sharper than they appear. Deviations of the void shape from a smooth circular shape caused an estimated error in measuring the diameter of an isolated void to be about 15%. The standard deviations of the histograms are 10 to 20 percent of the radius at the peak so that some of the spread in the distribution falls within experimental error.

The transformation curve proposed in Chapter 5 assumes that all the nuclei formed at once, at time τ. Figure 7.10 shows that this is not precisely true. The distributions do however show, in most cases, a peak which is narrow in comparison to the case where constant nucleation would be occuring. No voids on the small side of the peak were found even though they may have been easily detected with an optical microscope.

Application of the model to data: continuous films

If all the voids form at the same time, the area exposed, that is, the amount of light reaching the detector, should have a parabolic dependence on time before impingement of the voids (see equation 26). From equation 30, if impingement occurs, the natural logarithm of the untransformed fraction should have a parabolic dependence:

$$- \ln (1 - X) = N_{void} \pi u^2 (t - \tau)^2 \qquad \text{at any time t} \qquad (42)$$

where τ is the point in time where the nucleation of N_{void} voids occurs. If u is expressed in cm s^{-1}, then N_{void} in equation 42 must be in number per cm^2. Taking impingement into account, the equation to be fitted is:

$$- \ln (1 - X) = \mathbf{A} (t - \tau)^2 \ . \qquad (43)$$

where $\mathbf{A} = N_{void}\pi u^2$. Since there is assumed to be no transformation until the time τ, to fit the data, the best line/parabola combination for the dependence of -ln(1-X) on t, must be found (Fig.7.8b). A value of τ is chosen and the average value of the data up to τ is calculated. This baseline, $S_{cont's}$, represents the transmittance of the continuous film (Fig.7.8a). The fraction transformed, X, is obtained by subtracting from the laser trace,

S(t), this base transmittance, and dividing by the final value (before cooling) of the laser signal. This number is then multiplied by X_f, the measured area fraction at the end of the experiment from Table III:

$$X = \frac{S(t) - S_{cont's}}{S_{sample} - S_{cont's}} X_f \qquad (44)$$

Equation 44 is represented schematically in figure 7.8b).

Equation 43 is fitted using the method of least squares. The calculation is repeated with different values of τ until the best fit is found as indicated by a minimum in the sum of the squares of the deviations. The standard deviations in the fit to the line/parabola time dependence for each sample annealed were calculated from:

$$\text{standard deviation} = \sqrt{\frac{1}{n} \sum_i \delta_i^2} \qquad (45)$$

δ_i is the deviation of the data from the fitted curve and n is the number of data points used for the fit. Both experimental and fitted transformation curves, X vs t, are plotted in figure 7.11. The standard deviations are given for each curve. It can be seen from the standard deviations that data is fit better by the model (equation 42) in some cases than others.

Sample 3.2 was 80% transformed and the fitted curve fits the experimental curve very closely. This indicates that the assumption that all the voids formed at once is valid for this sample. The standard deviation for this sample is higher than many of the other samples because in the other cases, the extent of the transfomation was only about 25% and so only a small part of the total curve had to be described. Because of the extent of the transformation in sample 3.2, the void size distribution cannot be measured in sample 3.2. Sample 3.1, however, has a low standard deviation both in the fit and in void size, which indicates that the voids formed approximately simultaneously. Sample 4.1, is fully transformed. The fitted curve has a large standard deviation and the fit is particularly bad in the initial stages of the transformation. This sample is too far transformed to obtain void size distributions which would be expected to be quite broad. The agreement of the

Figure 7.11: Experimental and fitted traces, X vs t, for the continuous film listed in Table II. The solid lines are experimental curves and the dashed lines are drawn based on the best fit to equation 42:

$$\ln (1 - X) = N_h \pi u^2 (t - \tau)^2.$$

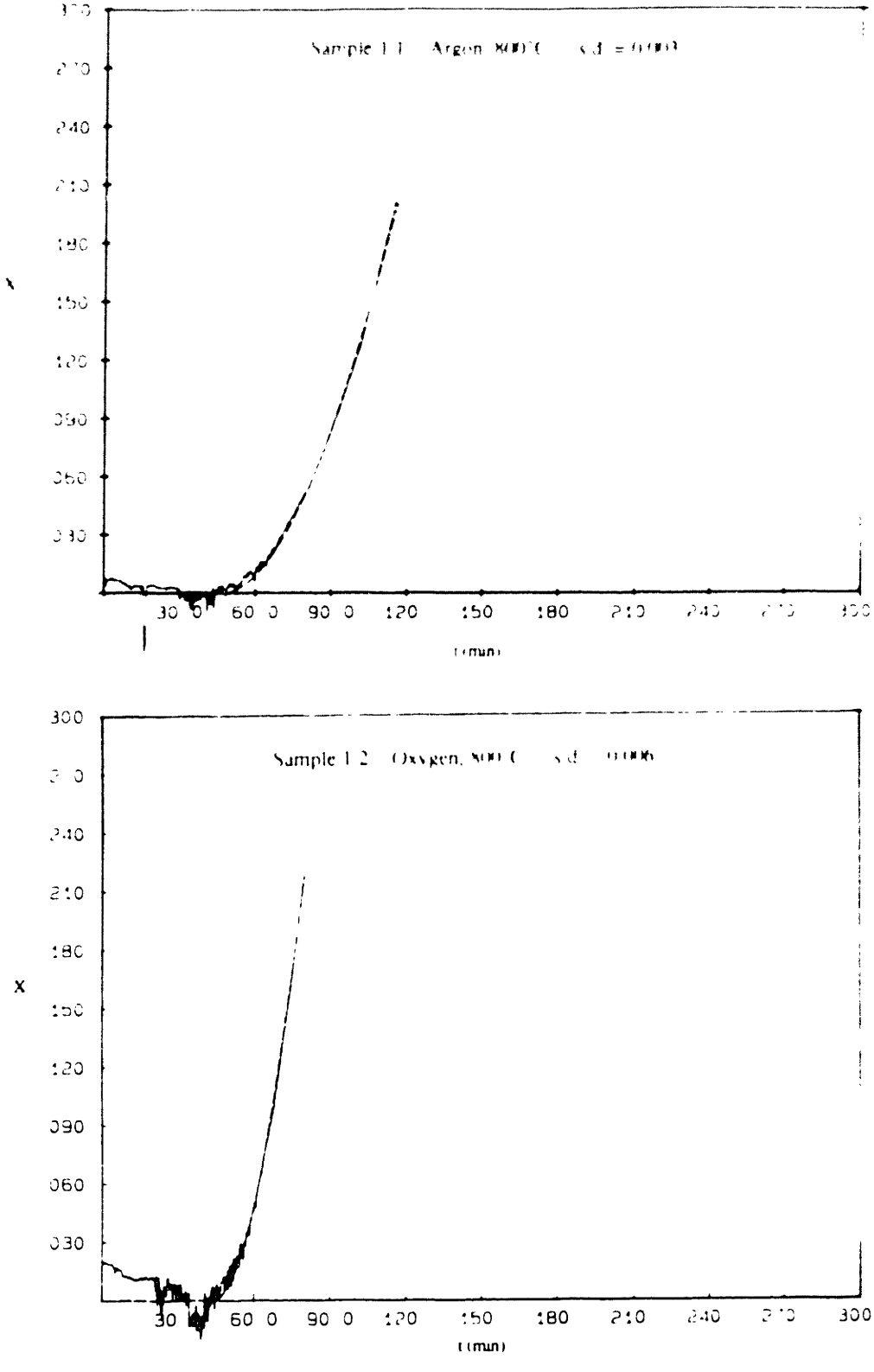

Figure 7.11: (continued from previous page)

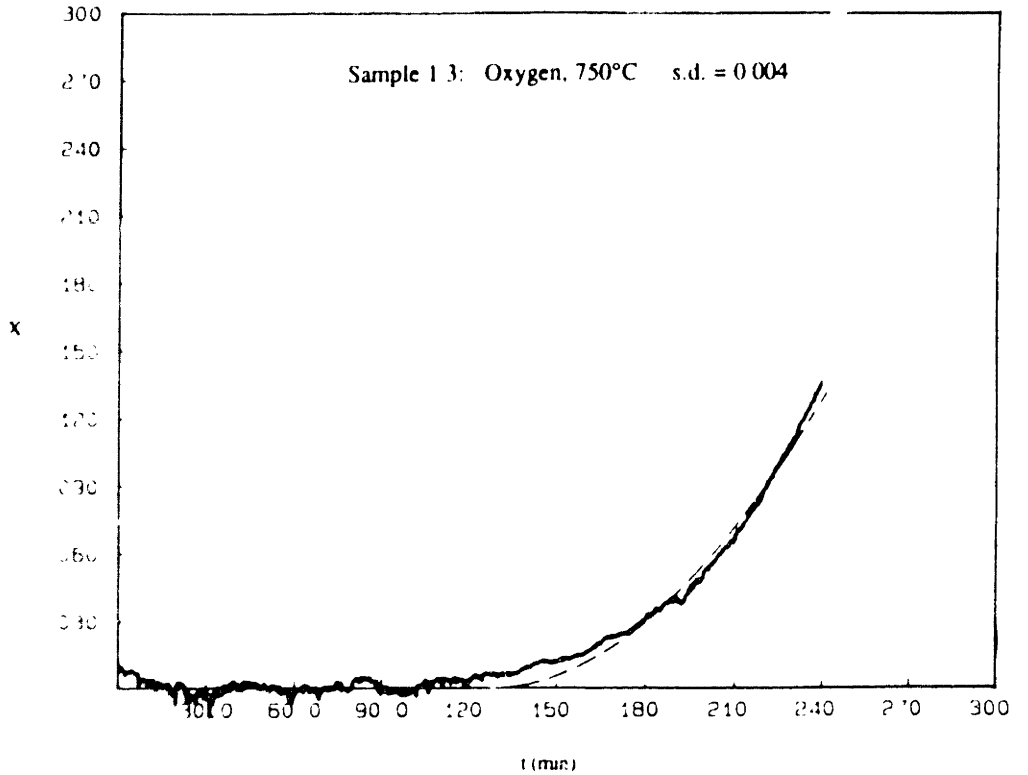

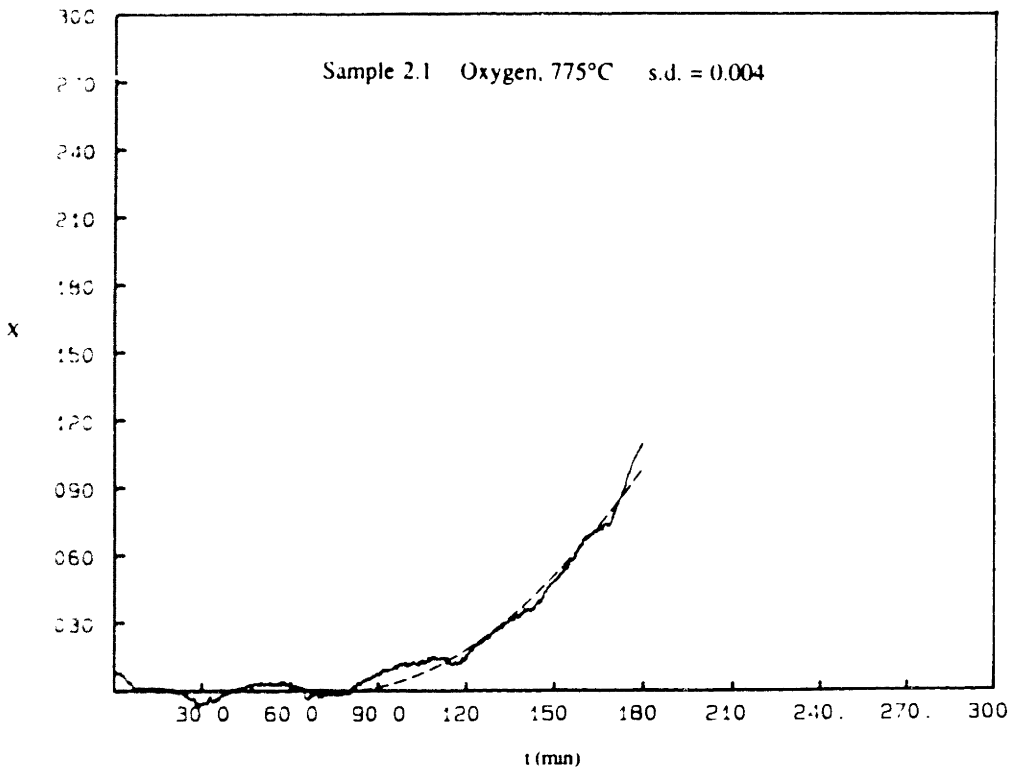

Figure 7.11: (continued from previous page)

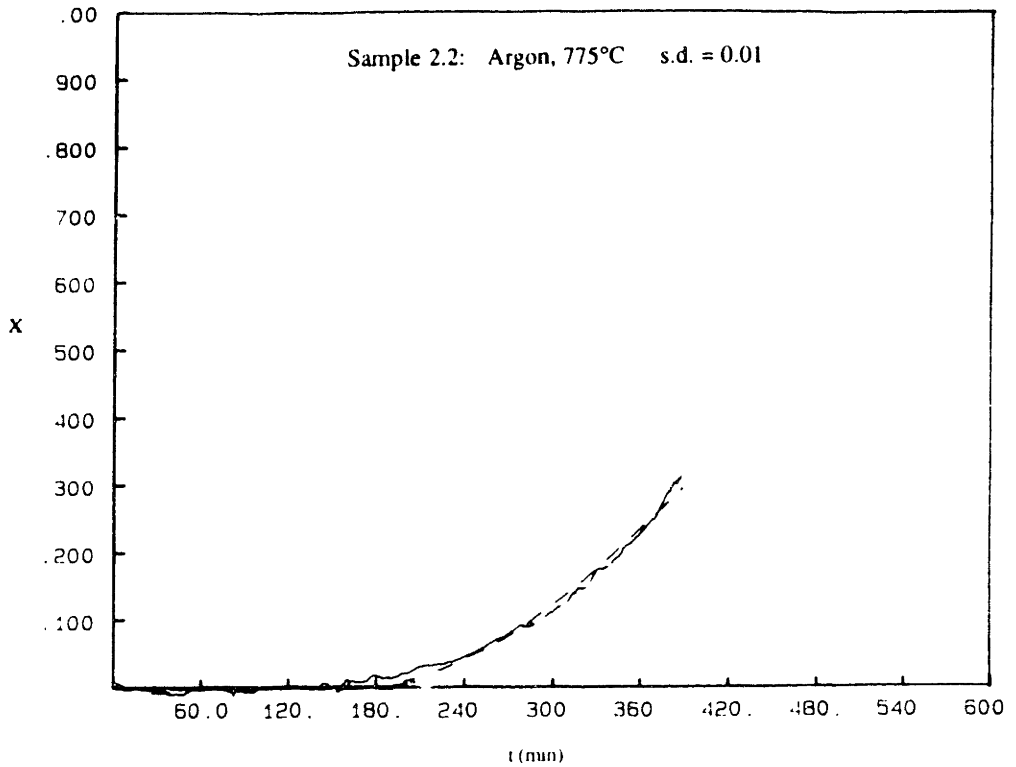

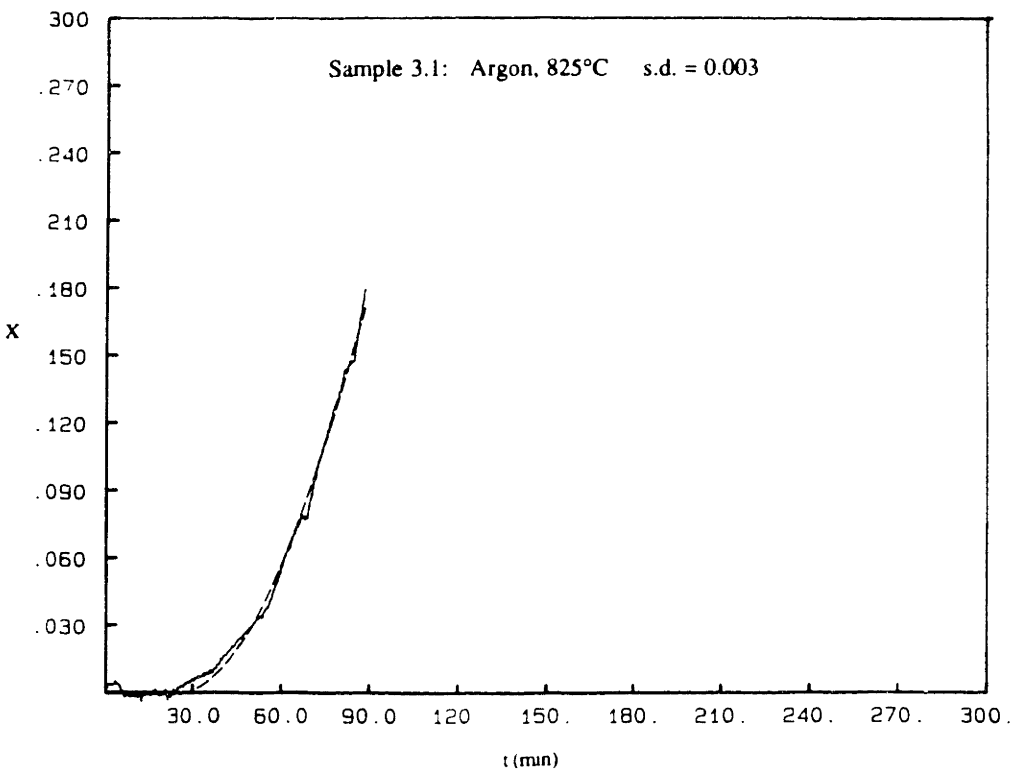

Figure 7.11: (continued from previous page)

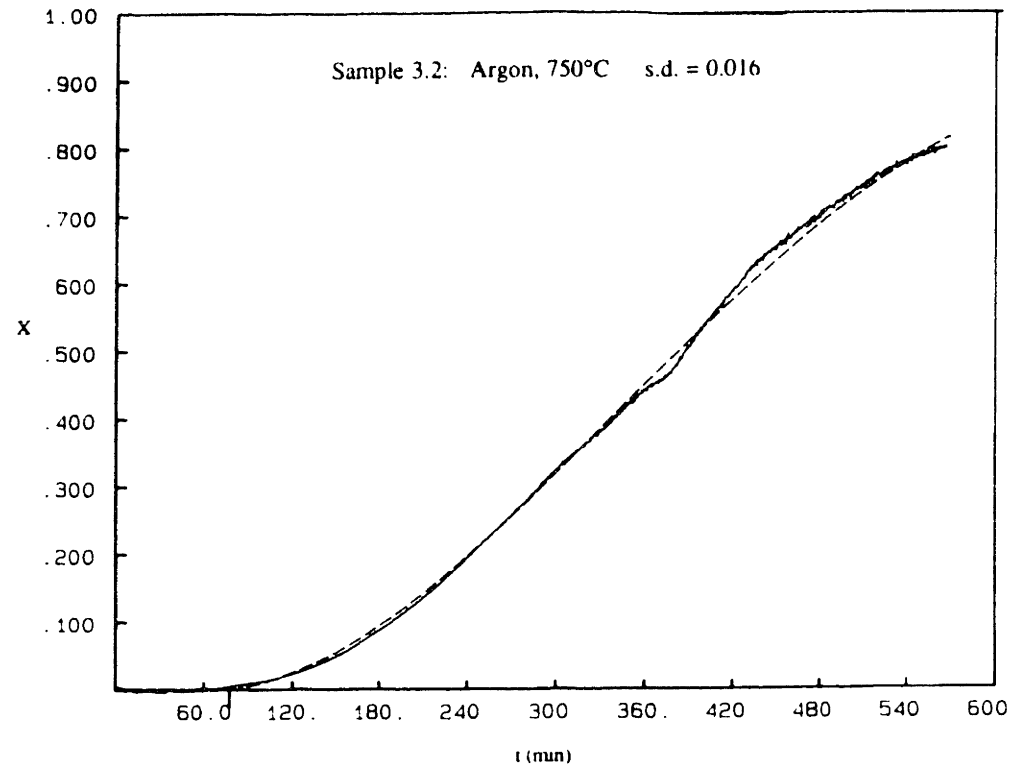

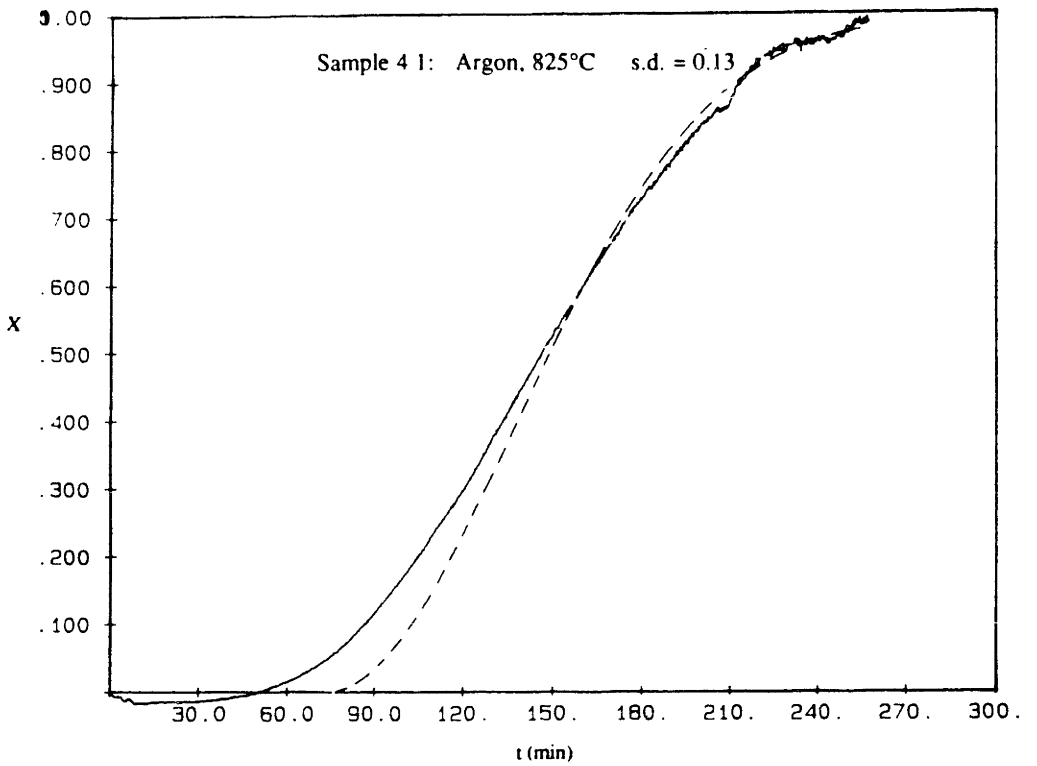

Figure 7.11: (continued from previous page)

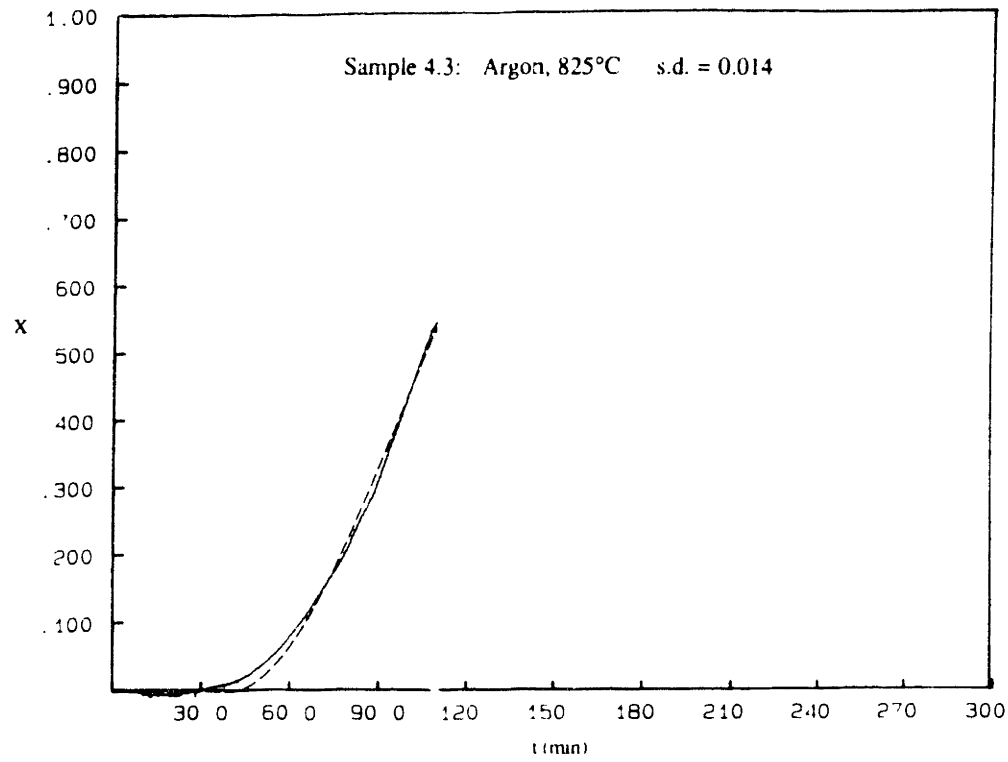

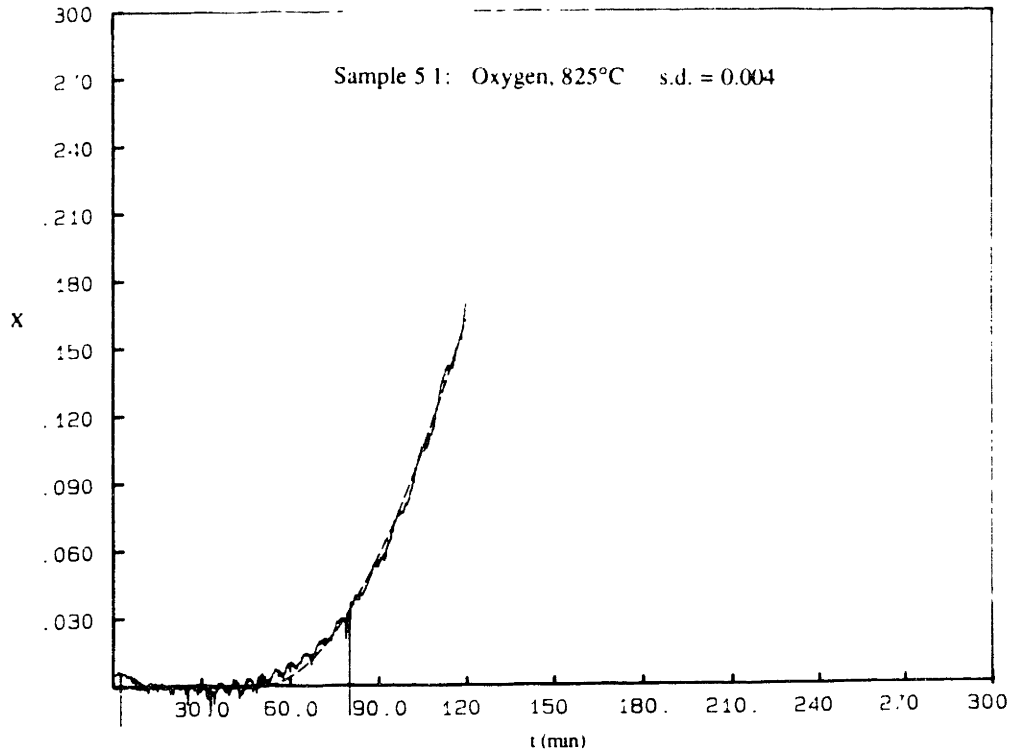

Figure 7.11: (continued from previous page)

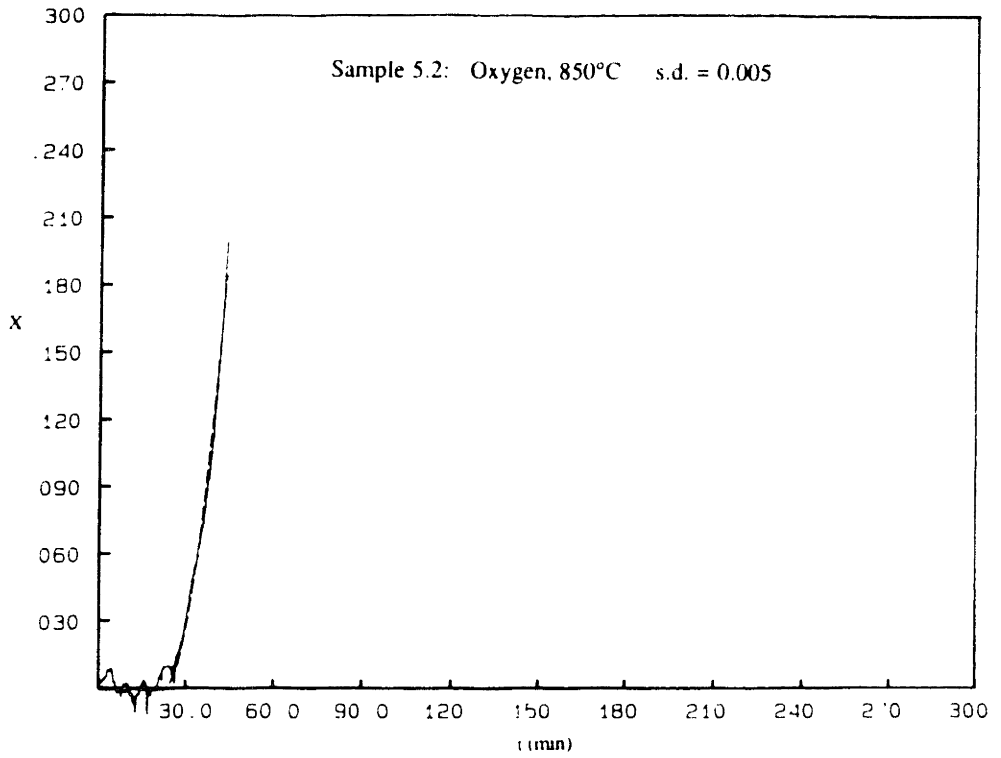
Sample 5.2: Oxygen, 850°C s.d. = 0.005
300
270
240
210
180
150
120
090
060
030
x
30.0
60 0
90 0
120
150
180
210
240
300
t (min)

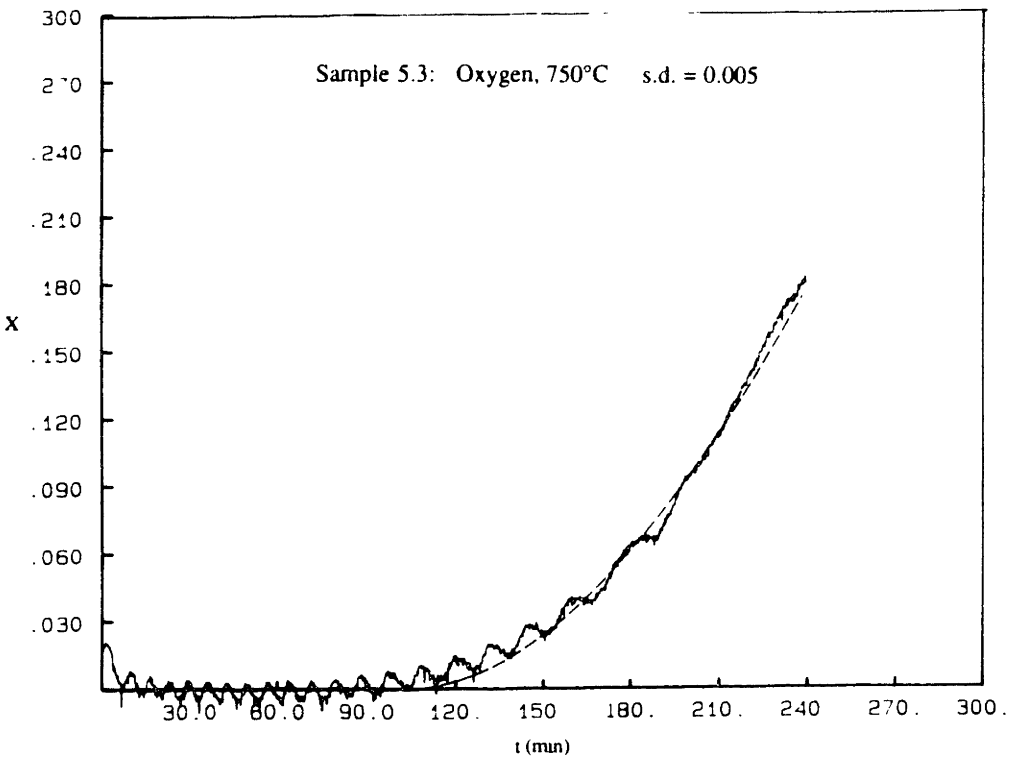
Sample 5.3: Oxygen, 750°C s.d. = 0.005
300
240
210
180
150
120
090
060
030
x
30.0
60.0
90.0
120.
150
180.
210.
240
270.
300.
t (min)

line/parabola combination found with the experimental curve depends on the viability of the assumption that all the nuclei formed simultaneously.

Determining the agglomeration front velocity in continuous films annealed in oxygen.

The agglomeration front velocity, u, can be calculated from the value:

$$\mathbf{A} = \pi u^2 N_{void} \qquad (46)$$

In the case of a parabolic dependence, N_{void} can be determined by counting the number of nuclei in a given area. For example, the value of $\mathbf{A}$ in sample 1.2 is 1.84×10^{-4} min^{-2} and the value of N_{void} is 142 in an area of about 0.01035 cm^2 (which is the size of the area in the photograph that was used to count the voids). This is approximately 1.4 voids in an area of 100×100 μm. The velocity of the interface is therefore 6.5×10^{-5} cm min^{-1} or 0.65 μm min^{-1}. The velocity of the agglomerating front determined from lines of the same thickness is 0.47 μm min^{-1}. The velocities calculated for samples annealed in oxygen are listed in Table IV and plotted against 1/kT in figure 7.12. The activation energy of 0.88 eV and D_o of 6×10^{-4} cm^2 s^{-1} do not agree well with the same constants determined from lines of this thickness.

Two alternative analyses.

There is too much scatter in the data of figure 7.12 to obtain a reliable fit. Two other methods can be used to verify the rates plotted in figure 7.12.

An alternative analysis is provided by considering the radius of the voids as the result of annealing at a fixed temperature for a length of time equal to t_{anneal}, less the incubation time τ (Fig.7.8b):

$$r = u (t_{anneal} - \tau) \qquad (47)$$

There is a distribution of void sizes in these experiments so the radius at the mode of the distribution of sizes was used to calculate the velocities. The signal should be dominated by

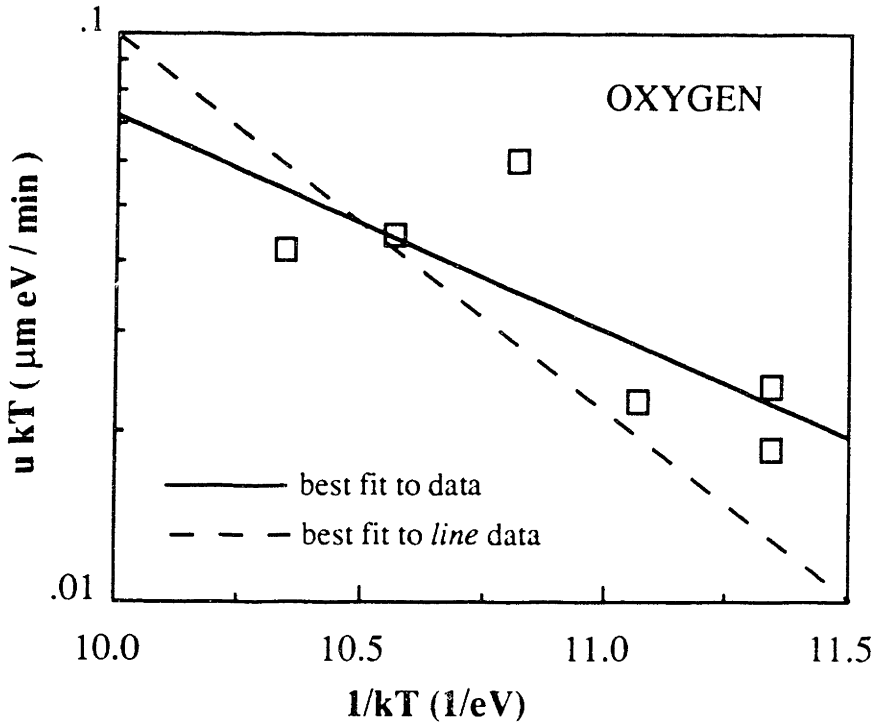

Figure 7.12: Arrhenius plot of agglomeration front velocity for continuous films annealed in oxygen. The front velocity was calculated based on equation 46. The solid line is the best fit to all the points and represents the equation:

$$u\,kT = 438 \exp\left(-\frac{0.88\ eV}{kT} \right)$$

The dashed line is the fit to the data from lines (see figure 7.6).

Temperature (Sample #)	A min^{-2}	N_{void}	u ($\mu m\ min^{-1}$)	τ (min)
750 (1.3)	1.07×10^{-5}	50	.27	127
750 (5.3)	1.00×10^{-5}	77	.21	100
775 (2.1)	9.53×10^{-6}	49	.25	75
800 (1.2)	1.84×10^{-4}	142	.65	44
825 (5.1)	3.5×10^{-5}	53	.47	49
850 (5.2)	4.37×10^{-4}	775	.43	22

TABLE IV: Agglomeration front velocity, u, calculated from equation 46, and the incubation times used to calculate u from equation 47, for anneals in oxygen.

nuclei of that size. Figure 7.13 is an Arrhenius plot of these velocities: log ukT vs 1/kT. The values of u agree with those obtained using equation 46.

Another way to determine the velocity from these samples, and do it directly, is to consider the agglomeration around the edge of the gold film (Fig.7.14). Knowing that the rate is constant, the velocity can be determined by measuring the extent of the agglomeration, Δx_{edge}, and dividing by the length of the experiment, t_{anneal}:

$$u_{edge} = \frac{\Delta x_{edge}}{t_{anneal}} \tag{48}$$

Both the velocities calculated from growth curves and from edge agglomeration, are presented in figure 7.15. The edge data falls close to the other data points. The line fitted to the edge data represents a fairly good fit, with an activation energy of 1.5 eV, which compares well with the data from lines. The value of D_o, 0.46 $cm^2\ s^{-1}$, is only about two times larger. This data agrees better than the data obtained from the fitting of the transformation curves mainly because of sample 5.2 which is the data point at 850°C. That particular sample was unevenly agglomerated: some areas had few voids, other areas had many. Therefore, the number of voids per unit area required for equation 46, might be in error.

Results for continuous films annealed in argon

Agglomeration velocities, calculated similarly to those in oxygen, were calculated for the anneals in argon. Figure 7.16 is an Arrhenius plot of agglomeration front velocity from equation 46. Data from oxygen anneals is plotted on the same graph as well as the measured void growth rates from experiments with 600Å thick lines. The activation energy is 1.0 eV and the pre-exponential of diffusivity is 3×10^{-3} $cm^2\ s^{-1}$. In figure 7.17, the front velocities have been calculated from equation 47, and the activation energy and D_o are respectively 1.6 eV and 1.3 $cm^2\ s^{-1}$. Both Arrhenius curve fits were based on only three data points. The velocities calculated from the extent of edge agglomeration,

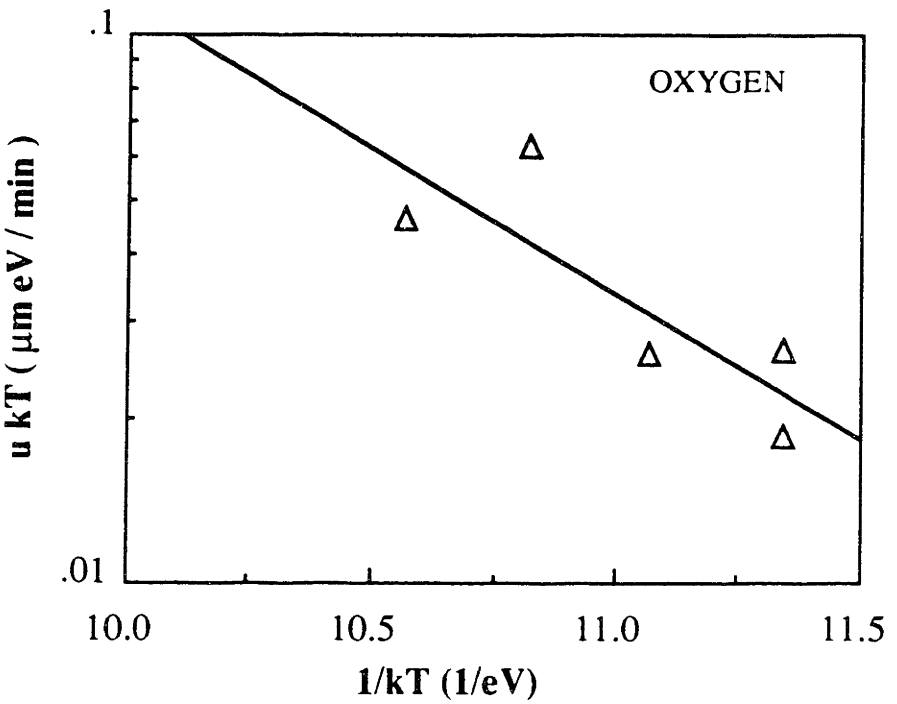

Figure 7.13: Arrhenius plot of agglomeration front velocity for continuous films annealed in oxygen. The velocity was calculated from the incubation time (equation 47) calculated by fitting a parabolic time dependence to ln (1-X).

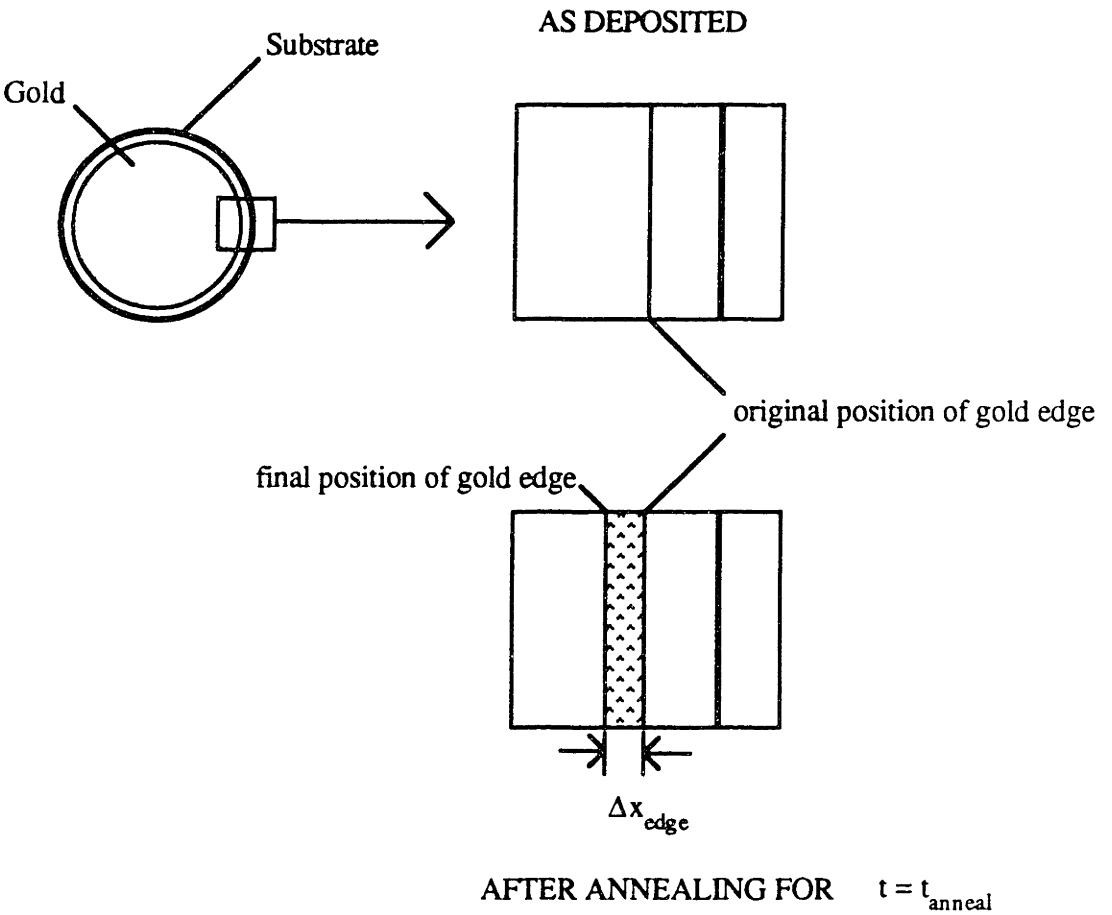

Figure 7.14: A schematic representation of the quantity used in equation 48. Because of the shadow cast by the lip on the evaporation plate (see figure 6.6) the continuous film has an edge around its periphery. Agglomeration begins at this edge as soon as the annealing temperature is reached.

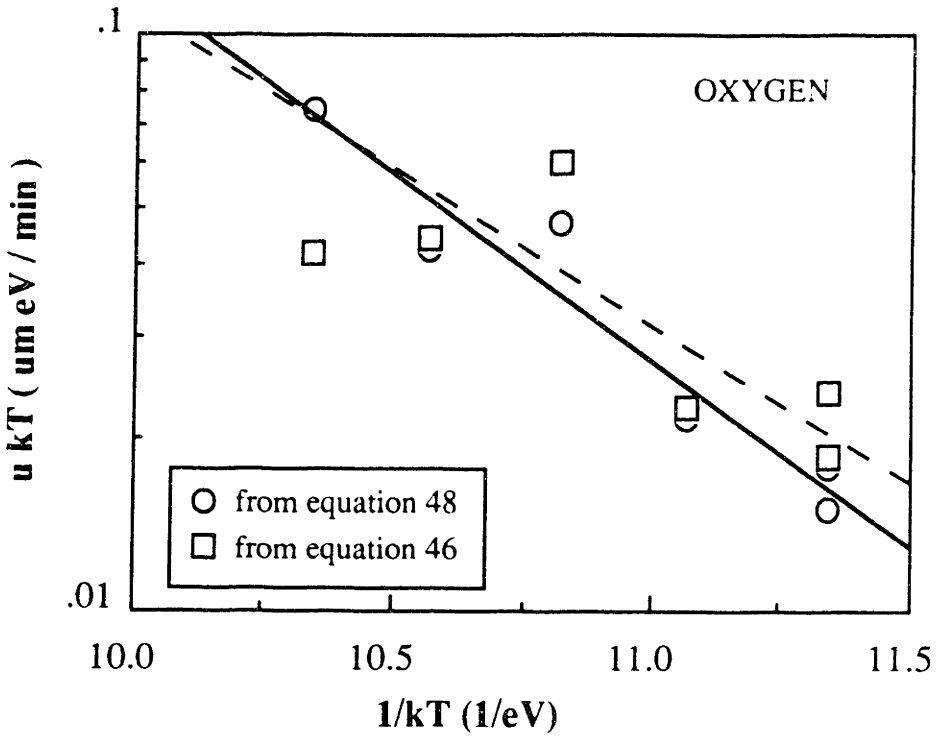

Figure 7.15: Arrhenius plot of agglomeration front velocity calculated from agglomeration of the film edge (equation 48) and from the number of voids and the best fit of the transformation curve (equation 46).
The solid line is the best fit based on the edge data:

$$u\,kT = 3.2 \times 10^{5} \exp\left(-\frac{1.5\,eV}{kT} \right).$$

The dashed line is the best fit to the data of figure 7.12, not including the point at 850°C:

$$u\,kT = 2.8 \times 10^{4} \exp\left(-\frac{1.2\,eV}{kT} \right)$$

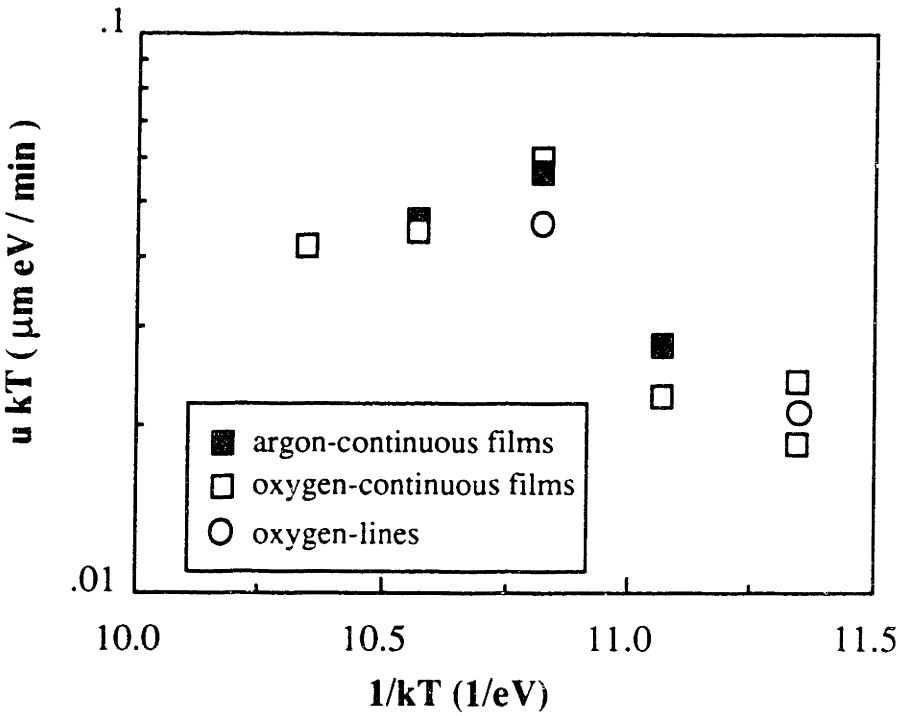

Figure 7.16: Arrhenius plot of agglomeration front velocity for continuous films annealed in argon.The velocity was calculated from equation 46: $\underline{A} = \pi u^2 N_{void}$ Oxygen data from figure 7.12 and line data for 600Å thick lines are included for comparison.

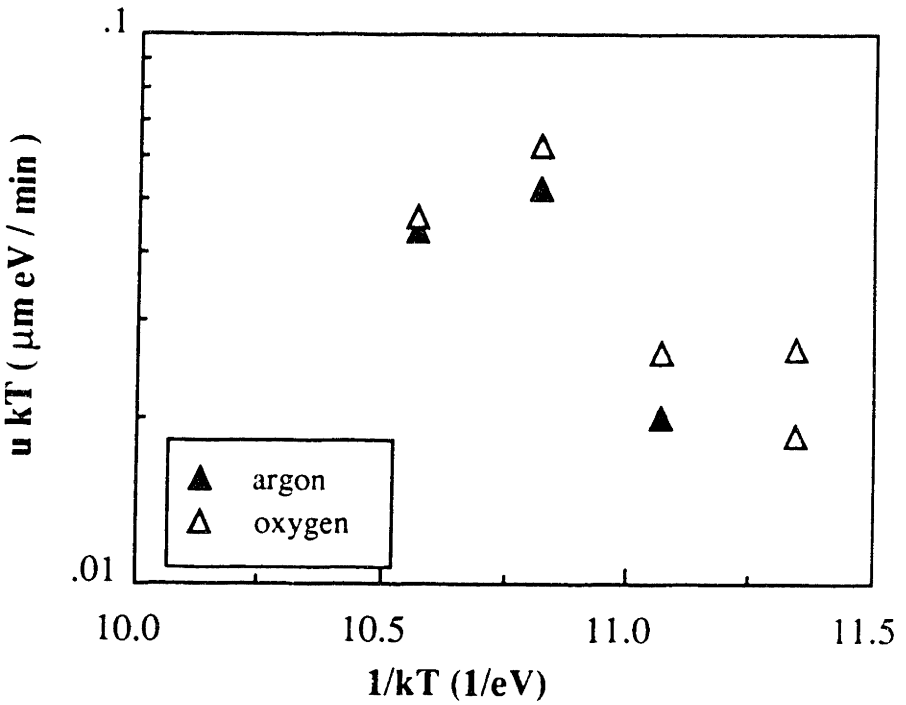

Figure 7.17: Arrhenius plot of agglomeration velocity for continuous films annealed in argon. The velocity was calculated from incubation times using equation 47. Oxygen data (from figure 7.13) are included for comparison.

equation 48, are plotted in figure 7.18. D_0 is 15 cm^2s^{-1} and the activation energy is 1.8 eV. While gold lines annealed in argon behaved differently from gold lines annealed in oxygen (see Appendix A), the oxygen data for continuous films is well within experimental error of the argon data. Because there is a lot of scatter in the data, the fit is poor, but the data from oxygen anneals serve to show that there is little difference between the oxygen and argon annealed films and that there is good agreement with the results from lines of the same thickness annealed in oxygen (Fig.7.16).

Summary

Lines of gold were annealed to directly measure the rate of agglomeration of thin films. The measured rates were used to extract the temperature and film thickness dependence of void growth for comparison with the proposed model in Chapter 5. The data obtained agreed very well with both the proposed temperature (Fig.7.6) and film thickness dependence (Fig.7.7b). In oxygen, the diffusivity extracted using the model in Chapter 5 was:

$$D_s = 0.18 \exp\left\{ -\frac{1.4\ eV}{kT} \right\} \qquad (39)$$

Continuous films 600Å thick were annealed in both oxygen and argon. These films were partially annealed to obtain void size distributions which reflect the time dependence of the nucleation rate. The void size distributions had some breadth to them, but were treated approximately as delta functions. Agglomeration of continuous films is marked by an incubation time and a parabolic time dependence if the nuclei all form at the same time. The transformation curves, X vs t, at different temperatures, were used to extract void growth rates according to equation 29 in Chapter 5. Continuous films annealed in oxygen and argon were found to agglomerate at similar rates to each other and there is also good agreement with data from gold lines of the same thickness annealed in oxygen.

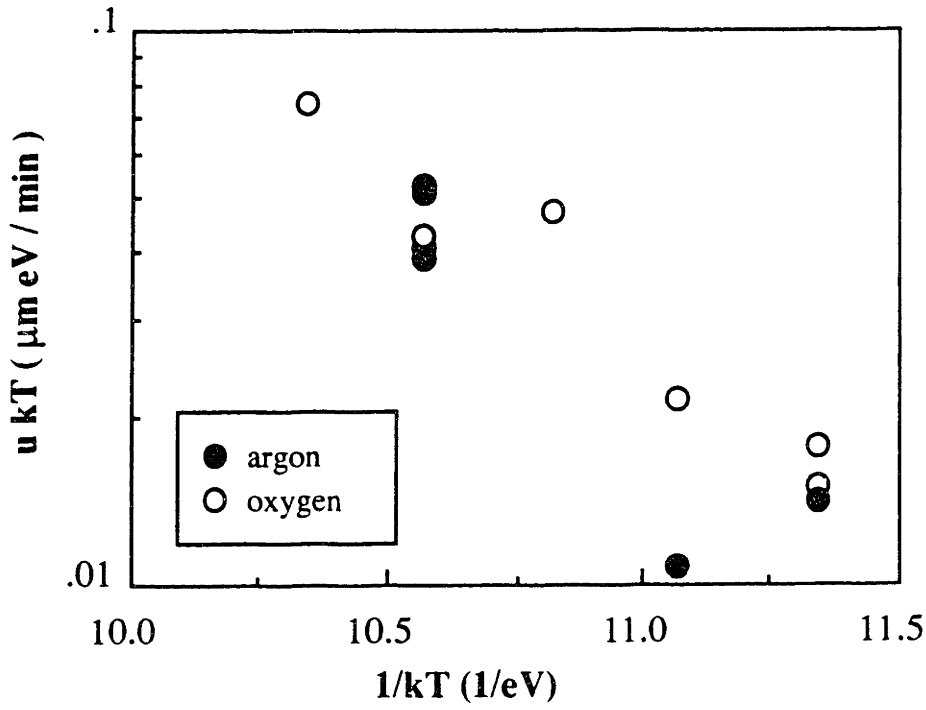

Figure 7.18: Arrhenius plot of agglomeration front velocity in argon, calculated from agglomeration of film edge using equation 48. Oxygen data (from figure 7.15) is included for comparison.

Chapter 8:

DISCUSSION

Discussion of the model

In Chapter 4, the morphology of the agglomerating edge was studied. It was found that agglomeration occurs by the breakdown of a thickened edge. The edge then recedes in a cellular or dendritic pattern, leaving behind beads or islands. The rate of agglomeration is determined by the velocity of the tips of these cells or dendrites which define an agglomeration front.

The temperature and film thickness dependence of the rate of agglomeration was modeled in Chapter 5 under the assumption that surface diffusion is the mechanism for mass transfer, that the moving edge is not subject to accumulation of material and that the film contact angle with the substrate is 90°. The last two conditions set the radius of curvature of the edge to be equal to the film thickness. From the expression for surface flux:

$$j_s = -\frac{D_s}{kT}\frac{\partial \mu}{\partial s} v, \qquad (50)$$

the volume of material and, therefore, the velocity with which the edge recedes can be derived. $\partial\mu/\partial s$ was expressed in terms of material parameters and the thickness of the film, h, using the Gibbs-Thompson equation and the geometry of the profile. This flux was then used to derive an expression for the rate of volume of material transferred and from this the velocity, dx/dt, of the receding edge. The result is (equation 24, Chapter 5):

$$\frac{dx}{dt} = \beta \frac{\exp\left(-\frac{Q_s}{kT}\right)}{kT\,h^3} \qquad \text{where} \quad \beta = D_o \Omega^2 \gamma_s \frac{2}{\pi} \qquad (51)$$

This result is independent of time and has an inverse cubic dependence on film thickness h. Deviations from a contact angle, θ, of 90° alter the radius of curvature for which the assumption of zero accumulation is valid. For smaller θ the radius of curvature would be higher and for larger θ, which is the case for gold on fused silica, the radius would be smaller. The derivation of the final equation would include a radius of curvature αh where α is determined by the contact angle and can be up to two. This results in a factor of two in equation 51, i.e., a D_0 half as large. As will be seen, in comparing the diffusivity calculated here with the diffusivity calculated by others, a factor of one half in D_0 is not significant.

The activation energies for diffusion determined from fitting equation 51 to data for each thickness (Fig. 7.4) appeared to vary with film thickness. If this dependence is not due to scatter in the experimental data, then it may come from two sources. As was discussed in Chapter 7, an incomplete description of actual processes in the derivation of the model may result in an apparent dependence on thickness. The increase of bead density in thinner films indicates that lateral diffusion might have to be taken into account in the thick films. If the activation energy is indeed changing with film thickness, the cause could be actual, physical changes due to, for example, impurities originating within the film which in small amounts in the volume may diffuse to the surface in amounts increasing with increasing film thickness. It could also be due to a transition in mechanism from surface to volume diffusion with increasing film thickness. If there is a transition from one mechanism to another, the contributions of the diffusive fluxes may produce a non linear Arrhenius dependence. The measured slope would vary depending on the regime in which the experiment was performed.

The agglomeration rate measured from the traces of transmittance versus time during the anneals of gold (patterned into wide lines) was constant, as predicted by

equation 51. The thickness dependence was determined experimentally, assuming a constant activation energy of 1.4 eV, to be $h^{-3.1}$. This is in very good agreement with the predicted dependence of h^{-3}.

The agglomeration of continuous films was modeled in Chapter 5 as a two dimensional phase transformation: from continuous film to beaded film, with a constant growth rate and a constant number of nuclei. Once nucleation occurs, taking impingement into account, the fraction transformed, X, has the following dependence on time (equation 30):

$$X = 1 - \exp\left\{ - N_h \pi u^2 \left(t - \tau \right)^2 \right\}. \qquad (52)$$

Although there was some time dependence in the nucleation frequency, traces of fraction transformed versus time obtained experimentally, are described very well by this equation.

From the measured number of voids, N_h, and the fit of equation 52 to the experimental data from 600Å thick films, the value of the transformation rate, u, was determined and agreed with the agglomeration rate determined from lines of the same thickness.

Interpretation of Incubation Time and Spread in Nucleation Times.

The purpose of studying continuous films was to include the effect of nucleation of voids. The transformation curves, figure 7.11, give information about the rate of void generation and, if the types of defects in the thin film are known, the defect that was responsible for agglomeration can be identified. One of the ways in which holes form in thin films is by grain boundary grooving. A grain boundary deepens as the 4th root of time, which means that a finite amount of time is needed for penetration of the film: an incubation time. The grain boundaries evolve at different rates depending on the orientations of the grains that meet. This would cause nucleation to occur over a long time

interval as different grain boundaries would intersect the substrate at different times. The result would be a distribution of void sizes as in figure 7.10. The thinner the film, the shorter the expected incubation time. Triple points are even more susceptible to penetration than grain boundaries. Srolovitz and Safran[3] found from equilibrium considerations that although conditions exist for a finite depth for both grain boundaries and triple junctions, the critical grain size for triple junctions is unrealistically small so that all triple junctions are expected to reach the substrate.

The void distributions varied from sample to sample. The number of each type of grain boundary is determined by the microstructure of the film. This in turn can be sensitive to the smoothness of the substrate as well as to other factors. The fact that voids formed preferentially at scratches in the substrate, so that a better polish was needed, could be a reflection of the fact that a grain boundary was pinned there during grain growth when the sample was heated, or that a special boundary was formed there during film deposition. The nucleation frequency might then be related to the polishing of a particular substrate and would appear random from one sample to the next. An advantage of having nucleation dominated by this interaction with the substrate is that the nuclei can be made to form far enough apart that they are able to assume a steady state morphology identical to that of the edges of lines. If the voids formed too close together, they might impinge before this morphology is established, i.e., before the thickened edge breaks down. Then a constant growth rate could not be assumed.

The beads themselves were elongated or often part of strands of grains, which remained stable for a long time. The limit to their stability seemed to be the fact that they were terminated at each end. The end grain is able to coarsen in the same manner that a terminated rod decomposed in Nichols and Mullins'[21] analysis. Experiments with much thinner lines resulted in a single row of beads(Appendix B). Although the anneal was long relative to the time that most of the substrate was exposed (the signal levelled off), long strands of gold still remained. This stability could be related to faceting. Sundquist[18]

found that elongated particles (single grain) could be as stable as (their shape may not change for as long a time as) shorter particles. This stability could also be related to the criteria of stability proposed by Srolovitz and Thompson[22] for thin lines, where the critical combination of grain size and cross-sectional area was predicted for stabilization of a line against agglomeration.

The role of impurities and comparison to surface diffusivities determined from other geometries.

In general, surface diffusion coefficients and activation energies are measured through the observation of morphological changes on heating. The evolution of the initial shape is modelled and compared with experiment. For gold, the diffusion coefficient or activation energy for surface diffusion have been measured by observing the smoothing of scratches[20,23,24,25] and of lithographically defined gratings[26] (driven by reduction of surface area), grain boundary grooving[20,25,27] (driven by minimization of grain boundary and surface energies), and evolution of field emitter tips (driven by the reduction of curvature). Different approaches have been used to detect diffusion at low temperatures. These involve the evolution of very fine structures of gold. A surface diffusion coefficient was measured [28] by observing the change in shape of very thin crystallites of gold on graphite at temperatures low enough (<500°C) that thickening of the crystallite was not observed. This phenomenon is driven by the reduction of edge length.* An activation energy for surface diffusion was also measured [29] by observing and modelling the growth of gold whiskers on a tungsten substrate. Agglomeration of thin patterned films would also appear to be useful, depending on the thickness of the film, in temperature ranges where bulk-based methods fail to yield results.

---

* First studied in the evolution of sodium chloride cleavage steps on heating:
H. Hoche and H. Bethge, *J. of Crystal Growth*, 33 (1976) 246.
H. Hoche, *J. of Crystal Growth*, 33 (1976) 255.

Equation 51 was applied to measured agglomeration rates and used to calculate a surface diffusivity in the temperature range from 700 to 825°C. The value of diffusivity, in cm^2s^{-1}, obtained is (equation 39):

$$D_s = 0.2 \exp\left(-\frac{1.4\,eV}{kT} \right) \quad cm^2\,s^{-1}. \tag{53}$$

Figure 8.1 shows this result in comparison with results from other methods. For comparison, the volume self-diffusivity of gold in the same temperature range is [19]:

$$D_v = 0.02 \exp\left(-\frac{2.2\,eV}{kT} \right) \quad cm^2\,s^{-1}. \tag{54}$$

Surface diffusivities obtained in this thesis and by other researchers using various methods are plotted in figure 8.1. McLean and Hirth[27] described a catastrophic decrease in surface diffusivity below 930°C. Gjostein[20] reported a sudden drop in diffusivity at 900°C and attributed it to the pinning of ledges by impurities. The impurities are thought to prevent surface diffusion so that volume, not surface diffusion, would be the dominant means of mass transport at those temperatures.

The value of the surface diffusion coefficient and activation energy measured experimentally, disagree from one study to the next. This has been attributed to impurities, originally in the bulk gold, diffusing to the gold surface and forming an inhibiting impurity layer [30].The atmosphere may also contain impurities which may adsorb to the gold surface. The type of atmosphere was found to play an important role. Carpenter and Mair[31] found that evaporation rates from a hot gold filament increased in the presence of oxygen (3mm mercury). This increase was attributed to the removal of a layer of impurities which prevented evaporation. Sundquist[18] found that oxygen produced an equilibrium shape of 1 μm particles of gold that was faceted. Pronounced faceting, however, was attributed to impurities. Olson *et al.* [26] found that patterning using lithography techniques contaminated the surface of the sample and prevented smoothing of a grating from taking

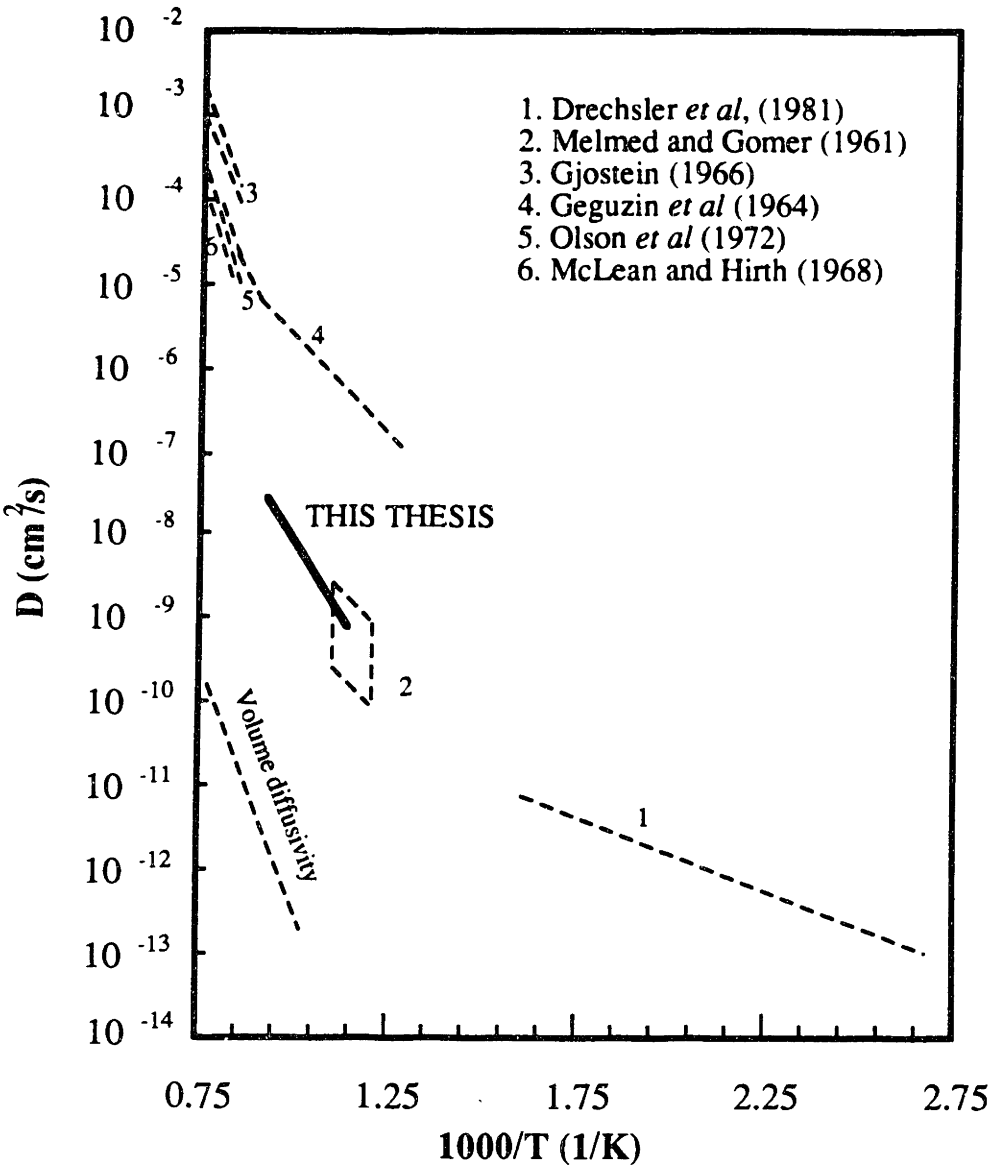

Figure 8.1: Surface diffusivity data from this thesis and from other work for comparison. Volume diffusivity was also included for comparison.

place unless the sample was first annealed at high temperature in oxygen or sputtered with argon ions for an extended period of time.

The following observations regarding possible contamination of the samples used in this thesis can be made:

1. Contamination between the film and the substrate due to the lift-off method, did not appear to affect agglomeration since the rates of agglomeration measured were similar for both patterned and continuous films annealed in oxygen.

2. While there was not much difference between continuous films annealed in oxygen and argon, the patterned films annealed in argon (Appendix A) produced much different results from those in oxygen, exhibiting an incubation time and agglomeration due in large part to void formation within the gold lines, even in thick gold deposits. This would be attributed to impurities on the gold surface of the receding edge which were not removed by the oxygen atmosphere used in the experiments of 1. If impurities retard the movement of the contaminated edge, the lines agglomerate by means of internal void formation.

The continuous films used are cleaner than the patterned films since no photoresist or solvents came in contact with either the substrate or the surface of the film. Since the data from oxygen and argon agreed in continuous films and disagreed in patterned films contamination from patterning was present. The fact that data from patterned films annealed in oxygen agreed with data from continuous films indicates that the oxygen successfully removed the contamination from the surface of the gold in patterned films.

Chapter 9:

SUMMARY AND CONCLUSIONS

The goal of this thesis was to study and model the process of agglomeration of thin films. The study was carried out in two parts. The first part was a TEM and SEM study of the movement of the agglomeration front and its relationship to the microstructure of the thin film. From these observations a model was derived to describe the kinetics of agglomeration. The second part of the study was based on measurement of the overall rate of transformation of a continuous film to an agglomerated film. The proposed model was applied to the transformation curves to test the time and temperature dependence against real data. Also from applying the model to the data from continuous films annealed in oxygen, a surface diffusivity for gold determined.

Agglomeration is driven by reduction of the surface area. A model was developed which was based on the observation that the actively receding part of the film edge is that part which has not thickened. The resulting kinetic equation

$$\frac{dx}{dt} = u = \beta \frac{\exp\left(-\frac{Q_s}{kT}\right)}{kT\,h^3} \qquad \text{where} \quad \beta = D_o \Omega^2 \gamma_s \nu \frac{2}{\pi} \qquad (55)$$

predicts a constant rate of agglomeration once a hole is formed and a film thickness dependence of h^{-3}, in contrast with previous theories and in agreement with our experiments.

Agglomeration can be treated as a transformation from one phase to another, consisting of the following steps:

1. nucleation of the second phase which includes beaded film,

2. growth of the second phase with a constant growth rate,

3. impingement of the nuclei.

A two dimensional Johnson-Mehl-Avrami analysis was used to propose the equation:

$$- \ln (1 - X) = N_h \pi u^2 (t - \tau)^2 \qquad (56)$$

for the case where the number of nuclei, N_h, and the growth velocity, u, are both constant.

It was found experimentally that the agglomeration rate was constant with time as is predicted by equation 55, and the thickness dependence was $h^{-3.1}$ which compares very well with the predicted h^{-3}. Experimental traces obtained from continuous films compared well with equation 56 which is based on a constant growth velocity of the beaded phase and a constant number of nuclei. Using the known value of N_h, the growth velocity, u, of the transformation in continuous films in equation 56 was calculated. It agreed with the value measured from experiments with patterned films.

Chapter 10:

FUTURE WORK

The modeling of the process of agglomeration in this thesis represents the simplest approach to both nucleation and growth. A more sophisticated model would include the effects of a contact angle other than 90°, a non-circular cross-section and a picture of diffusion in the third dimension as described in chapter 4. The last point includes the instability of the thickening edge (which would lead to a relationship between film thickness and bead density) and the exact shape including both curvatures of the dendrite tip (which might explain the apparent thickness dependence of the activation energy found in figure 7.4).

In continuous films, transformation curves may be more precisely described by taking into account time dependent nucleation of voids.

Experimentally, more studies with continuous films and wide lines are required in oxygen, other ambients and ultra high vacuum (UHV) systems. The special cleaning techniques developed for oxides can be taken advantage of to a greater extent in the line experiments. Lift-off used to pattern gold films leaves some residue which interacts with the gold surface. In argon, this retarded agglomeration. If, however, the substrate is etched after patterning of the resist, the pattern is transferred to the substrate as a series of high and low areas (Fig.10.1a). The advantage of this method is that all traces of the resist can be removed by a thorough cleaning before the gold is deposited. The gold then agglomerates away from the steps (Fig.10.2b).

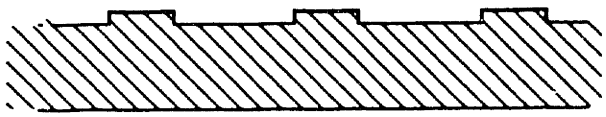

(a) Patterned substrate

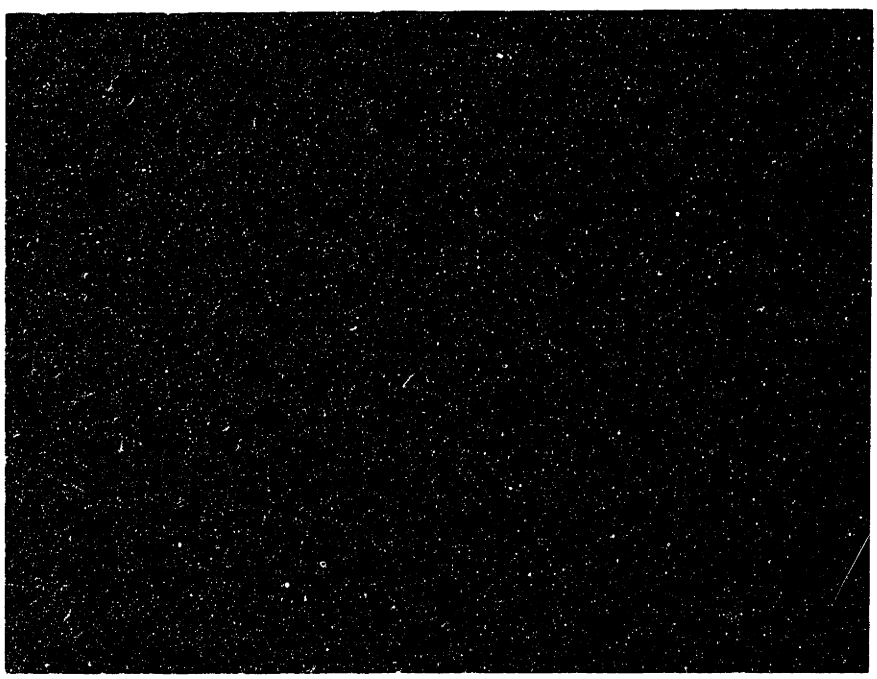

(b) Gold film deposited on such a substrate: after anneal. (optical dark field: only edges show)

Figure 10.1: Agglomeration of film into lines due to substrate patterning.

The deposition of the gold would ideally be carried out in UHV with the annealing performed *in situ* without breaking vacuum. The method of *in situ* monitoring using laser light would be particularly suited to this case.

APPENDIX A

Gold Lines Annealed in Argon

Gold lines created by lift-off were also annealed in argon. 400, 500 and 800Å thick lines were annealed, with observations made at the three temperatures, 750, 800 and 850°C, in the same anneal.The different slopes were measured and very high activation energies (up to 5 eV) calculated. In this case, however, annealing in this way did not yield the correct result. Samples annealed at one temperature only illustrate that the very small slope seen previously at 750°C was due to an incubation effect. After this incubation time, agglomeration proceeded at rates comparable to oxygen anneals, but the slope was not a straight line. The transformation curve resembled a transformation curve from continuous films and was actually due to significant void formation within the lines as well as agglomeration at the edges. The void formation complicated analysis of the transformation curve. This effect could be related to the observations of Olson *et al* who annealed gratings lithographically defined on gold surfaces. The gratings did not decay unless first annealed at high temperatures in oxygen or unless first cleaned by sputtering with argon ions. The photoresist in his case originally covered the surface of the grating, in this case, due to the lift-off procedure, it may be in contact with the line edges.

Therefore, in argon, agglomeration rate results from lines were inconclusive due to the inhibiting effect of impurities at the edges and void formation within the lines.

D. L. Olson, H. R. Patil and J. M. Blakely, *Scripta Metallurgica*, **6** (1972) 229.

APPENDIX B

Experiments with Gold Deposited on Patterned Substrates

A number of anneals were performed on patterned substrates. The advantage of patterning the substrate is that the substrate can be thoroughly cleaned before the gold is deposited. The gold pattern then consists of lines both where the substrate is etched and where it is not etched. One of the masks used had 12 μm wide spaces and 8 μm wide lines. The sample therefore had gold stripes of alternate widths. The gold on these samples was 700Å thick. The narrower stripes agglomerated into one row of beads down the center of the original cross-section, and the wider stripes agglomerated into two rows of beads. A mask with 25 μm spaces and 10 μm lines was also used and 600Å of gold was deposited on the patterned substrate. The 10 μm stripes had sections of both single and double bead rows. The 25 μm stripes had four to five rows of beads. The beads themselves were often strands of grains, which remained stable for a long time.

In the 8 μm lines, the material for the beads, which were about 2 μm across, was drawn from up to a distance of 3 μm. Therefore because two rows formed in a line 10 μm wide, we conclude that the edge became unstable after sweeping out a distance smaller than 3 μm.

References

1. Lord Rayleigh, *Proc. London Math. Soc.* **10**, 4 (1878).
2. D. J. Srolovitz and S. A. Safran, *J. Appl. Phys.* **60**, 247-254 (1986).
3. W. Mullins, *J. Appl. Phys.* **30** (1959) 77.
4. W. Mullins, *J. Appl. Phys.* **28** (1957) 333.
5. M. Lanxner, C. L. Bauer and R. Scholz, *Thin Solid Films* **150** (1987) 323.
6. D. J. Srolovitz and S. A. Safran, *J. Appl. Phys.* **60** (1986) 255.
7. R. H. Brandon and F. J. Bradshaw, R.A.E. (Farnborough) Rep. 66095 (1966)
8. A. E. B. Presland, G. L. Price and D. L. Trimm, *Prog. Surf. Sci.* **3** (1973) 63.
9. K. Sharma and J. Spitz, *Thin Solid Films* **65** (1980) 339.
10. W. M. Kane, J. P. Spratt and L. W. Hershinger, *J. Appl. Phys.*, **37** (1966) 2085.
11. R. E. Hummel, R. T. DeHoff, S. Matts-Goho and W. M. Goho, *Thin Solid Films*, **78** (1981) 1.
12. R. R. Zito, W. S. Bickel and W. M. Bailey, *Thin Solid Films*, **114** (1984) 241.
13. H. L. Caswell, J. R. Priest, and Y. Budo, J. Appl. Phys. 34 (1963) 3261.
14. M. L. Gimpl, A. D. McMaster and N. Fuschillo, *J. Appl. Phys.*, **35** (1964) 3572.
15. H. L. Caswell and Y. Budo, J. Appl. Phys. 34 (1963) 3461.
16. J. W. Christian, " The Theory of Transformation Rates in Metals and Alloys, Part I." (Pergamon Press, GB, 1975) p.18.
17. J. J. Metois and J. C. Heyraud, *Thin Solid Films*, **75** (1981) 1.
18. B. E. Sundquist, *Acta Metallurgica*, **12** (1964) 67.
19. W. Jost, *Diffusion* (Academic Press Inc., New York, 1952), p. 234.
20. N. A. Gjostein, *Trans. Met. Soc. AIME*, **239** (1967) 785.
21. F. A. Nichols and W. W. Mullins, *Trans. Metall. Soc. AIME*, **233** (1965) 1840.
22. D. J. Srolovitz and C. V. Thompson, *Thin Solid Films*, **139** (1986) 133.
23. N. A. Gjostein, *Trans. Met. Soc. AIME*, **236** (1966) 1267.
24. Ya. E. Geguzin and N. N. Ovcharenko, *Soviet Physics-Solid State*, **4** (1963) 2281.
25. Ya. E. Geguzin, G. N. Kovalev, and N. N. Ovcharenko, *Soviet Physics-Solid State*, **5** (1964) 2627.
26. D. L. Olson, H. R. Patil and J. M. Blakely, *Scripta Metallurgica*, **6** (1972) 229.
27. M. McLean and J. P. Hirth, *Surface Science*, **12** (1968) 177.
28. M. Drechsler, J. J. Metois and J. C. Heyraud, *Surface Science*, **108** (1981) 549.
29. A. J. Melmed and R. Gomer, *J. Chem. Phys.*, **34** (1961) 1802.
30. D.Clark, T. Dickinson and W. N. Mair,*Trans. Faraday Soc.*, **55** (1959) 1937.
31. D.Clark and W. N. Mair ,*Trans. Faraday Soc.*, **55** (1959) 1924.